OXYGEN TRANSPORT IN THE ARTERIAL VASCULATURE OF THE RESIDUAL LIMB AFTER TRANS-FEMORAL AMPUTATION

YAN FEI

PhD

The Hong Kong Polytechnic University

This programme is jointly offered by The Hong Kong Polytechnic University and Sichuan University

2019

The Hong Kong Polytechnic University

Department of Biomedical Engineering

Sichuan University

Institute for Disaster Management and Reconstruction

OXYGEN TRANSPORT IN THE ARTERIAL VASCULATURE OF THE RESIDUAL LIMB AFTER TRANS-FEMORAL AMPUTATION

YAN Fei

A thesis submitted in partial fulfillment of the requirements

for the degree of Doctor of Philosophy

August 2018

CERTIFICATE OF ORIGINALITY

I hereby declare that this thesis is my own work and that, to the best of my knowledge and belief, it reproduces no material previously published or written, nor material that has been accepted for the award of any other degree or diploma, except where due acknowledgement has been made in the text.

_____(Signed)

(YAN Fei)

ABSTRACT

Numerous musculoskeletal injuries are caused by earthquakes, such as lacerations, fractures, and soft-tissue contusions or sprains. And there are 3-20% of influenced people suffering crush injuries, in which injuries of the lower limb (74%) are the most common. Moreover, there were 2.26 million amputees in China by 2006. After Whenchuan and Lushan earthquakes, the number of amputees has considerably increased. It attracts a vast amount of public attention in contemporary society.

After the amputees wearing prostheses, there are a number of health problems in the residual limbs which are disruptive to amputees' daily lives. These problems hinder their clinical rehabilitation and may even threaten their physical health. The development of these problems including blisters, edema, pressure ulcers, damage to deep soft tissue and muscle atrophy is related to the biomechanical mechanism, while the fundamental mechanisms of these problems have not been fully elucidated. Thus, studies on residuum disorders are of great significance in biomechanical research.

The spatial vasculature of the residual limb is changed significantly by lower-limb amputation. Changes in the vasculature affect the hemodynamic status and oxygen transport in the circulatory system. And understanding the hemodynamic status and oxygen transport in the residuum is beneficial in evaluating the residuum status. Few investigations have focused on the blood flow and oxygen transport

systematically in the circulatory system of the residual limb due to the complex vasculature.

In order to understand the blood flow and oxygen transport systematically in the arterial system of the residual limb after amputation, computational and experimental investigations about oxygen distribution and hemodynamic responses were implemented in this study and included four parts as follows.

First, computational fluid dynamics models of the descending branches of the lateral femoral circumflex artery (DLFCA) coupled with oxygen transport in both the residuum and the sound limb were established, and three inflow velocities were applied at inlet to figure out the effect of exercise on oxygen transport in residuum DLFCA. Consequently, the investigation of oxygen transport in the residuum vasculature was suggested to be valuable in understanding the health status of the residuum after amputation, and the joint consideration of WSS and oxygen distribution was required in determining the rate of the atherosclerosis development in residuum arteries. Additionally, exercise was indicated to be favourable for enhancing oxygen content in DLFCA of the residual limb and reducing the possibility of the formation of the atherosclerotic plaque in residuum arteries.

Second, the oxygen concentration in the arteries could not be noninvasively monitored in clinical research, and a three-dimensional (3D) numerical simulation

of the systemic arterial tree is complicated and requires considerable computational resources and time. Thus, transmission line equations of oxygen transport in the arteries were firstly proposed according to the theory of oxygen transport and fluid transmission line equations. And these equations were numerically verified through the comparison between a 3D computational simulation of oxygen transport in the vascular model and a lumped parameter model of oxygen transport. These transmission line equations are treated as the theoretical basis for the establishment of the lumped parameter model of oxygen transport, and this model can be applied for numerically predicting the oxygen distribution in the systemic arterial tree with fewer computational resources and less time. Moreover, these transmission line equations of oxygen transport can also be regarded as the theoretical basis for developing transmission line equations of other substances in blood.

Third, transmission line equations of mass transport in arteries have been proposed, and these equations offer a more efficient scheme for investigating the systemic distribution of the substance in the arterial tree. Whereas, the derivation of these equations in arterioles and capillaries is lacked. Transmission line equations of mass transport in arterioles and capillaries were developed, and these equations were derived based on the transmission line equations of mass transport in arteries and mass transport theory in microvessels. These equations were verified through the comparison of the numerical prediction based on the developed equations with the previous *in vitro* experimental studies. The transmission line equations of mass

transport in arterioles and capillaries are not only applied in constructing the lumped parameter model of mass transport for predicting the systemic distribution of the substance concentration in the microvascular tree, but also regarded as the supplement to the theoretical basis for establishing the lumped parameter model of the entire vascular system including arteries, arterioles, and capillaries.

Forth, oxygen distribution in the residual limb changes due to the vasculature transformation after trans-femoral amputation, and changes in oxygen content play a significant role in the developments of health problems of the trans-femoral residuum. Oxygen content in the residual limb mainly depends on oxygen transport in the residuum vasculature. Few studies focused on oxygen transport in the arteries of the residual limb. We developed a coupling computational model of blood flow and oxygen transport in the residuum arteries to predict oxygen distribution, and the Windkessel model and the lumped parameter model of oxygen transport were applied as the boundary conditions at outlets of the vascular model. The boundary condition with the lumped parameter model of oxygen transport was verified through the comparisons between the non-elongated vascular models with the lumped parameter models and the elongated models. Moreover, an *in vitro* experiment with a three-dimensional (3D) printing replica of the residuum vasculature was carried out to validate the computational simulation. The proposed boundary condition with the lumped parameter model was determined to be reliable for simulating the effect of downstream vessels on oxygen transport in the vascular

model. According to the numerical results of the 3D computational model with the developed boundary condition of oxygen transport, the effect of inflow velocity on oxygen distribution was indicated to be much smaller than that of backflow during a pulsation cycle. Moreover, with the joint consideration of Sh, WSS, and oxygen content in tissues, the adjustment of inflow and backflow during a cycle was proposed to alleviate the risk of the residuum disorder.

PUBLICATIONS

Peer-reviewed Journal

1. Chen, Y, Yan, F., Jiang, W., Wang, Q., Fan, Y., (2013). Numerical study on effects of drug-coating position of drug-eluting stents on drug concentration. *Journal of Medical & Biological Engineering,* 34(5): *487-494.*
2. Chen, Y., Xiong, Y., Jiang, W., Yan, F., Guo, M., & Wang, Q., et al. (2013). Numerical simulation on the effects of drug eluting stents at different Reynolds numbers on hemodynamic and drug concentration distribution. *Journal of Mechanics in Medicine & Biology,* 13(04), 1350070.
3. Dong, R., Jiang, W., Yan, F., Zheng, T., & Fan, Y. (2015). Numerical analysis of the impact of atherosclerotic plaque and different stent spacing on drug deposition. *Journal of Mechanics in Medicine & Biology,* 15(01): 1550011.
4. Chen, Y., Xiong, Y., Jiang, W., Yan, F., Guo, M., Wang, Q., Fan, Y. (2015) Numerical simulation on the effects of drug eluting stents at different Reynolds numbers on hemodynamic and drug concentration distribution. *BioMedical Engineering OnLine*, 14(Suppl 1), S16.
5. Chen, Y., Guo, M., Xiong, Y., Jiang, W., Yan, F., & Wang, Q., et al. (2015). Experimental analysis of the 3D flow field of a virtual stent using particle image velocimetry. *Journal of Biomaterials & Tissue Engineering,* 5(1), 16-23(8).
6. Chen, Y., Xiong, Y., Jiang, W., Wong, M. S., Yan, F., & Wang, Q., et al. (2016). Numerical simulation on the effects of drug-eluting stents with different

bending angles on hemodynamics and drug distribution. *Medical & Biological Engineering & Computing,* 54(12), 1-12.

7. Dong, R., Li, X., Yan, F., Fan, Y., Jiang, W., & Wong, M. S. (2016). The spatial structure changes of thigh arterial trees after transfemoral amputation: case studies. *Journal of Medical Imaging & Health Informatics,* 6(3), 688-692.
8. Chen, T. L., Wong, D. W., Wang, Y., Ren, S., Yan, F., & Zhang, M. (2017). Biomechanics of fencing sport: a scoping review. *Plos One,* 12(2), e0171578.
9. Yan, F., Jiang, W. T., Dong, R. Q., Wang, Q. Y., Fan, Y. B., & Zhang, M. (2017). Blood flow and oxygen transport in descending branch of lateral femoral circumflex arteries after transfemoral amputation: a numerical study. *Journal of Medical & Biological Engineering,* 37(1), 1-11.
10. Bai, T., Chen, Y., Jiang, W., Yan, F., & Fan, Y. (2018). Studies on foam decay trend and influence of temperature jump on foam stability in sclerotherapy. *Vascular and Endovascular Surgery,* 52(2), 98-106.
11. Yan, F., Jiang, W. T., Xu, Z., Wang, Q. Y., Fan, Y. B., & Zhang, M. (2018). Developing transmission line equations of oxygen transport for predicting oxygen distribution in the arterial system. *Scientific Reports,* 8(1), 5369.
12. Li, Z., Yan, F., Yang, J., Chen, Y., Xu, Z., Jiang, W., Yuan, D. (2018). Hemodynamics and oxygen transport through pararenal aortic aneurysm treated with multilayer stent: numerical study. *Annals of Vascular Surgery,* 10.1016/j.avsg.2018.05.040.
13. Bai, T., Jiang, W., Chen, Y., Yan, F., Xu, Z., & Fan Y. (2018). Effect of multiple

factors on foam stability in foam sclerotherapy. *Scientific Reports,* 8(1), 15683.

14. Mei, J.[#], Yan, F.[#], Ni, M., Wang H., Zhang F., & Wang Z. Changes in intra-articular pressure on the blood supply in the retinaculum of the femoral neck. *Clinical Biomechanics.* ([#]These authors contributed equally) (Minor revision)
15. Yan, F., Jiang, W. T., Xu, Z., Wang, Q. Y., Fan, Y. B., & Zhang, M. Transmission line equations of mass transport in arterioles and capillaries: A complement to the theoretical basis for investigating mass transfer in the entire vascular system. (Under review in *Journal of Fluid Mechanics*)
16. Yan, F., Jiang, W. T., Dong, R. Q., Wang, Q. Y., Fan, Y. B., & Zhang, M. Use of transmission line equations of oxygen transport for understanding oxygen distribution in arteries of the residual limb after trans-femoral amputation. (Under review in *Journal of Biomechanics*)
17. 郭萌，蒋文涛，樊瑜波，郑庭辉，陈君楷，& 晏菲. (2010). 药物洗脱支架置入弯曲冠状动脉血管后药物浓度场及壁面切应力分布. *中国组织工程研究,* 14(42)，7857-7860.
18. 董瑞琪，蒋文涛，郑庭辉，晏菲，& 樊瑜波. (2011). 药物洗脱支架在弯曲动脉中药物沉积量的数值分析. *医用生物力学,* 26(1)，13-17.
19. 晏菲，蒋文涛，郑庭辉，樊瑜波，& 刘展. (2012). 药物洗脱支架高度对药物浓度和壁面切应力分布影响的数值分析. *医用生物力学,* 27(4)，451-455.
20. 晏菲，蒋文涛，郑庭辉，& 樊瑜波. (2012). 动脉粥样硬化斑块对药物洗脱支架药物扩散影响的数值分析. *医用生物力学,* 27(5)，510-514.

21. 吴昊，蒋文涛，晏菲，陈宇，& 樊瑜波．(2013)．两类药物洗脱支架药物释放曲线对血管壁内药物浓度影响的数值研究．*生物医学工程研究* 32(4)，206-211.

22. 陈宇，蒋文涛，熊艳，李小龙，& 晏菲．(2015)．基于 NoSQL 技术的心电数据库存储研究．*生物医学工程研究,* 34(4)，235-237.

23. 李小龙，晏菲，董瑞琪，陈宇，蒋文涛，& 樊瑜波．(2016)．一种表征残肢血管结构变形的参数方法．*医用生物力学,* 31(1)，19-23.

24. 李忠友,蒋文涛,陈宇,晏菲．(2018)．细胞喷墨打印喷嘴长度对流场影响的数值研究．*生物医学工程研究,* 37(1)，32-35.

25. 李忠友,蒋文涛,王振泽,晏菲,陈宇,樊瑜波．(2018)．老年人心血管疾病康复研究现状及展望．*生物医学工程与临床,* 22(3)，341-346.

26. 王振泽,徐智,晏菲,储照伟,蒋文涛,樊瑜波．(2018)．下肢假肢接收腔对残肢肌肉萎缩影响的数值研究．*生物医学工程学杂志*.(Accepted)

Book

1. 晏菲，董瑞琪，蒋文涛，张明．(2018) 下肢残肢的生物力学，in：樊瑜波，张明 (Eds.)，康复工程生物力学．上海交通大学出版社，上海，pp．1-15.

Conference proceedings

1. 晏菲，蒋文涛，郑庭辉，樊瑜波，刘展．药物洗脱支架高度及斑块对药物浓度分布影响的数值研究．2011中国力学大会暨钱学森诞辰100周年

纪念大会. 哈尔滨, 2011.8.22-24.

2. 晏菲, 蒋文涛, 郑庭辉, 樊瑜波. 动脉粥样硬化斑块药物扩散系数对药物洗脱支架药物扩散影响的数值分析. 第十届全国生物力学学术会议暨第十二届全国生物流变学学术会议. 成都, 2012.10.11-15.
3. Yan, F., Jiang, W., Dong, R., Wang, Q., Fan, Y., & Zhang, M. Numerical study on the effects of blood velocity on oxygen transport in the residuum vasculature. The 3rd Symposium on Fluid-Structure-Sound Interactions and Control. Perth, Australia, 5-9 July 2015.

ACKNOWLEDGEMENTS

First, I would like to express my gratitude to Hong Kong Jockey Club for supporting me to complete the Joint Ph.D Program of Sichuan University and The Hong Kong Polytechnic University. And I would devote myself to the studies about the management and reconstruction of the disaster.

Second, I am truly grateful for the guidance of my chief-supervisors Prof. Ming ZHANG and Prof. Wentao JIANG. They offer me a large amount of research experience and help for our studies. They not only provide the direct guidance for improving my research of interest, but also teach me the way to find your research interests and the logistical thought for conducting research. Moreover, their guidance about lives plays a significant role in my life. Additionally, I would like to express my gratitude to my co-supervisors Prof. Qingyuan Wang, Dr. M. S. WONG and Dr. Aaron LEUNG for their suggestions.

Third, I greatly appreciated help and suggestions from my research colleagues, Dr. Yu CHEN, Dr. Ruiqi DONG, Mr. Zhi XU, Mr. Daiquan ZHANG in Sichuan University and Dr. Duo WONG, Dr. Yan WANG, Mr. Tony CHEN, Ms. Shicong RENG in The Hong Kong Polytechnic University. And Ir. Xuejing HUANG in the Biomechanical Engineering Lab of Sichuan University provides an amount of guidance in the experimental study. My friends and colleagues (Junting XIANG and Meng GUO) help me release the pressure during my Ph.D period. Drinking

with my colleagues and friends helps me release the pressure and ease the mind during the most difficult period of research.

On top of that, I really appreciated the help from my families. Last year, my father and mother had severe diseases. I cost some time to take care of them, and they still supported me to continue my Ph.D study after their stable health status. I herein want to say thanks to my parents.

TABLE OF CONTENTS

LIST OF FIGURES

LIST OF TABLES

LIST OF ABBREVIATIONS

CFA: Common femoral artery

CFD: Computational fluid dynamics

CT: Computed tomography

DFA: Deep femoral artery

DLFCA: Descending branch of lateral femoral circumflex artery

EC: External carotid artery

FSI: Fluid-structure interaction

IC: Internal carotid artery

LDL: Low-density lipoprotein

LFCA: Lateral femoral circumflex artery

MFCA: Medial femoral circumflex artery

MRI: Magnetic resonance imaging

NIRS: Near-infrared spectroscopy

Pe: Péclet number

PO_2: Oxygen tension

RBCs: Red blood cells

Sh: Sherwood number

SFA: Superficial femoral artery

TLE: Transmission line equations

UDF: User-defined C-like function

UDS: User defined scalar

WSS: Wall shear stress

X-ray: X-radiation

3D: Three-dimensional

CHAPTER 1 INTRODUCTION

There are a number of musculoskeletal injuries due to earthquakes, such as lacerations, fractures (22%), and soft-tissue contusions or sprains (6%) (Mulvey et al., 2008). And there are 3-20% of influenced people suffering crush injuries (Gonzalez, 2005), in which injuries of the lower limb (74%) are the most common (Briggs, 2006).

In the meantime, there were 2.26 million amputees in China by 2006, of which 630 thousand amputees needed prostheses (Luo and Sun, 2009). After Wenchuan and Lushan earthquakes, the number of amputees has considerably increased (Zhao et al., 2008). It attracts a vast amount of public attention in contemporary society.

After the amputees wearing prostheses, there are a number of health problems related to the biomechanical mechanism. More specifically, friction and pressure would result in poor skin micro-circulation and skin problems, like blisters, edema, pressure ulcers and so forth (Lyon et al., 2000, Sanders et al., 1997). Moreover, muscle atrophy of the residuum is very common after amputation (Fraisse et al., 2008, Schmalz et al., 2001).

Skeletal muscle atrophy is considered as a problem with a decrease in the mass of the muscle after amputees wearing prostheses (Fraisse et al., 2008). It could cause the reduction in skeletal muscle strength of the residual limb, especially for the

patients with the short residuum (Isakov et al., 1996). And muscle wasting may be the main contributor to skeletal muscle atrophy (Lee and Vandenburgh, 2013). Skeletal muscle atrophy of the residual limb, regarded as a common disorder after trans-femoral amputation (Fraisse et al., 2008), has been always hindering efficient clinical rehabilitation and athletic capacity recovery for amputees. In general, the patient wants to wear the prosthesis for a long time. However, due to the residuum muscle atrophy, some patients' prosthetic sockets need to be accommodated periodically. It not only causes inconvenience to patients' daily lives, but also impedes athletic recovery for patients. If there is no accommodation of prosthetic sockets conducted for the patients who still suffer muscle atrophy in time, muscle atrophy could contribute to a number of problems, such as prosthetic socket loosening, abnormal gait, increasing friction and local stress concentration which could aggravate skin ulcers (Sanders et al., 2000, Sanders et al., 2009). Convincing arguments could be made that skeletal muscles are predominantly composed of protein, especially actin and myosin which are the main components of thick and thin filament. And there is a significant relationship between muscle force and the number of thick and thin filaments overlapping. More specifically, when the amount of thick and thin filaments overlapping has an increment, the corresponding muscle strength would increase as well. In other words, the homeostasis between muscle protein synthesis and degradation directly affects muscle quality, furthermore, has an influence in the muscle force and strength in the residual limb after trans-femoral amputation. Specifically, when the amount of synthesis in muscle protein is more

than that of degradation, there is manifestation of muscle hypertrophy appeared in the residual limb after trans-femoral amputation, vice versa, there would be the manifestation of muscle atrophy in the residual limb (Caron et al., 2009). In summary, there is a significant correlation between the change in muscle quality and the change in the physiological components of skeletal muscle in the residual limb after amputees wearing trans-femoral amputation.

In summary, these issues are increasingly disturbing amputees' daily lives after amputees wearing prostheses. Furthermore, these problems even would threaten physical health of these amputees at times.

Although a number of studies were carried out for understanding the relationship between the developments of these problems and the biomechanical status of the residual limb (Lee et al., 2004, Mak et al., 2001, Renström et al., 1982), the underlying mechanisms of these issues have not been clearly figured out. Since amputation significantly affects the arterial vasculature in residual limb (Dillingham et al., 2005, Gudmundsson et al., 2002, Erikson and Hulth, 1962), blood flow and oxygen distribution in residuum arteries transform in comparison with those of the sound contralateral limb (Yan et al., 2017). Change in oxygen concentration distribution of residual limb due to the vasculature transformation is supposed to be a factor in the developments of these health problems. Specifically, friction and pressure at the interface between residuum and socket cause impaired

microcirculation in superficial tissue of the residual limb. Poor microcirculation hinders oxygen transport and contributes to blisters, edema, and pressure ulcers (Lyon et al., 2000, Sanders et al., 1997). Moreover, muscle disuse is generally regarded as a reason for the development of muscle atrophy (Ferreira et al., 2008, Powers et al., 2005). Muscle disuse changes the spatial structure of arteries and results in the regression of microvascular structure and function, which leads to hypoxia in muscles. Thereafter, hypoxia induces muscle dysfunction and further causes muscle atrophy (Ottenheijm et al., 2006, Caron et al., 2009). In terms of muscle disuse, oxygen content plays a key role in the development of muscle atrophy. In summary, since oxygen in tissues of the residual limb is derived from blood flow in arteries, investigations of blood flow and oxygen concentration distribution in the transformed arterial vasculature are required for more fully elucidating the mechanisms of these problems in residuum.

There were several studies about arterial responses in the residual limb after trans-femoral amputation, and these studies mainly focused on changes in the geometry of the arterial trees in residuum (Dong et al., 2016), the relationship between hemodynamic state and health problems after lower-limb amputation (Dong et al., 2015) , and oxygen transport in an artery of the residual limb (Yan et al., 2017). Specifically, Dong et al. utilized a modified Hausdorff distance to determine the transformation of the spatial structure of the residuum arterial tree after amputation and suggested that using prothesis significantly affected the arterial vasculature of

the residual limb. Thereafter, she reviewed hemodynamic issues in preoperative assessment, operation, and complications after amputation, and it was concluded that more detailed researches about hemodynamic parameters and mass transport in residuum arteries were necessitated. Additionally, numerical simulations of the descending branches of the lateral femoral circumflex artery (DLFCA) in residual limb and sound limb were conducted to investigate blood flow and oxygen transport in these arteries. Nevertheless, few studies concentrated on oxygen transport in the arterial tree of the residuum after trans-femoral amputation.

Obviously, oxygen transport systems in the human body are supposed to be more complicated and efficient than the simple process of oxygen diffusion. The transport process of oxygen to cells has been composed of two specialized delivery systems (Fournier, 2011). At first, the circulatory system is one of the oxygen delivery systems, which utilizes the blood to take oxygen into the capillaries near the tissue. The hemodynamics could affect the oxygen transport in the blood of the circulatory system. In the capillaries, the red blood cells (RBCs) would release the oxygen. And then oxygen is transported close to the tissue by the coupling process of diffusion and convection. Hemoglobin, which exists in the RBCs, plays a significant role in the other delivery system of oxygen. The physiologic phenomenon of oxygen bound to the hemoglobin has increased the solubility of oxygen in the plasma. In the skeletal muscle, there is a significant correlation between sarcoplasmic myoglobin and oxygen transport (Wittenberg and Wittenberg, 1989). And it is concluded that

myoglobin has an impact on the oxygen concentration in the skeletal muscle (Millikan, 1939, Wittenberg, 1970, Wittenberg and Wittenberg, 1981, Kreuzer et al., 2011). In addition, exercise would contribute to the increment of myoglobin concentration in the myofibrils (Pattengale and Holloszy, 1967). The size of cells may affect the myoglobin content (Taylor et al., 1987).

Oxygen concentration distribution in microvessels and large arteries is supposed to be obtained through the experimental measurement and numerical prediction. Numerous measurements of oxygen concentration in blood were performed through using invasive procedures (Masamoto et al., 2008, Buerk and Goldstick, 1982, Vazquez et al., 2010, Yaseen et al., 2011). The most common technique for *in vivo* noninvasively measuring oxygen concentration in the microcirculation of brain and muscle was the near-infrared spectroscopy (NIRS) (Ferrari and Quaresima, 2012, Murkin and Arango, 2009, Wolf et al., 2007), whereas the depth of the detection site significantly affected the accuracy of the measurement (Wolf et al., 2007). Nevertheless, there were few *in vivo* noninvasive methods of systematically measuring oxygen concentration distribution in the circulatory system. The 3D computational fluid dynamic (CFD) simulation coupled with mass transport was utilized for determining oxygen concentration in the vessels (Tarbell, 2003, Murphy et al., 2015, Chen et al., 2014). Most of these numerical investigations emphasized oxygen distribution in local regions and neglected the systemic distribution of the oxygen concentration in the vascular tree. The oxygen distribution in the entire

vascular system could be acquired from a 3D CFD simulation coupled with mass transport. This simulation is complicated and requires considerable computational resources and time in terms of systemic circulation due to the complex vasculature of the arteries and microvessels. It is currently almost impossible for most of the research groups and clinical measurements to perform a 3D simulation of the systemic arterial tree or microvascular tree in the residual limb.

Few investigations have focused on the blood flow and oxygen transport systematically in the circulatory system of the residual limb due to the complex vasculature. First, to understand the difference of hemodynamic responses and oxygen distribution between the sound limb and the residual limb and the effect of exercise on the residuum, CFD models of the DLFCAs coupled with oxygen transport in both the residuum and the sound limb were firstly established, and three blood velocities with the gradual increment caused by exercise were applied at the inlet of the residuum vessel. Second, to predict the systemic distribution of oxygen concentration with the consideration of hemodynamics, the transmission line equations of oxygen transport in arteries and microvessels were firstly proposed according to the theory of oxygen transport and fluid transmission line equations. These transmission line equations can be applied for numerically predicting the oxygen distribution in the systemic arterial tree with fewer computational resources and less time, and also be regarded as the theoretical basis for developing transmission line equations of other substances in blood. Third, to investigate the

oxygen concentration distribution in the arteries of the residual limb, a coupling computational model of residuum arteries using transmission line equations of oxygen transport and blood flow was developed. In this model, a novel boundary condition with the lumped parameter model of oxygen transport was applied to simulate the effect of downstream vascular beds on oxygen transport in residuum arteries. Forth, to validate the computational model of oxygen transport in the residuum vasculature, an *in vitro* experimental platform with a 3D printing replica of the residuum vasculature was established.

CHAPTER 2 LITERATURE REVIEW

2.1 Residuum changes after amputees wearing prostheses

After the amputation, the changes of the residual limb may affect the fitting of the prosthetic socket (Lilja et al., 1998). The decrease of postoperative oedema would contribute to the decrease in the volume of the residual limb in the early rehabilitation phase (Lilja and Öberg, 1997). And it is demonstrated that a negative power function could quantify the volume change of the residuum followed by the time for definitive prosthetic fitting. In addition, Lilja et al. suggested that it was proper for the amputees to wear the definitive prosthesis four months after amputation. The volume of the residual limb not only changes, but the internal structure also transforms. In terms of measuring the changes of residuum muscles, magnetic resonance imaging (MRI) is a useful and non-invasive tool (Zhang et al., Jaegers, 1993).

2.2 Health problems after amputees wearing prostheses

2.2.1 Poor skin micro-circulation and skin problems

After the amputees wearing prostheses, there are numerous health problems related to the biomechanical mechanism. More specifically, friction and pressure would result in poor skin micro-circulation and skin problems, like blisters, edema, pressure ulcers and so forth (Lyon et al., 2000, Sanders et al., 1997). Lyon et al., which conducted a questionnaire study of 210 patients after amputation, found that

there were many problems of skin surface existed in lower-limb prosthesis users. In order to have a good knowledge of skin suffering capacity to the mechanical loading, Sanders et al. have developed an instrument for conducting the mechanical loading experiment which could figure out the relationship between skin and mechanical loading. And the damage of deep soft tissue is attributed to high stress in osteotomized bone ends (Portnoy et al., 2009). In order to explore the stress and strain in the soft tissue of the residual limb, Portnoy et al. developed a finite element model of the residual limb after trans-tibial amputation with a geometric model related to the MRI images of a specific amputee. Through this computational analysis, it is found that there is an individual difference of biomechanical information in the soft tissue of the residual limb among different amputees, which would contribute to the increment in the risk of deep pressure ulcer or deep tissue injury.

2.2.2 Muscle atrophy

Muscle atrophy of the residuum is very common after amputation (Fraisse et al., 2008, Schmalz et al., 2001). Fraisse et al. collected numerous research papers related to muscle atrophy from PubMed and Reedoc databases, for the sake of having a review about muscle changes in the residual limb after trans-tibial amputation in terms of different academic viewpoints. It is concluded that the manifestation of muscle atrophy in the quadriceps is most significant after

amputation and the circumstance of walking gait have been transformed a lot. Moreover, in order to find out the effects of muscle atrophy on thigh muscle changes after trans-tibial amputation, Schmalz et al. conducted a measurement in the physiological properties of thigh muscle belonged to the amputated limb, which revealed that muscle atrophy is most obvious in ventral muscles among trans-tibial amputees.

The amputees have the manifestation of muscle atrophy in the residual limb immediately after amputation (Baumgartner and Langlotz, 1980). In contrast, the muscle area of sound side has an increment with an initial reduction (Lilja et al., 1998). Moreover, physical activity, postoperative bandaging and prosthetic fitting could have an impact on the amount of muscle atrophy in the residual limb (Renström et al., 1982). In summary, it is concluded that both muscle atrophy and the decrease of postoperative oedema would cause the reduction in the muscle area, and the volume change of the residual limb is consistent with the decrease of muscle area in the rehabilitation phase (Lilja and Öberg, 1997, Golbranson et al., 1988).

2.2.3 Summary

These issues are increasingly disturbing amputees' daily lives after amputees wearing prostheses. Furthermore, these problems even would threaten physical health of these amputees at times. As a consequence, a large number of researches

have been carried out to investigate the mechanism of these problems and develop possible interventions to mitigate these. A computational model was employed in the analysis of the biomechanical circumstance between the surface of the residual limb and the prosthetic socket (Lee et al., 2004). And it is suggested that there has been a different distribution of stress and strain in different regions of the residual limb surface, which could be caused by the biomechanical mechanism of loading transfer. Mak et al. collected a number of research papers based on the investigation of the residuum biomechanical state, in order to analyse the causes and positions of pressure ulcers and soft tissue problems (Mak et al., 2001), and it is concluded that the consideration related to the mechanical understanding should be involved in the design of each components in the prosthesis, which would improve the biomechanical state in the surface of the residual limb. A measuring study has been employed to figure out the physiological properties of thigh muscle after trans-tibial amputation through using different measuring instruments (Renström et al., 1982). Thus, it is demonstrated that the decrease of muscle fibre size was the main contributor to muscle atrophy. Although there have already been these studies involved in the investigations of the reasons for these problems after amputees wearing prostheses, the fundamental mechanisms of these problems related to biomechanical and physiological understanding have not been fully elucidated according to the above investigations up to now. As a consequence, studies about these disorders of the residual limb after the amputation are still of great significance in biomechanical research.

2.3 Effects of muscle atrophy on prosthetic fitting

There are many research directions involved in the studies of stump muscle atrophy after amputees wearing prostheses. In general, the patient wants to wear the prosthesis for a long time. However, due to the residuum muscle atrophy, some patients' prosthetic sockets need to be accommodated periodically. It not only causes inconvenience to patients' daily lives, but also impedes athletic recovery for patients.

If there is no accommodation of prosthetic sockets conducted for the patients who still suffer muscle atrophy in time, muscle atrophy could contribute to a number of problems, such as prosthetic socket loosening, abnormal gait, increasing friction and local stress concentration which could aggravate skin ulcers (Sanders et al., 2000, Sanders et al., 2009). At the first stage, Sanders et al. carried out the experiment about the measurement of shear stress distribution between the surface of the residual limb and the prosthetic socket after trans-tibial amputation through using shear stress transducers. And it is demonstrated that muscle atrophy of the residual limb would contribute to the changes in pressure and shear stress distribution of different regions in the interface between the prosthetic socket and the stump. Thus, it is beneficial to make an optimal design for the prosthesis based on the biomechanical information which has been provided by these measuring instruments. In the recent time, a new way to measure the volume change of the

residual limb after trans-tibial amputation has been developed through measuring the biofluid volume before and after doing a short-term ambulation. As a result, the experimental results have provided some useful statistical information about the morphologic properties of the residual limb. Furthermore, the compared results may be useful for the optimal design of the prosthetic design and the intervention of residuum muscle atrophy after amputation.

2.4 The mechanisms of residuum muscle atrophy after amputation

Apparently, it is very significant for the improvement of amputees' restoration and prosthetic design to understand the pathological and biomechanical mechanism of residuum muscle atrophy after amputees wearing prostheses. Majority of researches, which are mainly focused on disuse muscle atrophy of the residual limb after amputation, have been conducted in terms of measurements in the physiological and mechanical properties of thigh muscle (Schmalz et al., 2001). More specifically, in order to find out the effects of muscle atrophy on thigh muscle changes after trans-tibial amputation, Schmalz et al. conducted a measurement in the physiological properties of thigh muscle belonged to the amputated limb, which revealed that muscle atrophy is most obvious in ventral muscles among trans-tibial amputees. In conclusion, it was suggested that muscle atrophy of residuum sartorius and quadriceps femoris, which was related to the disuse atrophy, was the most obvious after amputation.

Moreover, there were a number of studies involves in investigating the physiological and biomechanical state of different components in the residual limb, for the sake of having a good knowledge of the relationship between the residuum composition and muscle atrophy after amputation. More specifically, Sherk et al. conducted the experimental measurement of morphologic properties of different components in the residual limb among trans-tibial and trans-femoral amputees through using the x-ray imaging method, for the sake of exploring the relationship between the muscle and the adipose tissue in the residuum (Sherk et al., 2010). Furthermore, the experimental measurement would be useful for figuring out the mechanism of muscle atrophy based on the amount of the adipose tissue in the residual limb. Consequently, it is demonstrated that there was a clear correlation between muscle atrophy and adipose tissue in the residual limb, especially for trans-femoral amputees.

In order to understand the impact of electrical loading on the muscle changes, Boonyarom et al. made the rats suffered muscle atrophy through making their limbs disuse, and stimulated the limb muscle which suffered muscle atrophy electrically for a short-term experiment (Boonyarom et al., 2009). As a result, it is found that morphologic and histologic properties of muscle fibres, which have suffered a decrease in overlapping numbers of thin and thick filaments due to the disuse atrophy, would be transformed by the frequency of electrical stimulation.

For investigating the physiological and biomechanical mechanism of muscle atrophy, furthermore, to alleviate muscle atrophy of the residual limb after trans-femoral amputation, a number of scholars have investigated this disorder in terms of mechanical mechanism and microscopic pathological characteristics based on many measuring instruments. More specifically, there is a significant correlation between the reduction of muscle strength and muscle atrophy in the residual limb (Renström et al., 1982, Isakov et al., 1996, Tugcu et al., 2009). For the sake of demonstrating the relationship between the length of the residual limb and muscle atrophy after amputees wearing trans-tibial prostheses, Isakov et al. carried out a experimental measurement in the morphologic and physiological properties of muscle in the residual limb through using a new instrument based on electrical theory. As a consequence, it is found that there is a significant correlation between muscle atrophy and muscle strength in the residual limb, which are related to the change in the length of the stump after amputation.

In addition, in order to investigate the changes in the micro-structure of skeletal muscles in the residuum, an experimental measurement has been conducted to demonstrate the physiological and biomechanical properties of thigh muscle in the residual limb after trans-tibial amputation through using different measuring instruments (Renström et al., 1982). And it is demonstrated that the decrease of muscle fibre size was the main contributor to muscle atrophy. Meanwhile, the overlapping number of thick and thin filament in the residuum muscle could

influence muscle atrophy as well. For the sake of figuring out whether there existed a relationship between the physiological properties of bone and skeletal muscle in the residual limb after trans-tibial amputation, Tugcu et al. carried out an experimental measurement of muscle strength and the properties of bone in the thigh of the residual limb through using the X-ray measuring instrument. Consequently, it is demonstrated that there may not existed a correlation between the physiological properties of bone and muscle atrophy in the residual limb after amputees wearing prostheses.

Additionally, skeletal muscle apoptosis also plays a significant role in the muscle atrophy of the residual limb after amputation (Ferreira et al., 2008, Nagano et al., 2008). More specifically, Ferreira et al. conducted the experiment which made the limbs of the mice disuse for different time, and then measured the physiological and morphologic properties of skeletal muscle in the disuse limb, in order to demonstrate the correlation between muscle disuse and muscle atrophy in the limb in terms of the number of skeletal muscle cells. Subsequently, the measurement of muscle mass was employed after the short-term unloading for identifying the change in the number of skeletal muscle cells with time. Eventually, it is suggested that the change in the number of skeletal muscle cells could provide some evidences for the assessment of muscle atrophy in the early stage of muscle atrophy after skeletal muscle disuse.

In the meantime, for the sake of investigating the relationship between muscle atrophy and the biochemical mechanism of muscle apoptosis in the disuse limb of rats, Nagono et al. conducted the experiment of rats which suffered different temperature for a short time after a short-term limb disuse. And they also studied the molecule pathway of skeletal muscle cells and the micro-physiological characteristics of skeletal muscle in the limb after a short-term disuse. The results have revealed that there is a significant relationship between muscle atrophy and the molecule pathway of skeletal muscle cells in the limb after disuse, which determines that the molecule pathway of skeletal muscle cells is the main contributor to the biochemical mechanism of muscle atrophy.

On the other hand, it is due to the fact that skeletal muscles are predominantly composed of protein, especially actin and myosin which consist of thick and thin filament. And there is a significant relationship between muscle force and the number of thick and thin filaments overlapping. More specifically, when the amount of thick and thin filaments overlapping has an increment, the corresponding muscle strength would increase as well. In other words, the homeostasis between muscle protein synthesis and degradation directly affects muscle quality, furthermore, has an influence in the muscle force and strength in the residual limb after trans-femoral amputation (Fitts et al., 2000, VANDENBURGH et al., 1999, Fitts et al., 1986, Stein et al., 1999). Specifically, when the amount of synthesis in muscle protein is more than that of degradation, there is manifestation of muscle hypertrophy appeared in

the residual limb after trans-femoral amputation, vice versa, there would be the manifestation of muscle atrophy in the residual limb (Dan et al., 2011). In summary, there is a significant correlation between the change in muscle quality and the change in the physiological components of skeletal muscle in the residual limb after amputees wearing trans-femoral amputation.

Molecular signalling pathways

The homeostasis between skeletal muscle protein synthesis and degradation could be regulated by molecular signalling pathways (Glass, 2005). Specifically, in order to conclude the effects of molecular signalling pathways in the residual limb on the changes in the muscle quality after amputation, Glass et al. found that a number of scholars investigated the impact of protein molecular pathways in the skeletal muscle of the residual limb on the changes in the morphologic and biomechanical properties of the skeletal muscle after suffered the stimulation, which caused by the environment. The conclusion based on the review paper would provide theoretical basis for doing the research of the physiological and biomechanical mechanism of muscle atrophy in the residual limb after trans-femoral amputation.

In addition, for the sake of investigating the influence of one specific protein pathway on the muscle atrophy of the disuse limb, Bodine et al. carried out the biochemical experiment of the skeletal muscle protein molecular pathways after disuse coupling with the biomechanical mechanism, which would be beneficial to

find out the relationship between the biochemical and biochemical properties of skeletal muscle in the disuse limb (Bodine et al., 2001). Through the test of muscle protein molecular pathways in the disuse limb, it is concluded that activation of the Akt/mTOR pathway could prevent disuse muscle atrophy, which have provided an efficient way to treat skeletal muscle atrophy in the disuse limb.

And for the sake of investigating the influence of myostatin on the amount of skeletal muscle protein in the disuse limb based on the biochemical properties of skeletal muscle protein, Trendelenburg et al. have conducted a biochemical test of several protein factors which could control the muscle protein molecular pathways and identified the impact of different protein factors on the myostatin which is the main contributor to the changes in the amount of skeletal muscle cells in the disuse limb (Trendelenburg et al., 2009). Consequently, it is convinced that insulin-like growth factor 1 (IGF-1) among these factors of protein controlling could promote protein synthesis through inhibiting the activities of myostatin through affecting the pathways of skeletal muscle protein in the disuse limb.

Oxygen

On top of that, it is worth pointing out that the generation of muscle protein should necessitate oxygen consumption (Wagenmakers, 1998). Specifically, in order to study the influence of oxygen metabolism on the amount of skeletal muscle protein based on the biochemical properties of muscle protein pathways, Wagenmakers et

al. studied the amount of skeletal muscle protein after having the oxygen exercise through the biochemical measurement, and he tested the effects of TCA-cycle on the coupling function of oxygen metabolism and the amount of protein in the skeletal muscle. He has concluded that TCA-cycle is the main contributor to the changes in the protein homeostasis and biochemical process of oxygen metabolism in the skeletal muscle.

In addition, for the sake of figuring out the relationship between skeletal muscle protein metabolism and oxygen metabolism, Chance et al. carried out the measurement of the muscle mass after subjects having a consistent exercise, which would provide the significant evidences of the controlling function of oxygen metabolism in the skeletal muscle. Thus, it is noted that, based on the connection between oxygen and oxidative metabolism, the biochemical process of oxygen would have an influence on the homeostasis of muscle protein in skeletal muscle.

Moreover, the previous findings indicated that oxygen could have a significant impact on energy metabolism in skeletal muscle (McCully and Hamaoka, 2000). More specifically, McCully et al. conducted the experimental measurement of the oxygen concentration distribution in the skeletal muscle after having an exercise through using NIRS, in order to investigate the role of oxygen concentration distribution on the biochemical process of energy in the skeletal muscle. And it is suggested that the measurement of NIRS is an efficient way to have a good

knowledge of oxygen concentration distribution in the skeletal muscle and the amount of muscle energy metabolic process.

It is concluded that there existed an evident difference in regulated mechanism of oxygen concentration distribution in different skeletal muscles after the mechanical loading (Kushmerick et al., 1992). More specifically, through making use of the technique of particle magnetic physical capacity, Kushmerick et al. have measured the amount of oxygen concentration in the slow- and fast-twitch muscles which have suffered the mechanical loading under the constant temperature, for the sake of demonstrating the oxygen concentration distribution in different muscles after mechanical loading. This technique of particle magnetic physical capacity is beneficial to quantify the amount of oxygen in the skeletal muscle, which is helpful for investigating the oxygen concentration distribution in the skeletal muscle of the residual limb which has suffered muscle atrophy after the trans-femoral amputation.

Convincing arguments could be made that hypoxia in the skeletal muscle of the residual limb would facilitate muscle protein degradation with a decrease in muscle protein synthesis, which would contribute to skeletal muscle atrophy in the residuum after trans-femoral amputation (Caron et al., 2009). Specifically, Caron et al. has measured the amount of muscle protein from skeletal muscle for a constant time under the environment which was lack of oxygen, in order to make out the relationship between muscle atrophy and oxygen concentration in the residual limb

after amputees wearing prostheses. This study has provided the theoretical basis for the research of oxygen transport in the residual limb which would be beneficial to understand the mechanism of muscle atrophy in the residual limb after amputation in terms of oxygen concentration distribution in the vasculature of the stump. On the basis of the above investigations, oxygen concentration distribution in the vasculature of the residual limb plays a significant role in residuum muscle atrophy of trans-femoral amputees, and it is helpful to resolve the disorder of muscle atrophy based on the studies about oxygen transport in the vasculature of the residual limb.

2.5 Oxygen transport and hemodynamics

Meanwhile, it should be noted that the spatial vasculature of residuum has been changed significantly due to lower-limb amputation. The amputation would contribute to partial loss of the vasculature directly, and muscle atrophy would cause spatial structure changes and lumen reconstruction of branch vessel. In addition, the pressure in prosthetic socket causes extrusion of some vessels (mainly vein). In other words, there may be differences between residuum and contralateral normal limb in terms of the hemodynamic state.

Oxygen transport in human body mainly consists of convection and diffusion (Pittman, 2000). In the vascular system, the convection-diffusion equation is generally used to numerically describe the oxygen transport in blood. Hemoglobin is the oxygen carrier in vessels. Most of studies about oxygen transport in vessels

concentrate on 3D CFD simulations coupled with oxygen transport. In addition, oxygen transport in muscle tissues is mainly affected by diffusion, while myoglobin regulates oxygen transfer from microcirculation to the mitochondrion in muscle cells. Krogh cylinder is conventionally regarded as the theoretical basis for proposing the numerical model of oxygen transport in capillaries and tissues (Krogh, 1919).

2.5.1 3D computational simulations of oxygen transport in arteries

Moreover, a vast amount of research has already proved that there is a remarkable correlation between hemodynamic parameters and oxygen transport in the vasculature of other circulation systems (Qiu and Tarbell, 2000, Liu et al., 2010, Coppola and Caro, 2008, Tada and Tarbell, 2006, Bateman et al., 2003), some of which has employed the coupled numerical analysis of hemodynamic state and oxygen transport in the artery through utilizing theories of fluid dynamics and mass transfer.

At first, in order to investigate the oxygen concentration distribution in the vasculature of the arterial circulation, Qiu et al. has established a computation fluid dynamic model of coronary arteries which consisted of a curved vasculature geometric model through coupling the simulation of oxygen transport in the

vasculature and in the arterial wall. As a consequence, the results reveal that the geometric model and hemodynamic parameters of the vasculature in the circulation system play a significant role in oxygen concentration distribution.

Subsequently, for the sake of figuring out the correlation between the spiral flow and oxygen concentration distribution in the artery, Liu et al. have employed three computational fluid dynamic models which are composed of different geometric model of arteries through using the theoretical method of oxygen transport in the vessels. As a result, it is found that there is a significant correlation between the spiral flow and oxygen concentration distribution, which provides a theoretical basis for the research of oxygen transport in the circulation system in terms of meaningful physiology.

Then Coppola et al. have established three numerical models of different arterial geometries, in order to understand the relationship between oxygen concentration distribution in the arterial vessels and the geometric characteristics of the vessels coupling with the comparison with the wall shear stress. Eventually, convincing argument should be made that the hemodynamic characteristics belonged to different geometries of the vessels have a cooperative influence in the wall shear stress and oxygen transport in the vessels of the circulation system.

For the aim of investigating the oxygen concentration distribution in the bifurcation

artery, Tada et al. has built a fluid mechanics model coupling with the theoretical knowledge of oxygen transport in the circulation system, using a commercial software FLUENT. And the results reveal that the geometric structure of the bifurcated artery plays a significant role in the distribution of oxygen concentration and WSS. Moreover, for the sake of exploring the oxygen concentration distribution in the micro-fluid circulation system of the human body, it is concluded that there is a significant correlation between oxygen transport and the physiological properties of the micro-fluid circulation system by Bateman et al.

Most of these numerical investigations emphasized the oxygen distribution in local regions and neglected the systemic distribution of the oxygen concentration in the vascular tree. The oxygen distribution in the entire vascular system could be acquired from a 3D CFD simulation coupled with mass transport. This simulation is complicated and requires considerable computational resources and time in terms of systemic circulation due to the complex vasculature of the arteries and microvessels. It is currently almost impossible for most of the research groups and clinical measurements to perform a 3D simulation of the systemic arterial tree or microvascular tree.

2.5.2 Lumped parameter model of blood flow

The lumped parameter model of blood flow based on the fluid transmission line

model is a useful tool in predicting the systemic distribution of blood flow and pressure in the arterial tree. Noordergraaf et al. (Noordergraaf et al., 1963) developed a lumped parameter model of the whole circulatory system, including the left ventricle, and compared the results with the human longitudinal ballistocardiogram. The input impedances, wave travel, blood flow, and pressure in the lumped parameter model of the human systemic arterial tree were compared with the measured data. These comparisons indicated that the lumped parameter model was reliable in obtaining the behaviors of a real circulatory system (Westerhof et al., 1969). Lacourse et al. (Lacourse et al., 1986) applied the lumped parameter model of the upper circulatory system to simulate stenosis at different locations of the arterial tree and investigate the effects of atherosclerosis on the systemic distribution of hemodynamic parameters. The lumped parameter model of blood flow could be used not only to determine the effects of cardiovascular diseases on the systemic hemodynamics of the circulatory system, but also to predict the hemodynamic responses of clinical interventions. Liang et al. (Liang et al., 2014a, Liang et al., 2014b) developed a lumped parameter model of the entire circulatory system based on patient-specific clinical data to predict the effects of the Fontan operation on the systemic hemodynamic data. The terminals of the arterial tree in the aforementioned models were simulated with rather simple boundary conditions (e.g., constant resistance condition or Windkessel condition). Thus, the effects of wave propagation were not involved in these numerical simulations. Herein, Olufsen (Olufsen, 1999) added the consideration of wave

propagation in the development of a lumped parameter model by attaching a structured tree to the outflow condition of the systemic arterial tree.

2.5.3 Oxygen transport in the arterial tree

The systemic distribution of the oxygen concentration in the arterial tree was not investigated in most of studies. Only a simplified mathematical expression that included the hemoglobin concentration was coupled with the lumped parameter model of blood flow to calculate the oxygen concentration from a systemic circulation perspective (Broomé et al., 2013, Yao et al., 2008). The expression included the hemoglobin concentration, the oxygen saturation, and the volume of the vascular segment. The volume of the vascular segment was related to the lumped parameter model of blood flow. Acquiring the systemic distribution of the oxygen concentration in the entire circulatory system was suggested to be helpful for understanding the relationship between the oxygen distribution and developments of diseases, and further improving the clinical interventions. Moreover, the effects of hemodynamics on the oxygen concentration distribution were neglected in the numerical investigations with the lumped parameter model of blood flow. Hemodynamics plays a significant role in oxygen transport in the arteries and should be considered for an accurate calculation (Tada, 2010, Liu et al., 2010, Tsai et al., 2003).

Convection and diffusion of oxygen transfer are the main components of oxygen transport in the vascular system. Both of them correlate with the oxygen concentration. And there exists a correlation between convection and diffusion in oxygen transport. In mass transport, convection enhances diffusion (Fannjiang and Papanicolaou, 1994, Fannjiang and Papanicolaou, 1997), which is due to the convective flow. Moreover, the fluid flow contributes to a faster rate of substance transfer than the diffusive term (Wilkinson, 2000), which further increases the gradient of substance concentration and thus causes the augmentation of the diffusive flux. This is due to the Fick's first law which correlates the diffusive flux to the concentration gradient. In summary, convection increases diffusion in mass transport and relates to the gradient of diffusion. In addition, in terms of heat transfer, there is the similar rule that the heat generation due to the fluid flow linearly correlates to the diffusion gradient (Ramachandran, 2014).

In terms of oxygen transmission in arteries, convection dominates diffusion (Douglas and Russell, 1982), whereas diffusion slightly affects convection (Cussler, 2009). Moreover, blood flow is hardly affected by oxygen diffusion (Ramachandran, 2014), and convection is caused by blood flow (Patankar, 1980b). Thus, diffusion hardly affects convection. In terms of heat and mass transfer, diffusion hardly affects the forced convective flow (Deen, 1998), thus, diffusion has little effect on convection as well. Overall, in terms of oxygen transport in the arterial tree, convection plays a significant role in diffusion, while diffusion rarely has an

influence on convection. Thereafter, the convective transport of oxygen is equal to the diffusive flux out of the blood (Tsai et al., 2003), and the diffusion term from blood to vascular walls is the major source of oxygen consumption in the arterial tissue (Popel, 1989).

2.5.4 Effects of oxygen transport in downstream arteries and microvessels

These numerical studies mainly focused on the local distribution of oxygen concentration in arterial wall and hardly paid attention to the overall nature of oxygen distribution in the arteries. Moreover, oxygen concentration at the outlet boundary conditions of numerical investigations was generally simplified as a constant value. Thus, effects of the downstream arteries and microvessels on oxygen transport in arteries of interest were ignored in these computational simulations.

Ignorance of arteries and microvessels causes a decrease in the accuracy of the numerical prediction of oxygen distribution and blood flow in the vessels of interest. In terms of blood flow, the values of pressure or flowrate fraction at the outlet of the vascular model are assumed to be constant without the consideration of effects of the downstream vasculature. Compliance and resistance of the downstream arterial bed and microvascular bed are neglected in these settings of outlet boundary

conditions. Several schemes have been developed for coupling the effects of the downstream vessels in the 3D computational fluid dynamic (CFD) simulations of the arteries. Lumped parameter models and one-dimensional vascular tree model in these numerical methods are conventionally applied at outlets of these computational models (Schaaf and Abbrecht, 1972, Stettler et al., 1981, Stergiopulos et al., 1992, Stergiopulos et al., 1999, Stergiopulos et al., 1995, Olufsen et al., 2000). Studies have proved that blood flow closely correlates with oxygen transport in arteries and microvessels (Qiu and Tarbell, 2000, Liu et al., 2011, Coppola and Caro, 2008, Duling, 1972, Prewitt and Johnson, 1976, Sullivan and Johnson, 1981). Oxygen consumption in tissue is primarily supplied by oxygen transfer from blood to tissue. The way of transferring oxygen from blood to tissue is dependent on blood flow in arteries, arterioles, and capillaries. Eventually, oxygen in tissue is derived from mass transport from microvessels to tissues in microcirculation. Moreover, oxygen content in arteries of interest relates to oxygen transport in the downstream arteries and the corresponding microcirculation (Ivanov et al., 1999, Pittman and Duling, 1975, Swain and Pittman, 1989). In summary, to acquire a more precise prediction of oxygen concentration distribution in the artery of interest, the consideration of effects of oxygen transport in the downstream vessels is required in the 3D simulation of blood flow and oxygen transport. Although the 3D model of the whole vascular tree including the artery of interest, the downstream arteries, and microvessels is supposed to be used for performing the coupling of the artery of interest and the downstream vessels, it

needs considerable computational resources and consumes a large amount of time. Most of research groups barely have enough resources to perform the simulation of the entire vascular tree.

2.5.5 Oxygen transport in muscles

Oxygen transferring from microvessels to muscles is dominated by oxygen diffusion under near-constant oxygen tension in the sarcoplasm. The gradient of the oxygen tension between blood and tissue is the driven force of oxygen transfer to the mitochondrion in muscles. Moreover, oxymyoglobin transport enhances oxygen diffusion in muscles, and the augmentation mediates a high proportion of oxygen transmitted flux from interstitium to muscle fibers. Thereafter, the oxygen consumed in the mitochondrion is carried by myoglobin as well.

The difference of oxygen tension in the muscle fiber is small and is approximated to 2-3 torr (Wittenberg and Wittenberg, 1985, Katz et al., 1984), while the difference between blood and sarcoplasm is large and is about 15-20 torr (Hellums, 1977, Federspiel and Popel, 1986). Oxygen diffusion from capillaries to muscle tissues mainly depends on the gradient of oxygen tension, and the gradient is mainly influenced by the difference. The change in blood flow affects the oxygen tension in vessels, and further alters the difference. Thus, blood flow is a factor to influence the oxygen transport from blood to tissues. Moreover, oxygen in the vascular

system includes dissolved oxygen and hemoglobin-bound oxygen, while dissolved oxygen and myoglobin-bound oxygen are the components of oxygen in muscles. Previous studies have suggested that changes in blood flow affect the concentrations of oxygen, hemoglobin, and myoglobin (Stainsby and Otis, 1964, Shoemaker et al., 1996). In summary, blood flow plays a significant role in the oxygen transport in vessels and muscle tissues. Additionally, the working myocytes during exercise require more oxygen to perform contractile function. The number of open capillaries increases during exercise and enhances the blood flow in the capillary beds. Thus, the change in blood flow is supposed to alter oxygen content in muscles.

Currently, studies about blood flow and oxygen transport in arteries and tissues of the residual limb are few and only focuses on the microcirculation in the residuum skin (Macchi et al., 2004, Mak et al., 2001, Zhang and Roberts, 1993). The relationship between blood flow in residuum arteries and oxygen distribution in vessels and tissues is ignored. Amputation and muscle atrophy change the spatial structure of residuum arteries, and further affect the blood flow and oxygen transport in vessels and muscles after amputation (Troedsson, 2013). As a consequence, investigations about blood flow and oxygen transport in residuum arteries are needed to more precisely evaluate the status of the residuum muscles and to understand the correlation between oxygen transport and developments of health problems in the residuum.

2.6 Objectives

To propose transmission line equations of oxygen transport in arterioles and microvessels for predicting oxygen concentration distribution in the whole circulatory system with less computational cost and time.

To apply transmission line equations of blood flow and oxygen transport in the development of the coupling computational model of blood flow and oxygen transport for more precisely predicting oxygen concentration distribution.

To investigate the oxygen concentration distribution in the arterial system of the residual limb after trans-femoral amputation using the coupled numerical model.

To numerically and experimentally validate the lumped parameter model of oxygen transport that is developed on the basis of the transmission line equations.

CHAPTER 3 METHODS

3.1 Subjects

Our research team selected six unilateral trans-femoral amputees as volunteers according to medical records and regarded three of them as the follow-up subjects. We used a computed tomography (CT) system (Siemens Somatom Definition Flash, Siemens Healthcare Sector, Germany) to obtain the vasculature images of the residuum and the contralateral sound limb. Moreover, the hemodynamic parameters of the main blood vessels were measured by using Doppler ultrasound (iU22, Philips Medical Systems, Bothell, WA, USA), such as the blood flow, pressure, velocity and resistance coefficient. The application for the ethical review of this study has been approved by the Human Subjects Ethics Sub-committee of The Hong Kong Polytechnic University.

Table 3-1 The inclusion criteria of amputees.

Category	Criterion
Age	18-60 years old
Amputation time	Within one year
Residuum status	Medium or long
Postoperative status	Accepted a good postoperative

A 21-year-old female volunteer with the left mid-thigh amputation was selected as the subject. This study acquired the angiographic images and hemodynamic parameters of the subject as the numerical analysis data.

3.2 Computational models of DLFCAs in the residual limb and the sound limb

Methods introduced in this section are applied in the establishment of the computational simulations of DLFCAs in both sides of a trans-femoral amputee (see chapter 4).

3.2.1 Geometric model and meshing

In the first place, the angiographic images of the residuum and the contralateral sound limb were imported into the medical image processing software (MIMICS v10.0 Materialise, Leuven, Belgium) to carry out three-dimensional reconstruction. These images were collected from a 21 years old female volunteer who underwent left mid-thigh amputation. And there were 717 slices with the thickness of 1 mm in the angiographic imaging. The field of view, the image resolution, and the pixel size were 377×377 mm^2, 512×512 pixels, and 0.736 mm, respectively.

It should be noted that muscle atrophy of residuum sartorius and quadriceps femoris, which was related to the disuse atrophy, was the most obvious after amputation

(Schmalz et al., 2001). And the descending branch of lateral femoral circumflex artery is the main vessel which supplies nutrition and oxygen for these muscles (Standring et al., 2005). Consequently, the geometric models of the vessels in both the residuum and the contralateral sound limb were established and entity modelled in a general-purpose pre-processor (Gambit 2.4) (shown in Fig. 3-1).

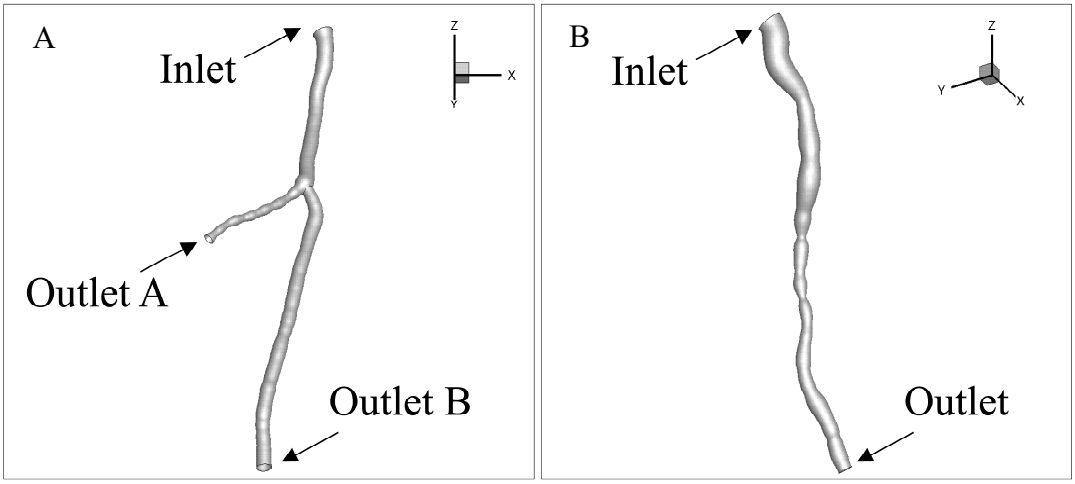

Figure 3-1 Geometric models of the vessels in both the contralateral sound limb (A) and the residual limb (B).

3.2.2 Meshing

Subsequently, the geometric models were employed into Gambit 2.4 for meshing (shown in Fig. 3-2). And there were 126853 mixed elements in the vascular model of the contralateral sound limb (shown in Fig. 3-2A), which consisted of 56663 tetrahedral elements in the interior and 70190 high quality wedge elements within the boundary layer. In addition, there were 75076 mixed cells in the vascular model

of the residual limb (shown in Fig. 3-2B), which included 30361 tetrahedral elements in the interior and 44715 high quality wedge elements within the boundary layer. It was beneficial for enhancing the computational accuracy to mesh more elements within the boundary layer.

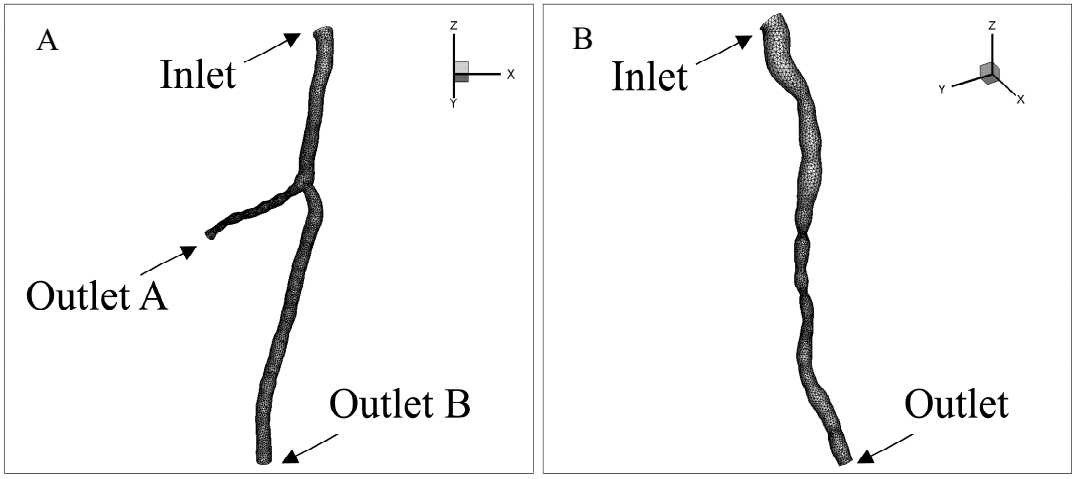

Figure 3-2 Meshed models of the vessels in both the contralateral sound limb (A) and the residual limb (B).

3.2.3 Computational fluid dynamics (CFD) analysis

The meshed models were imported into the commercial CFD software (FLUENT v10.0) for numerical analysis. And this simulation employed a couple numerical analysis of hemodynamics and oxygen transport through using theories of fluid mechanics and mass transfer.

Blood flow

Assumptions

Three assumptions were employed in this numerical analysis of blood flow: (1) blood is a homogeneous, incompressible fluid (Ku, 1997); (2) the walls of vessels are rigid and no-slip (Friedman et al., 1992, Moore et al., 1994); (3) blood flow is steady and uniform.

Governing equations

For the sake of investigating the effects of blood constitutive models on blood flow and oxygen transport, two blood constitutive models were considered: Newtonian and non-Newtonian (Casson).

In the simulation of blood flow, three-dimensional continuity equation and Navier-Stokes equation were employed.

$$\begin{cases} \dfrac{\partial u_j}{\partial x_j} = 0 \\ \rho \dfrac{\partial u_i}{\partial t} + \rho \dfrac{\partial u_j u_i}{\partial x_j} = -\dfrac{\partial P}{\partial x_i} + \mu \dfrac{\partial}{\partial x_j}\left(\dfrac{\partial u_i}{\partial x_j} + \dfrac{\partial u_j}{\partial x_i} \right) \end{cases} \qquad (i, j = 1,2,3) \qquad (3.1)$$

Where u_i was the velocity vector of blood, and P was the pressure. Moreover, ρ and μ were the density and dynamic viscosity of blood, respectively: ρ =1055 kg/m^3 (Wentzel et al., 2001). In the Newtonian model, μ =3.5×10^{-3} kg/m·s. Through utilizing the mathematic expression of Newtonian fluid in terms of Casson equation ($\sqrt{\tau} = k_0 + k_1\sqrt{\dot{\gamma}}$), the apparent viscosity of the Casson model could be derived as $\mu = \frac{1}{2\sqrt{D_{II}}}\left(k_0 + k_1\sqrt{2\sqrt{D_{II}}}\right)^2$. Where τ and $\dot{\gamma}$ were shear stress and shear strain, respectively; k_0^2 and k_1^2 were Casson yield stress and Casson viscosity, respectively; D_{II} was the second invariant of strain rate tensor. The modified viscosity was applicable for the Casson model. And the apparent viscosity of the Casson model was employed into a commercial software (Fluent, version 6.3, ANSYS, Inc.) through compiling a user-defined C-like function (UDF).

Boundary conditions

A zero-pressure boundary condition was applied at the outlet: $P|_{outlet} = 0$. Since it was concluded that exercise would contribute to an increase in the velocity of blood flow (Shoemaker et al., 1996), it was necessary to investigate the impact of exercise on the oxygen transport in the descending branch of lateral femoral circumflex artery. In order to find out the effects of different velocities on the oxygen transport

of the vessels, the profile with three velocities was applied at the inlet of the vascular model:

$$\begin{cases} V_z\big|_{inlet} = 0.091\,m/s \quad (velocityA), \quad 0.245\,m/s \quad (velocityB), \quad 0.321\,m/s \quad (velocityC) \\ V_r\big|_{inlet} = 0 \end{cases}$$

(Shoemaker et al., 1996).

Oxygen transport

Oxygen transport equation

Oxygen transport of the blood flow could be composed of convection and diffusion terms, which was expressed by the equation as follow:

$$\left(1+\frac{[Hb]}{\alpha}\frac{dS}{dPO_2}\right)\vec{u}\cdot\nabla PO_2 = \nabla\cdot\left[D_b\left(1+\frac{[Hb]}{\alpha}\frac{D_c}{D_b}\frac{dS}{dPO_2}\right)\nabla PO_2\right] \tag{3.2}$$

Where PO_2 was the oxygen tension in blood flow. The ability of hemoglobin to carry oxygen in blood was expressed by $[Hb]$. And α was the oxygen solubility. D_b and D_c were the diffusion coefficients of free oxygen and oxyhemoglobin. The ratio of oxyhemoglobin to total hemoglobin, S referred to as the saturation function, was given by the Hill equation: $S = \frac{PO_2{}^n}{PO_2{}^n + PO_{50}{}^n}$ (Fournier, 2011). For the sake of investigating the contribution of hemoglobin to oxygen transport,

two cases were considered: (1) with hemoglobin, i.e., oxygen in blood included free oxygen and oxygen carried by hemoglobin; (2) without hemoglobin ($[Hb]=0$).

Table 3-2 The parameters in oxygen transport.

Parameter	Value	Source
$[Hb]$	0.2 *mL O_2/mL blood*	(Back et al., 1977)
α	2.5×10^{-5} *mL O_2/mL blood/mmHg*	(Schneiderman and Goldstick, 1978)
D_b	1.2×10^{-9} *m^2/s*	(Stein et al., 1971)
D_c	1.5×10^{-11} *m^2/s*	(Caro et al., 1978)
n	2.7	(Moore and Ethier, 1997)
PO_{50}	26.6 *mmHg*	(Moore and Ethier, 1997)

The user-defined scalar (UDS) in FLUENT was used for solving the oxygen transport equation with the user-defined C-like function (UDF).

$$\frac{\partial \rho \varphi_k}{\partial t}+\frac{\partial}{\partial x_i}\left(\rho u_i \varphi_k-\Gamma_k \frac{\partial \varphi_k}{\partial x_i}\right)=S_{\varphi_k} \qquad k=1,\ldots,N \tag{3.3}$$

Where ϕ_k was an arbitrary scalar. Γ_k and S_{ϕ_k} were the diffusion coefficient and source term, respectively, which were supplied for each of the N scalar equations.

Boundary conditions

At the inlet of the vessel, the boundary condition of oxygen tension was set as $PO_2|_{inlet} = 85mmHg$; the flux of oxygen tension at the outlet was specified as $\frac{\partial PO_2}{\partial n} = 0$; and oxygen tension of the vascular wall was set as $PO_2|_{wall} = 60mmHg$ (Moore and Ethier, 1997, Buerk and Goldstick, 1982, Liu et al., 2009).

Computational settings in FLUENT

This software applied the finite volume method to solve the equations of blood flow and oxygen transport, and the solver was based on pressure. More specifically, the computational model utilized the three-dimensional single precision and segregated solver. In the solution controls, the SIMPLEC method was set for pressure-velocity coupling; the solution of pressure applied standard discretization; and the first-order upwind was employed in the discretization of momentum and oxygen tension. The residual value of 0.0001 was selected as the absolute convergence criterion of all the variables.

3.3 Computational simulation and experimental study of oxygen transport and blood flow in the residual limb

A more precise prediction of oxygen distribution in the 3D vascular model needs the consideration of effects of the downstream vessels on oxygen transport. The lumped parameter model of oxygen transport in the downstream vascular bed is employed as the boundary condition of oxygen transport at the outlet of the 3D vascular model in order to realize the effects of the downstream vessels. The transmission line equations of oxygen transport are treated as the theoretical basis of the development of the lumped parameter model and expressed as follows:

$$\begin{cases} -\dfrac{\partial J_{diff}}{\partial x} = R_0 J_{con} + L_0 \dfrac{\partial J_{con}}{\partial t} \\ -\dfrac{\partial J_{con}}{\partial x} = -J_{diff}\Big|_{\text{From blood to wall}} = -2\pi a\left(\Gamma \dfrac{\partial C}{\partial r}\right)_{r=a} \end{cases}, \tag{3.4}$$

where J_{con} and J_{diff} are the convective flux and the diffusive flux, respectively; a is the radius of the vessel; r-direction and x-direction represent the radial direction and the direction of blood flow; L_0 and R_0 represent the properties of oxygen convection per unit distance and are equal to $-\dfrac{1}{v_x}$ and $\dfrac{\partial}{\partial t}\left(-\dfrac{1}{v_x}\right)$, respectively. The electrical analogue including resistance (R) and current sink is assumed to be the representation of the lumped parameter model of oxygen transport (Fig. 3-3). In the coupling model of the 3D vascular model and the lumped parameter model of oxygen transport, the convective flux at outlet of the 3D model is regarded as the inlet boundary condition of the lumped parameter model, while the diffusive flux at the beginning of the lumped parameter model is applied in the setting of the outlet boundary condition of the 3D model. Moreover, the diffusive

flux at end of the lumped parameter model (J'_{diff}) is set through using the oxygen gradient between the terminal artery and the first-order arteriole.

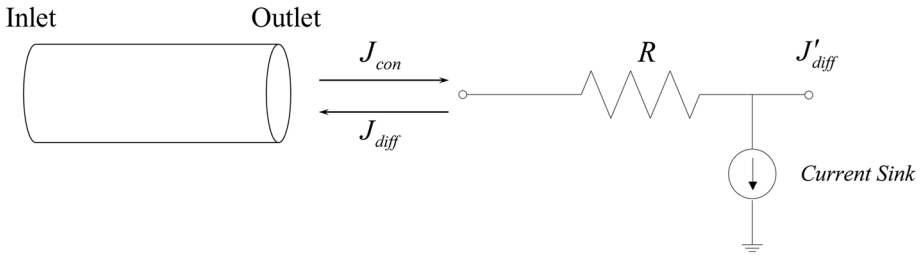

Figure 3-3 Schematic diagram of the coupling model of the 3D vascular model and the lumped parameter model of oxygen transport. The convective flux and diffusive flux (J_{con} and J_{diff}) of oxygen transport are analogous to current and voltage in the circuit. R is the resistance of oxygen transport in the entire vascular tree and represents the remaining portion of oxygen content. The current sink represents the total flux of oxygen diffusion from blood to arterial wall. J'_{diff} is the diffusive flux of oxygen transport at the end of the downstream arteries.

In the CFD simulations of the 3D arteries, the governing equations were the continuity equation and the Navier-Stokes equation. Blood was assumed to be homogeneous, incompressible, and Newtonian fluid (Ku, 1997, Friedman et al., 1992, Moore et al., 1994). Since the difference in hemodynamic parameters of femoral arteries between the simulation ignoring the elasticity of the vascular wall and that with the consideration of the elastic vascular wall was proved to be relatively small (Kim et al., 2008), the elasticity of the arterial wall was neglected in these simulations. The convection-diffusion equation was treated as the

governing equation of oxygen transport (Liu et al., 2010, Yan et al., 2017). Parameters in the governing equations of blood flow and oxygen transport were same to those in our previous study about oxygen transport of residuum DLFCA.

We applied the commercial software (Fluent, version 6.3, ANSYS, Inc.) to perform the CFD simulation coupling with oxygen transport. The numerical investigation of the convection-diffusion equation was conducted through applying the user-defined scalar (UDS) and the user-defined C-like function (UDF) in Fluent. Moreover, a UDF was compiled to apply the lumped parameter model of oxygen transport in the setting of the outlet boundary condition of the 3D computational model. The residual value in Fluent was generally treated as the convergence criterion and was set as 0.0001. The settings in Fluent were derived from our previous study as well.

This study was divided into three parts; first, three regular vascular models were employed to numerically verify the developed boundary condition with the lumped parameter model of oxygen transport; second, the computational simulation of the residuum arteries after trans-femoral amputation was carried out, and the developed boundary condition of oxygen transport was applied in this simulation; third, the *in vitro* experiment with the 3D printing vascular model of the residuum arteries was conducted to validate the computational simulation. And methods elucidated in this section were used in numerical verifications of the developed boundary condition

of oxygen transport, in the computational simulation of oxygen transport and blood flow in arteries of the trans-femoral residuum, and in the experimental validation of the computational model of residuum vasculature (see chapter 7).

3.3.1 Numerical verification

Three regular vascular geometries were used in this numerical verification and included a straight vessel, a 90° curved vessel, and a bifurcated vessel (Fig. 3-4). The values of the geometric parameters were listed in Tab. 3-3. The effect of the outlet boundary conditions of oxygen transport and blood flow would be almost eliminated with the elongation of the vascular model (Ma et al., 1994, Ma et al., 1997). Thus, for the sake of verifying the boundary condition of the lumped parameter model of oxygen transport, the straight vessel and these two branches of the bifurcated vessel were straightly extended, while the curvature angle of the curved vessel was increased by 100° to minimize the effect of the boundary condition (Austin and Seader, 1973). The flowrate profiles were set as the inlet boundary conditions of blood flow in these vascular models (Fig. 3-5). The pressure at the outlets of the elongated straight vessel and the 190° curved vessel was set as zero, while the pressure at the outlets of the original straight vessel and the 90° curved vessel was calculated based on the elongated model. The constant resistance models were applied at the outlets of the elongated bifurcation vascular model, and the values of the resistances were set as 4.712×10^{9} Pa·s/m^{3} (External carotid artery)

and 2.8897×10^9 Pa·s/m^3 (Internal carotid artery) (Boileau et al., 2015). The pressure at the outlet of the non-elongated bifurcation model was derived from the elongated bifurcation model as well. Oxygen tensions at the inlets of the straight models, the curved models, and the bifurcated models were set as 85 mmHg, 85 mmHg, and 85.3 mmHg, while those at the arterial walls were determined as 60 mmHg, 48 mmHg, and 55.5 mmHg (Richardson, 2008, Santilli et al., 1995, Moore and Ethier, 1997). Zero gradient of oxygen tension was employed in the settings of the outlet boundary conditions of oxygen transport in these elongated models, whereas the lumped parameter models of oxygen transport in the extension portion of these elongated models were regarded as the boundary conditions of the outlets in the non-elongated models.

Table 3-3 Values of the geometric parameters in three vascular models.

Model	Parameter	Value	Parameter	Value
Straight vessel	D_s	18 mm		
	L_s	200 mm		
Curved vessel	d_c	4.4 mm		
	R_c	22 mm		
	α_c	90°		
Bifurcated vessel	D_{cc1}	6 mm	D_{ic5}	5.16 mm
	D_{cc2}	6 mm	D_{ic6}	4.26 mm
	D_{ic1}	6.26 mm	D_{ec1}	4.16 mm
	D_{ic2}	6.66 mm	D_{ec2}	3.41 mm
	D_{ic3}	6.66 mm	D_{ec3}	3.41 mm
	D_{ic4}	6.19 mm	β	50°

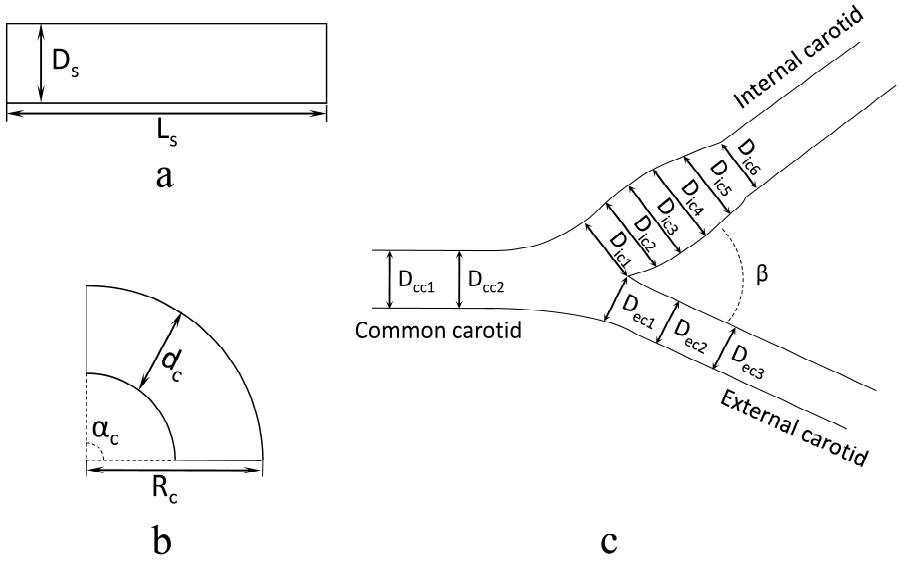

Figure 3-4 Schematic diagrams of the regular vascular models of (**a**) the straight artery, (**b**) the 90-degree artery, and (**c**) the bifurcated artery. D_s and L_s are the diameter and the length of the straight artery; d_c, R_c, and α_c are the diameter of the curved artery, the radius of the curvature and the angle of the curvature, respectively; $D_{cc\gamma}$ (γ=1, 2), $D_{ic\delta}$ (δ=1, 2, 3, 4, 5, 6), $D_{ec\varepsilon}$ (ε=1, 2, 3), and β are the diameters of the common carotid artery, the diameters of the internal carotid artery, the diameters of the external carotid artery and the bifurcation angle, respectively.

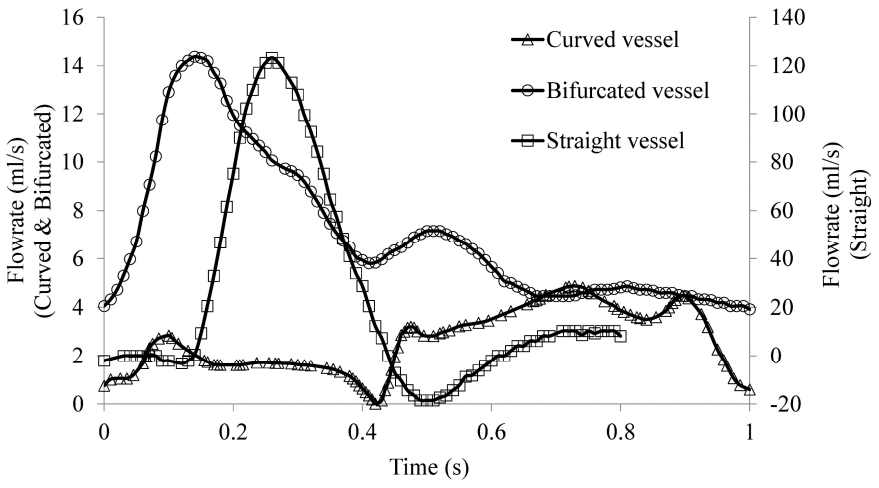

Figure 3-5 Flowrate profiles at inlets of three arteries.

3.3.2 Computational simulation of residuum arteries

The geometric model of the residuum arteries after trans-femoral amputation was built through the reconstruction with the angiographic images of an amputee (Fig. 3-6a), which was based on our previous study (Yan et al., 2017). The vascular model included common femoral artery (CFA), superficial femoral artery (SFA), deep femoral artery (DFA), lateral femoral circumflex artery (LFCA), and medial femoral circumflex artery (MFCA). The blood velocity profile in the femoral artery of the residual limb was measured by Doppler ultrasound (iU22, Philips Medical Systems, Bothell, WA, USA) and was applied at inlet of the CFD model (Fig. 3-6b). The three-element Windkessel model, which was established on the basis of the fluid transmission line equations, was used for developing the boundary conditions of the outlets in residuum arteries (Fig. 3-6c). The resistances and the capacitance in the Windkessel model were derived from the literatures (Seeley, 2011, Reymond et al., 2009) and blood velocity data measured by ultrasound (Fig. 3-6d). In terms of oxygen transport, the oxygen tensions at inlet and wall were specified as 75.9 mmHg and 60 mmHg (Buerk and Goldstick, 1982). And the aforementioned boundary conditions of oxygen transport in this study, which were based on the coupling model of the 3D CFD analysis and the lumped parameter models of oxygen transport in the downstream vessels, were employed at the outlets of the vascular model.

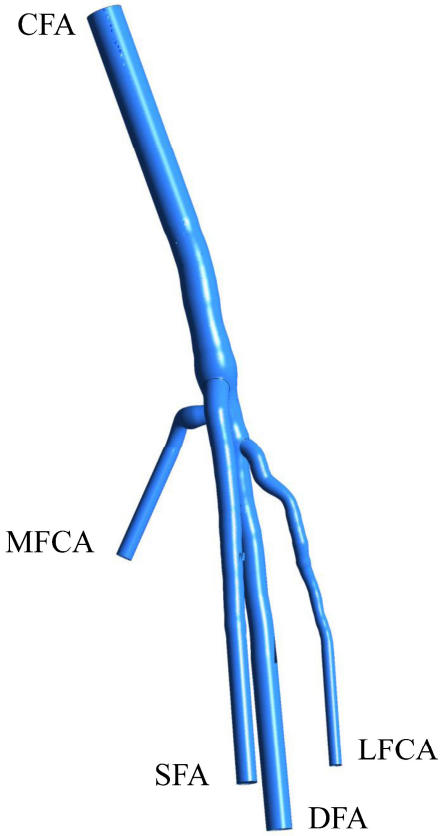

a

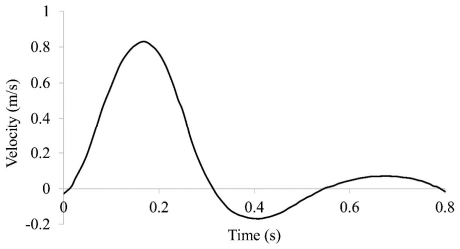

b

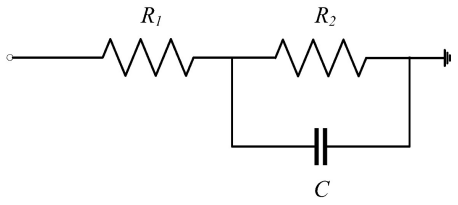

c

Outlet	R_1 (Pa·s/m^3)	R_2 (Pa·s/m^3)	C (m^3/Pa)
SFA	7.997223×10^{8}	1.914788×10^{11}	9.309412×10^{-12}
DFA	6.263715×10^{8}	1.017174×10^{10}	1.657698×10^{-10}
LFCA	2.549714×10^{9}	1.892255×10^{10}	8.336336×10^{-11}
MFCA	1.666656×10^{9}	2.735587×10^{10}	6.167622×10^{-11}

d

Figure 3-6 The geometric model of the residuum arteries (**a**), the blood velocity profile at inlet (**b**), the electrical analogue of the Windkessel model (**c**) and the values of parameters in Windkessel models of different outlets (**d**).

3.3.3 In vitro experiment

The *in vitro* experiment was established using a 3D printing vascular model (Materialise, Leuven, Belgium) of the residuum vasculature in order to validate the computational simulation of oxygen transport and blood flow in these residuum

arteries (Fig. 3-7). The 3D printing vascular model was fabricated according to the digital 3D model of the residuum vasculature which has been developed based on the angiographic images. The material of the printing model is TuskXC2700T, and the transparent stereolithography is used on the internal and external surfaces of the vascular model. The printing layer thickness, the standard accuracy, and the wall thickness are 0.1 mm, ±0.2%, and 2 mm, respectively. A peristaltic pump (Masterflex L/S, Cole-Parmer, USA) was used for producing the corresponding pulsatile inflow with the computational simulation. Electronic proportional valve (EPV-375B, Hass Manufacturing Company, USA) and airtight container were applied to simulate the resistance and the capacitance of the Windkessel model at each outlet of the vascular model. The setting of the proportional valve and the development of the airtight container were based on the values of the resistance and the capacitance. In addition, flowrate in the experiment was measured by the electromagnetic flowmeter (FMG71B-A, Omega Engineering, Inc., USA). Thereafter, the measurements of oxygen concentration in the solvent were performed at inlet and each outlet of the vascular model through using the oxygen analyzer (JPBJ-608, INESA Scientific Instrument Co.， Ltd., China). To implement oxygen consuming of the downstream arteries, two valves were installed at the upside and downside of the downstream tube, respectively. More specifically, oxygenated water in the tube was removed through the downside valve to simulate the oxygen loss, meanwhile the same amount of oxygen-free water was produced through mechanical ventilation with nitrogen in oxygenated water and introduced

in the upside valve to remain the total amount of fluid. The amount of the oxygen loss was determined through the measurement of oxygen concentration in the removed oxygenated water. Moreover, the temperature remained unchanged during the experiment. In this experiment, the solvent was water, while the settings and the parameters of the corresponding computational model were adjusted according to the development of the *in vitro* experiment. The experimental results were compared with those in the corresponding computational simulation to validate the coupling model of the 3D CFD analysis and the lumped parameter model of oxygen transport.

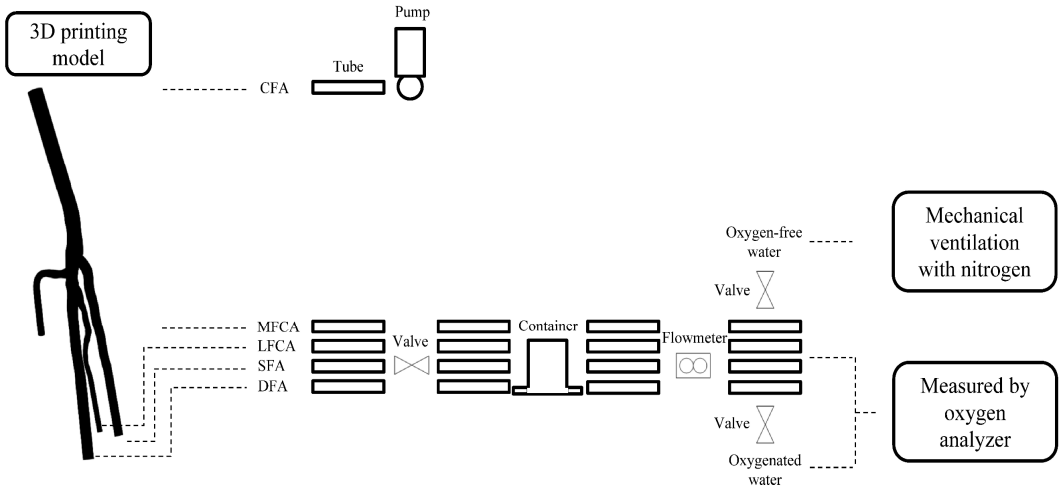

Figure 3-7 Schematic diagram of the development of the experimental platform.

CHAPTER 4 COMPUTATIONAL SIMULATIONS OF BLOOD FLOW AND OXYGEN TRANSPORT IN DLFCAS OF THE RESIDUAL LIMB AND THE SOUND LIMB

Computational simulations of blood flow and oxygen transport in DLFCAs of the residual limb and the sound limb were carried out to determine the differences of hemodynamic responses between the residual limb and the sound limb. Moreover, in order to figure out the effects of exercise on blood flow and oxygen transport in the residuum artery, three velocities during rest, exercise, and steady-state exercise were employed at inlet of the vascular model.

Angiographic images of residuum arteries in a trans-femoral amputee were applied to reconstruct the geometric model. Section 3.2 in chapter 3 introduces details in the computational simulations of DLFCAs. This chapter introduces the blood flow and oxygen distribution in the residuum DLFCA under different inlet velocities, moreover, the differences of blood velocity and oxygen concentration between the sound limb and residual limb are showed.

4.1 Velocity of blood flow

4.1.1 Different velocities at the inlet (residuum)

The profile with three velocities was applied at the inlet of the residuum vascular model: 0.091 m/s (velocityA); 0.245 m/s (velocityB); and 0.321 m/s (velocityC), which was beneficial for finding out the effects of different velocities on the velocity of blood flow in the vascular model.

Newtonian

For the sake of investigating different velocity distribution in the vascular model based on different velocities at the inlet boundary, three velocities were selected for the vascular model with Newtonian fluid. For Newtonian fluid, it was shown that different inlet boundaries with various velocities could contribute to different velocities of blood flow in the vascular model (shown in Fig. 4-1). Specifically, the increase in the velocity of the inlet caused the increment of the blood velocity in the vessel. However, the streamline distribution of three inlet boundaries was the same. In summary, the change in the velocity at the inlet boundary could cause different velocities of blood flow in the vessel, whereas could not transform the streamline distribution of blood flow.

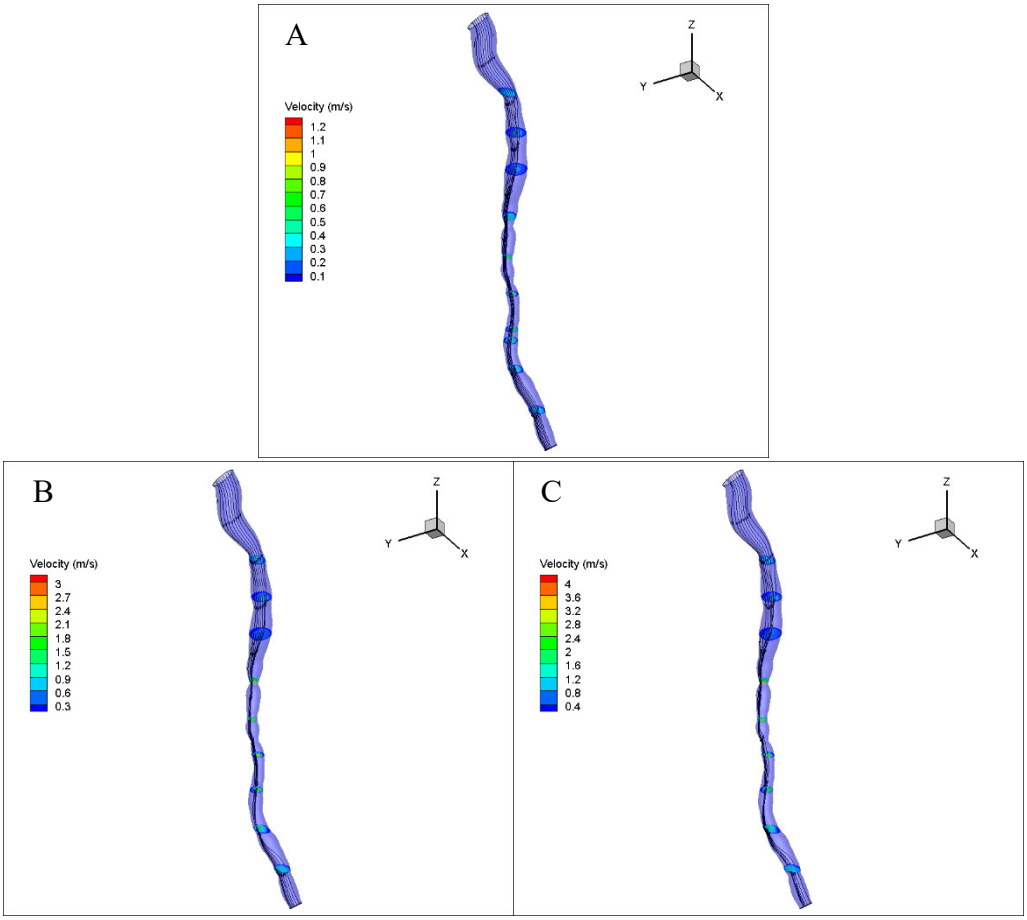

Figure 4-1 The velocity of blood flow with Newtonian fluid: velocityA (A), velocityB (B), and velocityC (C).

Non-Newtonian (Casson)

In addition, Casson fluid was employed into this vascular model, in order to find out the difference of velocity distribution between Newtonian and non-Newtonian. As shown in Fig. 4-2, it was noted that the velocity of blood flow increased followed by the increment in the velocity at the inlet boundary for non-Newtonian fluid. For most regions of the vascular model, there was no difference of streamline distribution among three inlet boundary conditions. However, the streamline distribution in the region close to the outlet was disturbed in terms of velocityB and

velocityC (shown in Fig. 4-2B and Fig. 4-2C). Specifically, there existed an elongated recirculation close to the outlet of the vascular model. In summary, the increment of the velocity at the inlet boundary could contribute to the increase in the velocity of blood flow in terms of non-Newtonian fluid, and result in the formation of recirculation in the region near the outlet of the vascular model.

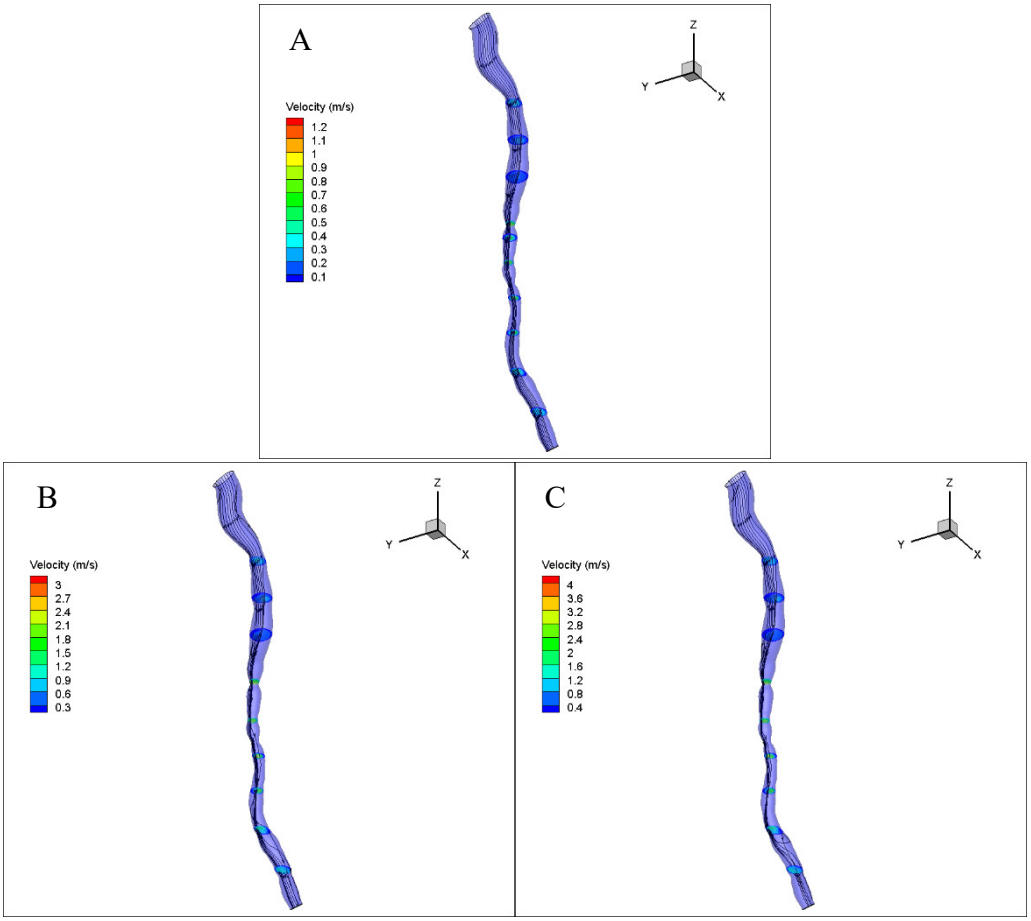

Figure 4-2 The velocity of blood flow with non-Newtonian fluid: velocityA (A), velocityB (B), and velocityC (C).

For Newtonian and non-Newtonian fluid, the increment of the velocity at the inlet boundary could cause the increase in the velocity of blood flow. The streamline

distribution of three inlet boundaries was the same for Newtonian. In terms of non-Newtonian, there was no difference of streamline distribution in most regions of the vascular model among three inlet boundary conditions, while an elongated recirculation was formed near the outlet for velocityB and velocityC. And the increase in the velocity at the inlet boundary would cause the formation of recirculation in the region close to the outlet for non-Newtonian fluid. Through comparing the results of Newtonian with those of non-Newtonian, it was found that the velocity of blood flow did not change in this vascular model, and the streamline distribution of non-Newtonian fluid transformed in the region near the outlet with the increment of the velocity at the inlet boundary.

4.1.2 Vascular models of both residuum and contralateral sound limb

The DLFCA in contralateral sound limb was regarded as the reference. The blood flow of this branch in the residual limb was compared with that of the contralateral sound limb, which was beneficial to find out the difference of blood flow between the amputated limb and the contralateral sound limb.

Newtonian

Firstly, the inlet boundary with velocityA and Newtonian fluid were applied in two vascular models of residuum and contralateral sound limb. As shown in Fig. 4-3, it

should be noted that the spatial vasculature of the DLFCA in the residual limb changed significantly due to the amputation and muscle atrophy, through the comparison with the DLFCA in contralateral sound limb. The velocity of blood flow in this vascular model of residuum was different from that of the contralateral sound side. Meanwhile, there lied the difference of the streamline distribution between the two vascular models (shown in Fig. 4-3), which was result from the change in the spatial vasculature of the residuum DLFCA.

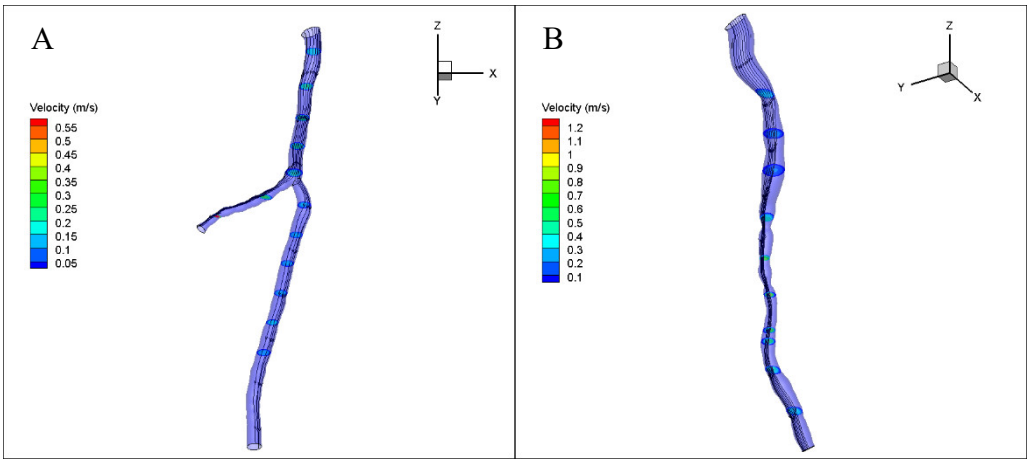

Figure 4-3 The velocity of blood flow with Newtonian fluid: contralateral sound limb (A) and residuum (B).

Non-Newtonian (Casson)

Secondly, the inlet boundary with velocityA and non-Newtonian model were employed in two DLFCA models of residuum and contralateral sound limb, which would illustrate the effects of non-Newtonian model on the velocity and streamline distribution. Followed by the results of two DLFCA models with Newtonian fluid, there still existed the difference of the blood velocity and the streamline distribution

between two vascular models of residuum and contralateral sound limb (shown in Fig. 4-4).

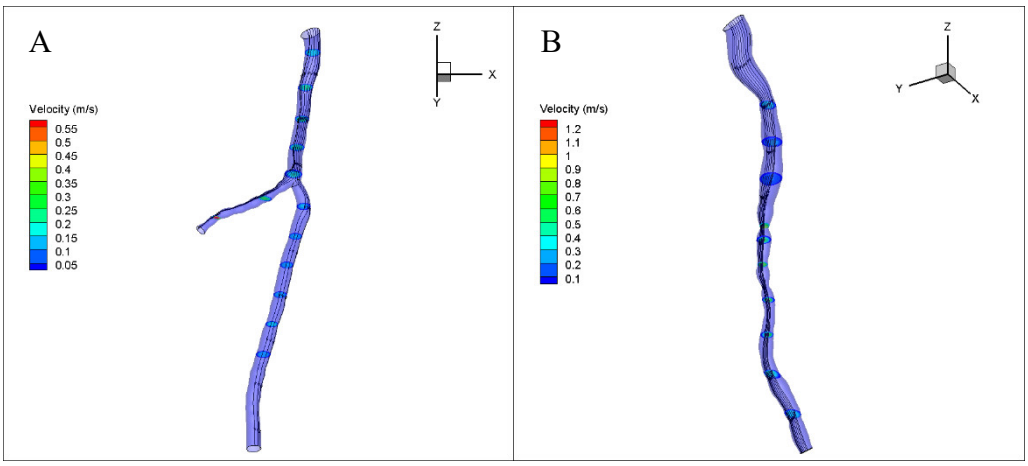

Figure 4-4 The velocity of blood flow with non-Newtonian fluid: contralateral sound limb (A) and residuum (B).

Through comparing the results of Newtonian fluid with those of non-Newtonian fluid in two DLFCA models of residuum and contralateral sound limb, it was convinced that there was no difference of the blood velocity and streamline distribution between Newtonian and non-Newtonian, based on Fig. 4-3 and Fig. 4-4. On top of that, the change in the spatial vasculature of the DLFCA in the residual limb was the main contributor to the difference of the velocity and streamline distribution between two DLFCA models of residuum and contralateral sound limb.

4.2 Wall shear stress (WSS)

The wall shear stress (WSS) of the vessel plays a significant role in the evaluation of vascular diseases. WSS value, which is smaller than 0.4 Pa, is unfavorable for the vessel (Palumbo et al., 2002). And it may contribute to the development of vascular diseases. The region of the vascular wall with WSS value smaller than 0.4 Pa is referred to as low WSS region.

4.2.1 Different velocities at the inlet (residuum)

The boundary conditions with three velocities were employed at the inlet of the residuum DLFCA model: 0.091 m/s (velocityA); 0.245 m/s (velocityB); and 0.321 m/s (velocityC), which was helpful for understanding the impact of different velocities at the inlet boundary on WSS distribution.

Newtonian

As shown in Fig. 4-5, there existed low WSS regions only in residuum DLFCA model with velocityA at the inlet boundary for Newtonian fluid. More specifically, the low WSS regions were observed in the curved regions of the vascular model close to the inlet and outlet (shown in Fig. 4-5A). There was no low WSS region in the residuum DLFCA model with velocityB and velocityC based on Fig. 4-5B and Fig. 4-5C. And the value of WSS increased followed by the increment of the velocity at the inlet boundary. That is, the increase in the velocity at the inlet boundary of the DLFCA would contribute to the increment of WSS and cause the

decrease in low WSS region. Consequently, the increase in the velocity at the inlet boundary may reduce the risk of vascular diseases.

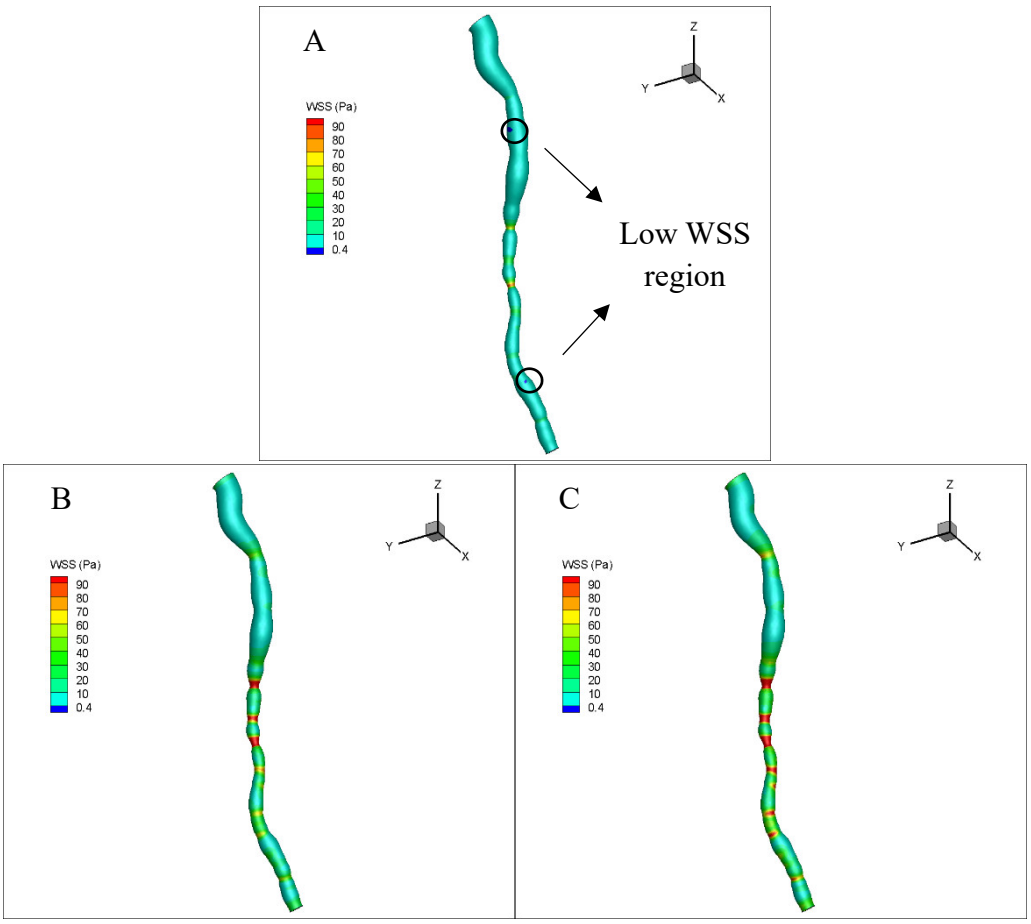

Figure 4-5 WSS with Newtonian fluid: velocityA (A), velocityB (B), and velocityC (C).

Non-Newtonian (Casson)

For non-Newtonian fluid, the low WSS region was only observed in the DLFCA model with velocityA at the inlet boundary (shown in Fig. 4-6A), as well. And the low WSS region was observed in the curved region of the vessel near the outlet. In addition, there was no low WSS region in the vascular model with velocityB and

velocityC at the inlet boundary, as shown in Fig. 4-6B and Fig. 4-6C. The value of WSS had an increment followed by the increase in the velocity at the inlet boundary for non-Newtonian, which was consistent with the results of Newtonian.

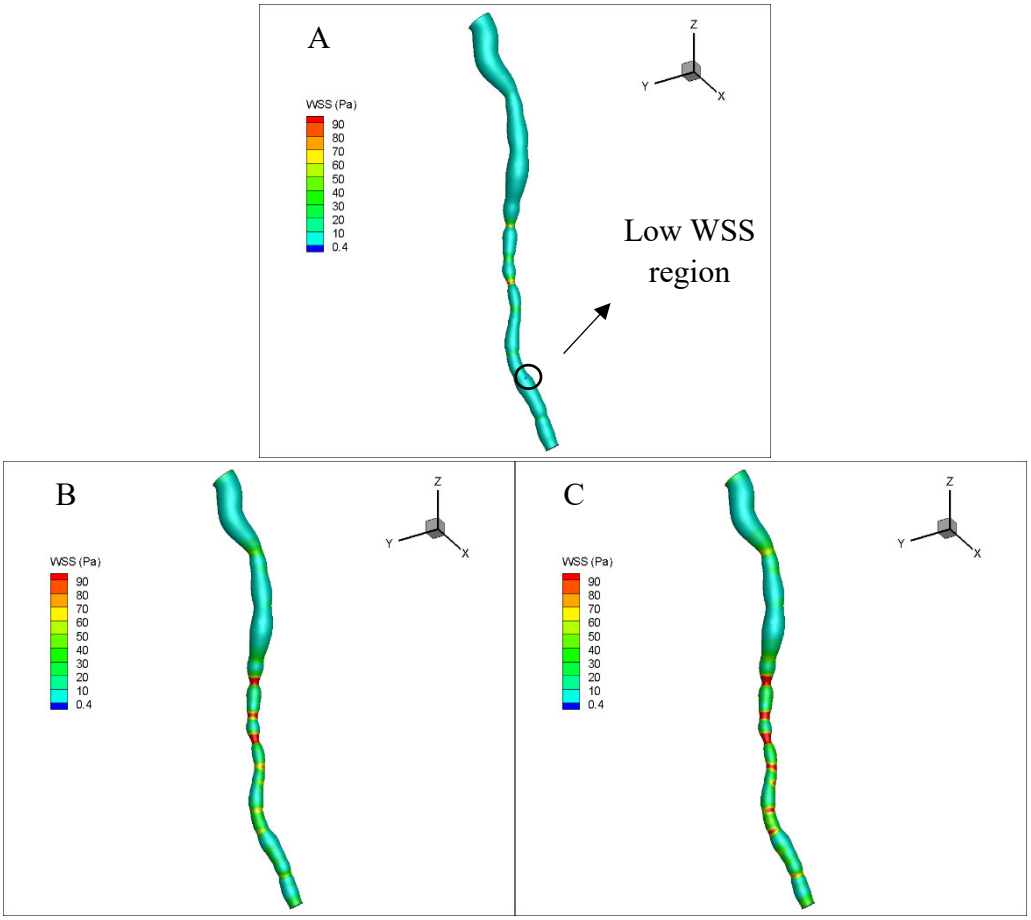

Figure 4-6 WSS with non-Newtonian fluid: velocityA (A), velocityB (B), and velocityC (C).

For Newtonian and non-Newtonian, the low WSS region was only observed in the arterial wall of residuum DLFCA with velocityA at the inlet boundary. And the increase in the velocity at the inlet boundary of the vascular model would result in the increment of WSS, and cause the decrease in low WSS region. Thus, the

increase in the velocity at the inlet boundary may reduce the risk of vascular diseases. Through comparing the results of Newtonian and non-Newtonian, it was illustrated that the area of low WSS region in the vascular model with non-Newtonian fluid was smaller than that of the vascular model with Newtonian fluid, which was consistent with the numerical simulation results of the previous study (Fan et al., 2009).

4.2.2 DLFCA model of contralateral sound limb

Although the WSS of DLFCA model in the residual limb plays a role in the evaluation of amputees' health status, it is necessary to investigate the WSS of the vascular model in contralateral sound limb. Two blood constitutive models (Newtonian and non-Newtonian) with velocityA at the inlet boundary were applied in the DLFCA model of the contralateral sound limb, for the sake of investigating the WSS distribution of the vascular model in the contralateral sound limb after amputation.

Newtonian and non-Newtonian (Casson)

As shown in Fig. 4-7, the low WSS regions were observed near the bifurcation and the outlet of the DLFCA model in terms of both Newtonian and non-Newtonian. Specifically, there existed the largest low WSS region just before the bifurcation of the vascular model with Newtonian and non-Newtonian, which was consistent with

the computational results of the previous research (Fan et al., 2009). The area of low WSS region in the DLFCA model with Newtonian fluid was larger than that of the vascular model with non-Newtonian fluid based on the comparison of Newtonian with non-Newtonian (shown in Fig. 4-7), which was consistent with the results of the DLFCA model in the residual limb.

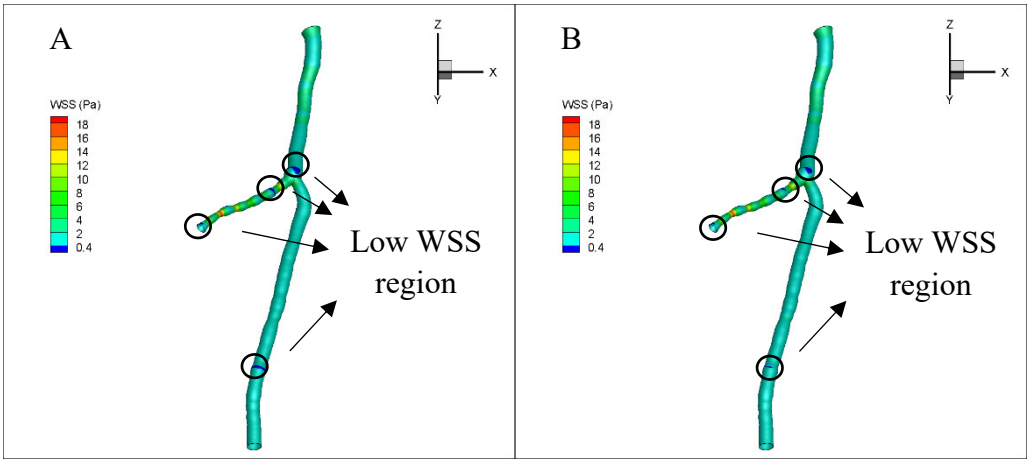

Figure 4-7 WSS distribution of the DLFCA in contralateral sound limb: Newtonian (A) and non-Newtonian (B).

4.3 Sherwood number

It should be noted that hypoxia (low oxygen tension) would occur in the region of the vascular wall where Sherwood number was smaller than the Damköhler number (Tarbell, 2003, Okamoto et al., 1983, Qiu and Tarbell, 2000). Sherwood number, which could be given by the expression ($Sh = k\frac{a}{D}$), is known as the dimensionless coefficient for mass transfer process. In the equation, k denotes the coefficient of mass transfer; a represents the mean diameter of the vessel; and D is defined as

the diffusion coefficient of oxygen. The Damköhler number is regarded as the dimensionless wall consumption rate coefficient which could be expressed as $Da_w = \frac{\dot{Q}Ta}{KDP_b}$ (Fournier, 2011). Where $\dot{Q}$ is known as oxygen consumption rate of arterial tissue; a represents the mean diameter of the vessel; T is defined as the thickness of the arterial wall; K is referred to as Henry's law constant; D denotes the diffusion coefficient of oxygen; and the bulk oxygen partial pressure is expressed by P_b. The estimated value of the Damköhler number was 39 for simplification (Tarbell, 2003). The post-processing with the user-defined C-like function (UDF) in FLUENT was employed for calculating the Sherwood number.

4.3.1 DLFCA in residuum

For investigating the effects of different velocities on the oxygen transport of the residuum DLFCA, the boundary conditions with three velocities were employed at the inlet of the vascular model: 0.091 m/s (velocityA); 0.245 m/s (velocityB); and 0.321 m/s (velocityC). In the meantime, two settings were applied in the user-defined scalar (UDS) in FLUENT with the UDF: (1) with hemoglobin, i.e., oxygen in blood included free oxygen and oxygen carried by hemoglobin; (2) without hemoglobin ($[Hb] = 0$), which was helpful for investigating the contribution of hemoglobin to oxygen transport in residuum DLFCA with Newtonian and non-Newtonian.

Newtonian

Although the blood is regarded as a complex non-Newtonian fluid (Batra and Jena, 1991, Johnston et al., 2006, Chen and Lu, 2006), the investigation of the oxygen transport in the Newtonian fluid is still required (Tarbell, 2003, Liu et al., 2010, Qiu and Tarbell, 2000, Coppola and Caro, 2008, Tada and Tarbell, 2006).

As shown in Fig. 4-8, in terms of three velocities at the inlet boundary, hypoxia zones were observed near the inlet and in the middle of the residuum DLFCA model with hemoglobin in oxygen transport. Followed by the increase in the velocity at the inlet boundary, the Sherwood number within the wall of the vascular model increased in terms of oxygen transport with hemoglobin. Thus, the number and area of hypoxia zones in the residuum DLFCA reduced with the increment of the velocity at the inlet boundary. Consequently, the increase in the velocity at the inlet boundary of the DLFCA was main contributor to the decrease in the number and area of hypoxia zones within the vascular wall, which was beneficial for oxygen transfer with hemoglobin in the vessel.

The Sherwood number of the residuum DLFCA model without hemoglobin increased due to the increment of the velocity at the inlet boundary (shown in Fig. 4-9), which was consistent with the results with hemoglobin. For the residuum DLFCA model without hemoglobin, the increase in the velocity at the inlet boundary would still cause the increment of the Sherwood number; thereby

contribute to the reduction of the number and area of hypoxia zones within the vascular wall.

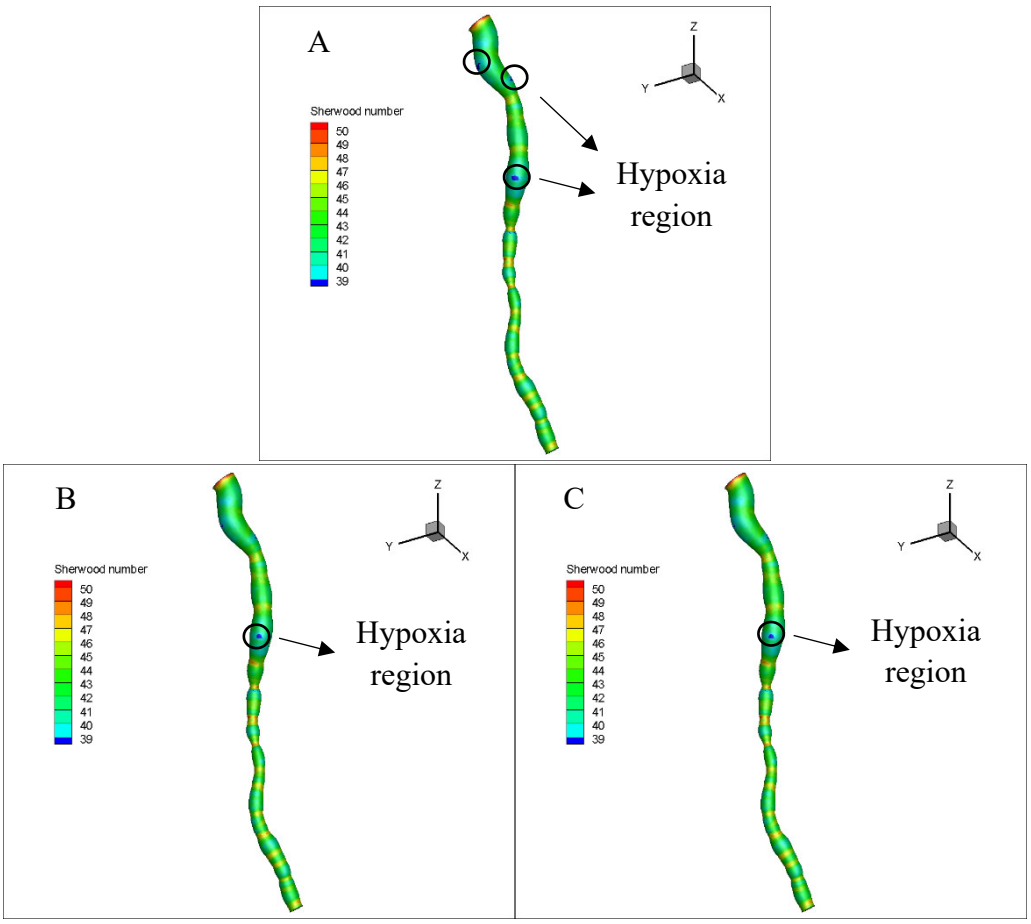

Figure 4-8 Sherwood number with hemoglobin in Newtonian fluid: velocityA (A), velocityB (B), and velocityC (C).

Compared with the Sherwood number of the residuum DLFCA model with hemoglobin, it was indicated that the Sherwood number without hemoglobin decreased remarkably based on Fig. 4-8 and Fig. 4-9. In other words, in terms of the DLFCA in the residual limb, the value of Sherwood number without hemoglobin was lower than that with hemoglobin, which was consistent with the

computational results of the previous study (Moore and Ethier, 1997, Liu et al., 2010). Thus, it was found that the number and area of hypoxia zones in residuum DLFCA model without hemoglobin were larger through the comparison with the results of oxygen transport with hemoglobin.

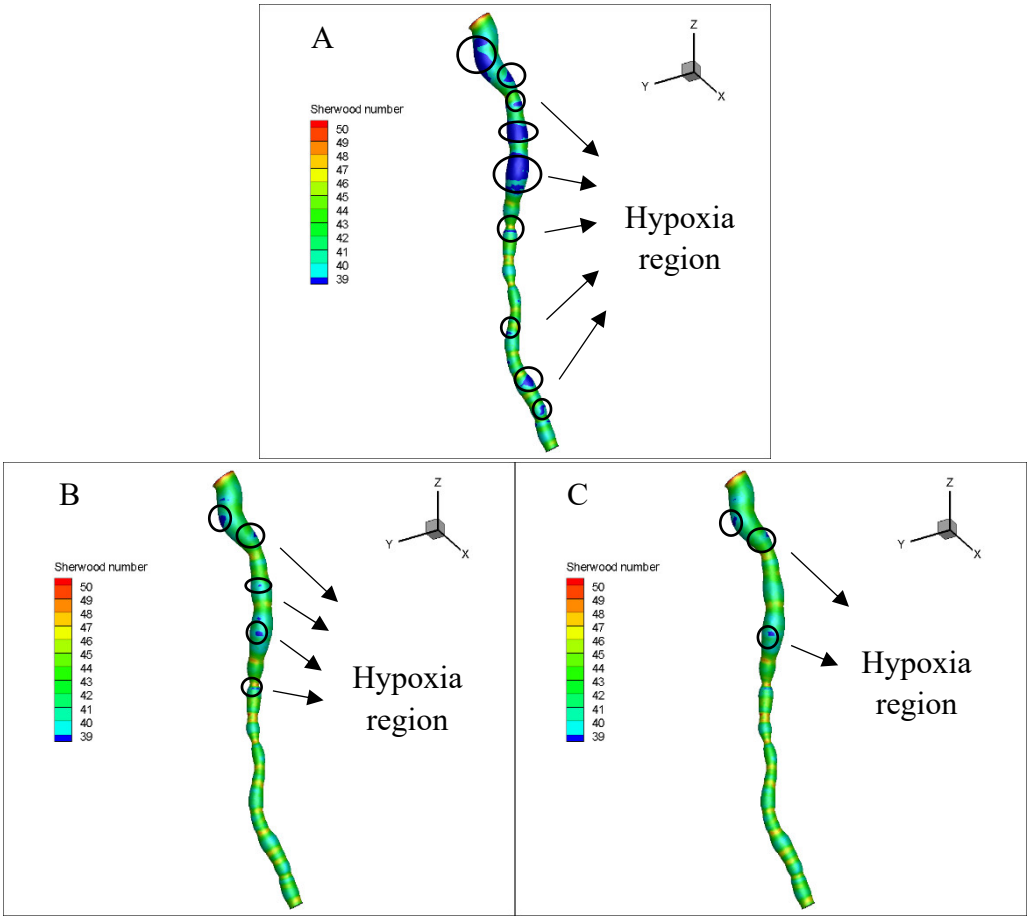

Figure 4-9 Sherwood number without hemoglobin in Newtonian fluid: velocityA (A), velocityB (B), and velocityC (C).

Non-Newtonian (Casson)

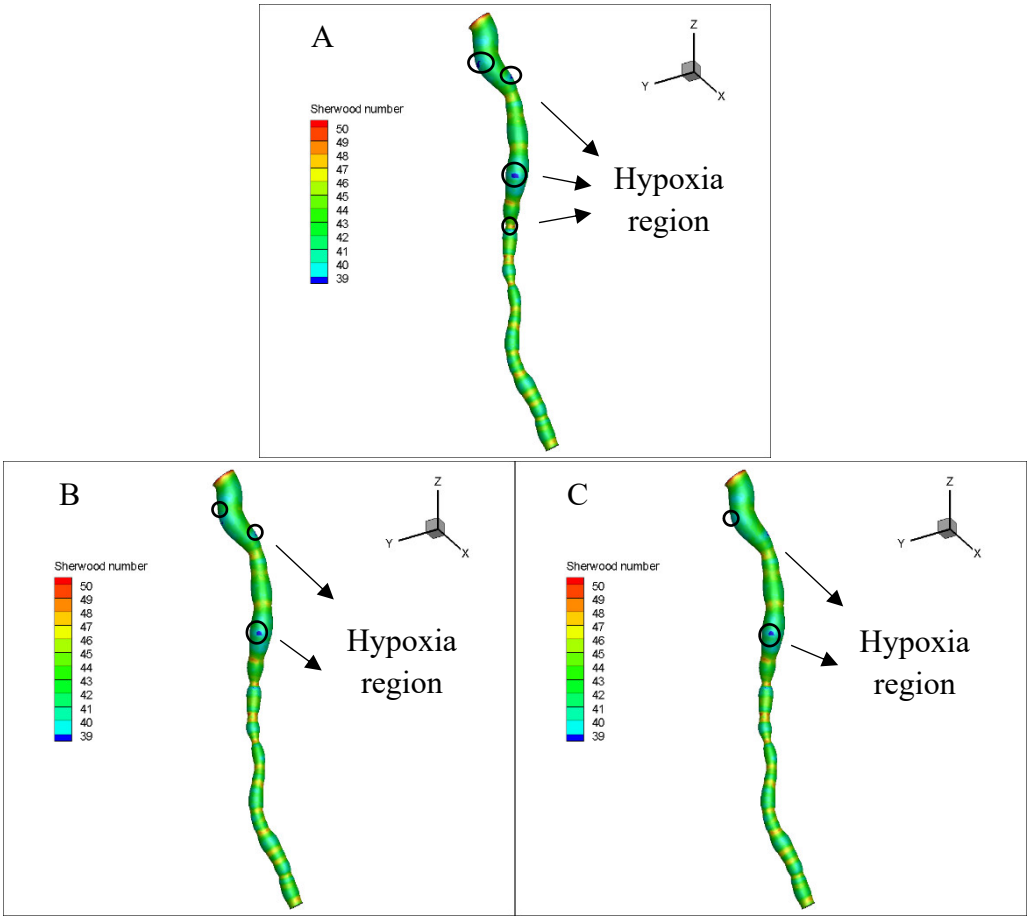

Figure 4-10 Sherwood number with hemoglobin in non-Newtonian fluid: velocityA (A), velocityB (B), and velocityC (C).

For non-Newtonian fluid, in terms of three velocities at the inlet boundary, hypoxia zones were observed near the inlet and in the middle of the residuum DLFCA model with hemoglobin in oxygen transport (shown in Fig.4-10). The increase in the velocity at the inlet boundary caused the increment of the Sherwood number within the wall of the vascular model in terms of oxygen transport with hemoglobin; thus, contributed to the reduction of the number and area of hypoxia zones in the residuum DLFCA model with non-Newtonian fluid.

As shown in Fig. 4-11, in terms of the residuum DLFCA model with non-Newtonian fluid, the Sherwood number without hemoglobin increased followed by the increment of the velocity at the inlet boundary, which was consistent with the results with hemoglobin. For the residuum DLFCA model with non-Newtonian fluid, the increment of the velocity at the inlet boundary would still contribute to the increase in the Sherwood number in terms of oxygen transport without hemoglobin; and cause the decrease in the number and area of hypoxia zones within the vascular wall.

Through the comparison with the results of oxygen transport with hemoglobin, it was demonstrated that the Sherwood number without hemoglobin decreased remarkably in terms of the residuum DLFCA model with non-Newtonian fluid (shown in Fig. 4-10 and Fig. 4-11). For non-Newtonian fluid, the value of Sherwood number without hemoglobin was lower than that with hemoglobin. And it was indicated that the number and area of hypoxia zones with hemoglobin were smaller in terms of residuum DLFCA model with non-Newtonian fluid, compared with the results of oxygen transport without hemoglobin.

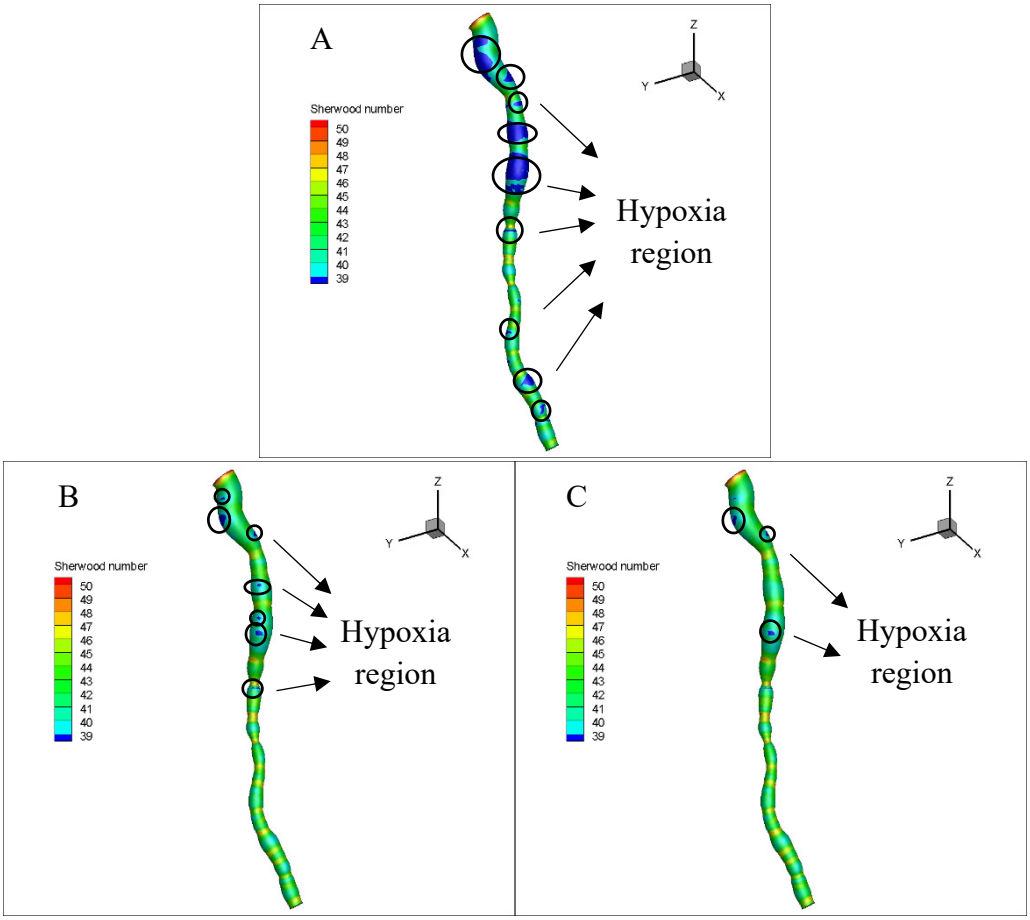

Figure 4-11 Sherwood number without hemoglobin in non-Newtonian fluid: velocityA (A), velocityB (B), and velocityC (C).

4.3.2 DLFCA in contralateral sound limb

It is necessary to investigate the Sherwood number of the DLFCA model in contralateral sound limb, although the Sherwood number of the vascular model in the residual limb plays a role in the evaluation of oxygen transport in the vessel. Two blood constitutive models (Newtonian and non-Newtonian) with velocityA at the inlet boundary were employed in the DLFCA model of the contralateral sound limb, in order to investigate the oxygen transport of the vascular model in the

contralateral sound limb after amputation. And two settings were applied in the user-defined scalar (UDS) in FLUENT with the UDF: (1) with hemoglobin, i.e., oxygen in blood included free oxygen and oxygen carried by hemoglobin; (2) without hemoglobin ($[Hb]=0$), which was beneficial for investigating the contribution of hemoglobin to oxygen transport in the DLFCA of contralateral sound limb.

Newtonian

For Newtonian fluid, the hypoxia zone was observed near the inlet of the vessel, in terms of oxygen transport with hemoglobin (shown in Fig. 4-12A). As shown in Fig. 4-12B, the hypoxia zones were observed near the inlet, just before the bifurcation and near the outlet of the vascular model without hemoglobin. Obviously, the value of Sherwood number with hemoglobin was higher than that without hemoglobin in the DLFCA of contralateral sound limb, which was consistent with the results of the DLFCA in the residual limb. The number and area of hypoxia zones without hemoglobin were larger than that with hemoglobin in terms of the vascular model with Newtonian fluid.

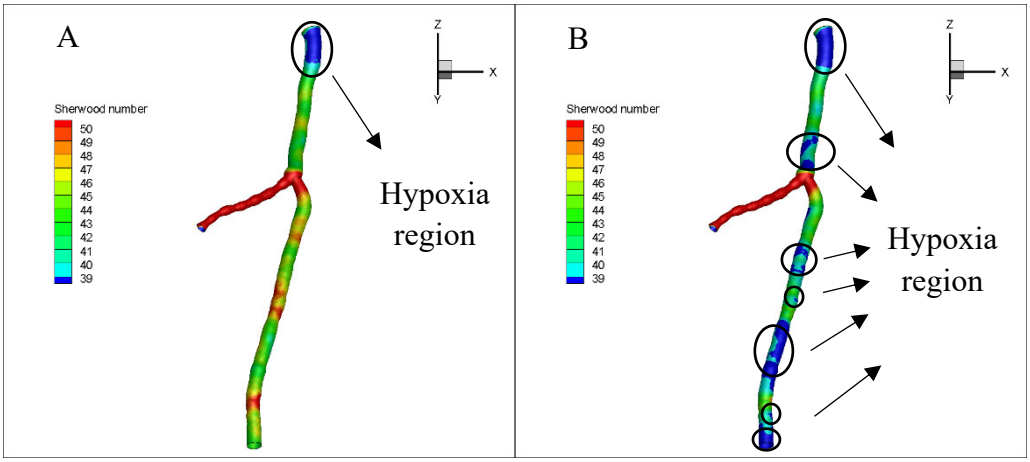

Figure 4-12 Sherwood number in Newtonian fluid: with hemoglobin (A) and without hemoglobin (B).

Non-Newtonian (Casson)

As shown in Fig. 4-13A, in terms of non-Newtonian fluid, the hypoxia zone was observed near the inlet of the DLFCA model with hemoglobin. For oxygen transport without hemoglobin, the hypoxia zones were observed near the inlet, just before the bifurcation and near the outlet of the vascular model (shown in Fig. 4-13B). And for non-Newtonian fluid, it was demonstrated that the value of Sherwood number without hemoglobin was lower than that with hemoglobin in the DLFCA of contralateral sound limb, which was consistent with the results of the DLFCA in the residual limb. Thus, the number and area of hypoxia zones with hemoglobin were smaller than that without hemoglobin in terms of the vascular model with non-Newtonian fluid.

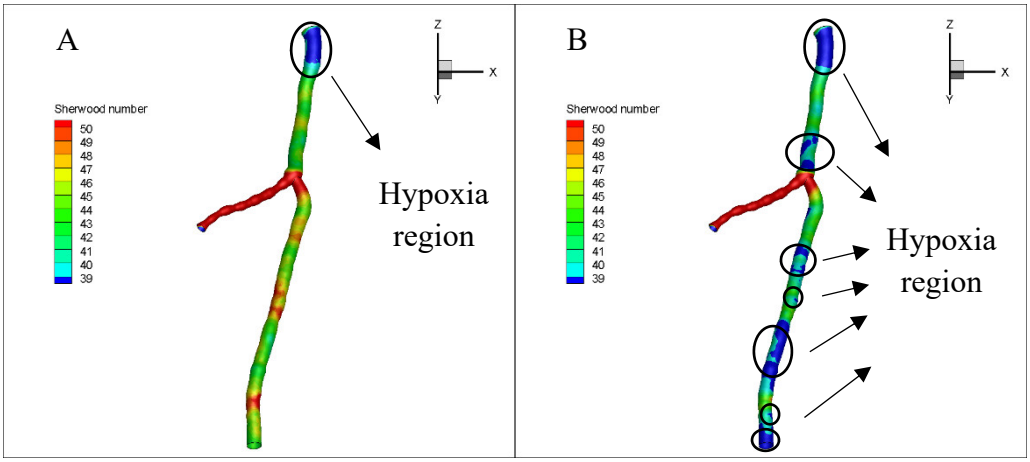

Figure 4-13 Sherwood number in non-Newtonian fluid: with hemoglobin (A) and without hemoglobin (B).

For the DLFCA model with both Newtonian and non-Newtonian in the contralateral sound limb, the value of Sherwood number without hemoglobin was lower than that with hemoglobin within the vascular wall, which was consistent with the results of the vascular model in the residuum.

4.4 Summary

In terms of the residuum DLFCA model with both Newtonian and non-Newtonian fluid, the increment of the velocity at the inlet boundary could cause the increase in the velocity of blood flow. Through comparing the results of Newtonian with those of non-Newtonian, it was found that the velocity of blood flow did not change in this vascular model, and the streamline distribution of non-Newtonian fluid transformed in the region near the outlet with the increment of the velocity at the inlet boundary. In addition, through comparing the results of Newtonian fluid with

those of non-Newtonian fluid in two DLFCA models of residuum and contralateral sound limb, it was convinced that there was no difference of the blood velocity and streamline distribution between Newtonian and non-Newtonian. On top of that, the change in the spatial vasculature of the DLFCA in the residual limb was the main contributor to the difference of the velocity and streamline distribution between two DLFCA models of residuum and contralateral sound limb.

The low WSS region was only observed in the arterial wall of residuum DLFCA with velocityA at the inlet boundary in terms of both Newtonian and non-Newtonian fluid. The increase in the velocity at the inlet boundary of the vascular model would result in the increment of WSS and cause the decrease in low WSS region. Thus, the increase in the velocity at the inlet boundary may reduce the risk of vascular diseases. Through comparing the results of Newtonian and non-Newtonian, it was illustrated that the area of low WSS region in the vascular model with non-Newtonian fluid was smaller than that of the vascular model with Newtonian fluid, which was consistent with the numerical simulation results of the previous study (Fan et al., 2009).

For oxygen transport with hemoglobin and without hemoglobin, the increase in the velocity at the inlet boundary of the residuum DLFCA model with Newtonian fluid was main contributor to the decrease in the number and area of hypoxia zones within the vascular wall, which was consistent with the results of the vascular model

with non-Newtonian. Thus, it was suggested that the increment of the velocity in the residuum DLFCA model would be beneficial for oxygen transfer in the vessel. And the value of Sherwood number without hemoglobin was lower than that with hemoglobin in the residuum DLFCA model in terms of both Newtonian and non-Newtonian fluid, which was consistent with the computational results of the previous study (Moore and Ethier, 1997, Liu et al., 2010). Moreover, for the DLFCA model with both Newtonian and non-Newtonian in the contralateral sound limb, the value of Sherwood number without hemoglobin was lower than that with hemoglobin within the vascular wall as well.

CHAPTER 5 TRANSMISSION LINE EQUATIONS OF OXYGEN TRANSPORT IN ARTERIES

Oxygen plays a significant role in the physiological status of the tissues in human body. Oxygen transport in arteries, arterioles, and capillaries is the main way to supply oxygen and nutrients for the tissues. Moreover, oxygen diffusive flux from the blood to arterial wall is the main component of oxygen consumption in the arterial tissue. Abnormality of oxygen tension distribution contributes to the hypoxia in the arterial wall (Moore and Ethier, 1997), which further causes the development of the atherosclerotic plaque (Crawford and Blankenhorn, 1991, Zemplenyi et al., 1989, Matsushita et al., 2000).

Numerous studies about numerical predictions and experimental measurements in microcirculation and large arteries were conducted to determine the oxygen concentration in vessels and tissues. Buerk et al. (Buerk and Goldstick, 1982) carried out *in vivo* measurement of arterial oxygen content in the dog blood vessels using the oxygen tension (PO_2) electrode which penetrated into the lumen, and it was indicated that the arterial PO_2 values in the thoracic aorta and femoral artery were 84 mmHg and 89 mmHg, respectively; Vazquez et al. (Vazquez et al., 2010) positioned the oxygen sensors with tips in tissue and blood in order to simultaneously record tissue and arterial PO_2, and the results showed that the changes in arterial PO_2 could directly affect the tissue oxygenation and function; Yaseen et al. (Yaseen et al., 2011) conducted the tracheotomy and cannulation of

the femoral artery, and then used the confocal phosphorescence lifetime microscopy to measure arterial PO_2; and Masamoto et al. (Masamoto et al., 2008) carried out arterial blood sampling for measuring systemic PO_2 and placed a microelectrode beneath the cortical surface to record PO_2 in the cortex. According to these literatures, it was suggested that there were few non-invasive ways to measure the oxygen concentration in arteries. Thus, for the sake of investigating the oxygen distribution in the arterial blood and arterial wall, numerous numerical simulations of oxygen transport in the arteries were performed (Moore and Ethier, 1997, Buerk and Goldstick, 1982, Liu et al., 2010, Qiu and Tarbell, 2000, Tada, 2010). Specifically, computational fluid dynamic (CFD) models coupled with the convection-diffusion equation of oxygen transport were established in these simulations to predict the distribution of oxygen concentration. In summary, experimental investigations and numerical simulations of the oxygen transport mainly focused on the PO_2 distribution in local regions of the arteries and tissues, whereas most of them did not consider the systemic distribution of oxygen concentration in terms of the whole circulatory system perspective. Nevertheless, a simplified mathematical expression including the hemoglobin concentration was applied in the lumped parameter model for calculating blood oxygen concentration in terms of the systemic circulation perspective (Broomé et al., 2013, Yao et al., 2008), and the effects of hemodynamics on oxygen concentration distribution were neglected in the expression. However, hemodynamics plays a significant role in oxygen transport in the arteries (Tada, 2010, Liu et al., 2010, Tsai et al., 2003).

In fact, a mathematical model for predicting blood flow in terms of the systemic circulation perspective has been employed for a few years (Noordergraaf et al., 1963, Westerhof et al., 1969, Raines et al., 1974, Reymond et al., 2011). Lumped parameter model of blood flow, which was on the basis of fluid transmission line model, was widely used for predicting blood velocity and pressure in the whole circulatory system (Lacourse et al., 1986, Snyder et al., 1968, van de Vosse and Stergiopulos, 2011). With reference to fluid transmission line equations, transmission line equations of oxygen transport were firstly developed in this study. Lumped parameter model of oxygen transport, which is established based on the transmission line equations of oxygen transport, is supposed to be valuable for predicting the systemic distribution of oxygen concentration in the whole circulatory system.

5.1 Theoretical considerations

5.1.1 The integrated form of oxygen transport equation

In the derivation of the oxygen transmission line equations, mass transport equation in cylindrical coordinates is firstly applied.

$$\frac{\partial C}{\partial t}+\frac{v_r}{r}\frac{\partial}{\partial r}(rC)+\frac{v_\theta}{r}\frac{\partial C}{\partial \theta}+v_z\frac{\partial C}{\partial z}=\frac{\Gamma}{\rho}\left[\frac{1}{r}\frac{\partial}{\partial r}\left(r\frac{\partial C}{\partial r}\right)+\frac{1}{r^2}\frac{\partial^2 C}{\partial \theta^2}+\frac{\partial^2 C}{\partial z^2}\right]+S, \quad (5.1)$$

where r, θ and z are radial coordinate, angular coordinate and axial coordinate, respectively; C is the concentration of the solute; Γ and ρ are the diffusion

coefficient of the solute and the density of the fluid, respectively; v_r, v_θ and v_z are the components of the fluid velocity in r-direction, θ-direction and z-direction in the cylindrical coordinate system, respectively; S is the source term, and it is supposed to be zero in terms of oxygen transport in the blood vessel. v_r and v_θ are usually assumed to be zero in the numerical simulation of blood flow. Subsequently, each term of equation (5.1) multiplies r, which yields

$$\frac{\partial(rC)}{\partial t}+v_z\frac{\partial(rC)}{\partial z}=\frac{\Gamma}{\rho}\left[\frac{\partial}{\partial r}\left(r\frac{\partial C}{\partial r}\right)+\frac{\partial^2(rC)}{\partial z^2}\right]. \tag{5.2}$$

Then we integrate each term of equation (5.2) over the cross-section of blood vessel and use the Leibniz rule for differentiating an integral (Equation (5.3)) to rewrite these integrals.

$$\frac{\partial}{\partial t}\int_{\alpha(t)}^{\beta(t)} f(x,t)\,dx=\int_{\alpha(t)}^{\beta(t)}\frac{\partial f(x,t)}{\partial t}dx+\left\{f\left[\beta(t),t\right]\frac{\partial\beta(t)}{\partial t}-f\left[\alpha(t),t\right]\frac{\partial\alpha(t)}{\partial t}\right\} \tag{5.3}$$

Thus, equation (5.2) is transformed into

$$\frac{\partial\left(\int_0^R 2\pi rCdr\right)}{\partial t}+v_z\frac{\partial\left(\int_0^R 2\pi rCdr\right)}{\partial z}=\frac{\Gamma}{\rho}\left[\int_0^R 2\pi\frac{\partial}{\partial r}\left(r\frac{\partial C}{\partial r}\right)dr+\frac{\partial^2\left(\int_0^R 2\pi rCdr\right)}{\partial z^2}\right], \tag{5.4}$$

where R is the radius of the vessel. The oxygen content of the whole cross-section (M) is presented by the expression: $M=\int_0^R 2\pi rCdr$. Moreover, the first term at the right-hand side of equation (5.4) could be rewritten by $\int_0^R 2\pi\frac{\partial}{\partial r}\left(r\frac{\partial C}{\partial r}\right)dr=2\pi\left(r\frac{\partial C}{\partial r}\right)\Big|_{r=0}^{r=R}=2\pi R\left(\frac{\partial C}{\partial r}\right)_{r=R}$.

Consequently, the integration of the oxygen transport equation without the consideration of hemoglobin over the cross-section of blood vessel is showed as follow:

$$\rho \frac{\partial M}{\partial t} + \rho v_z \frac{\partial M}{\partial z} = 2\pi R \left(\Gamma \frac{\partial C}{\partial r} \right)_{r=R} + \Gamma \frac{\partial^2 M}{\partial z^2}. \tag{5.5}$$

Thus, in this equation, ρ and v_z are the blood density and blood velocity, respectively; M is the oxygen content of the whole cross-section in the vessel; z -direction is the direction of blood flow; Γ is the diffusion coefficient of oxygen in the blood; and R is the radius of the vascular lumen.

The convective flux is expressed as $J_{con} = \rho v_z M$, and the diffusive flux is expressed as $J_{diff} = \Gamma \frac{\partial M}{\partial z}$. In the equation (5.5), z represents the direction of fluid flow. x is utilized to replace z in the following. Therefore, the equation (5.5) should be transformed into

$$\frac{\partial}{\partial t}\left(\frac{J_{con}}{v_x} \right) + \frac{\partial}{\partial x}\left(J_{con} \right) = \frac{\partial}{\partial x}\left(J_{diff} \right) + 2\pi R \left(\Gamma \frac{\partial C}{\partial r} \right)_{r=R}. \tag{5.6}$$

In the mathematic derivation of the aforementioned equation, three assumptions are applied: the vessel is treated as a uniform tube; the velocity distribution is uniform over the entire cross-section of the vessel; and the value of vascular radial deformation is much smaller than the radius. These assumptions were employed in the derivation of fluid transmission line equations as well (Raines et al., 1974,

Horsten et al., 1989).

5.1.2 Transmission line equations of oxygen transport

In mass transport, the distribution of solute concentration is mainly influenced by the convective flux and diffusive flux. And there exists a correlation between the convective flux and diffusive flux (Patankar, 1980a). The convective flux could cause the increment of oxygen concentration gradient, and then enhance the diffusive flux (Fannjiang and Papanicolaou, 1994, Fannjiang and Papanicolaou, 1997). In contrast, the diffusion is supposed to affect the convective flow which dominates the convective flux (Cussler, 1984). There exists the similar relationship between the convective flux and diffusive flux in oxygen transport as well (Buerk and Goldstick, 1982). Moreover, the heat generated by convection is proportional to the gradient of the thermal diffusion in heat transfer of the plane coquette fluid flow (Ramachandran, 2014). The fluid transmission line equations ($\begin{cases} -\frac{\partial P}{\partial x} = Z_X Q \\ -\frac{\partial Q}{\partial x} = \frac{1}{Z_r} P \end{cases}$) are regarded as the theoretical reference for the development of the transmission line equations of oxygen transport in this study, where P is the pressure, Q is the volumetric flow rate, Z_X is the transverse impedance, Z_r is longitudinal impedance, and x represents the direction of fluid flow as well. In conclusion, the transmission line equations of oxygen transport are developed:

$$-\frac{\partial J_{diff}}{\partial x} / J_{con} = Z_{con} \tag{5.7}$$

And

$$-\frac{\partial J_{con}}{\partial x} / J_{diff} = Z_{diff}, \tag{5.8}$$

where the ratio of the gradient of diffusive flux to convective flux is defined as the convective impedance and denoted as Z_{con}, and the ratio of the gradient of convective flux to diffusive flux is defined as the diffusive impedance and denoted as Z_{diff}.

In oxygen transport, on one hand, diffusion is mainly influenced by convection (Jim Douglas and Russell, 1982); on the other hand, convection is dominant by blood flow (Patankar, 1980a), and diffusion rarely has an impact on convection (Cussler, 1984, Ramachandran, 2014, Deen, 1998, Wilkinson, 2000). Based on mass balance of oxygen transport in a vessel, the following relationships were figured out: convective transport = diffusive flux out of the blood = oxygen consumption (Tsai et al., 2003). Consequently, the equation (5.8) could be rewritten as

$$-\frac{\partial J_{con}}{\partial x} = -J_{diff}\Big|_{\text{From blood to wall}} = -2\pi R\left(\Gamma \frac{\partial C}{\partial r}\right)_{r=R}, \tag{5.9}$$

where $-2\pi R\left(\Gamma \frac{\partial C}{\partial r}\right)_{r=R}$ is the diffusive flux of oxygen from blood to vascular wall.

Since there is phase difference between the pressure gradient and volumetric flow rate, one of the fluid transmission line equations could be written as

$$-\frac{\partial P}{\partial x} = Z_X Q = R' Q + L' \frac{\partial Q}{\partial t}, \tag{5.10}$$

where $R^{'}$ and $L^{'}$ represent the resistivity and inertance, respectively. There exists phase difference between the gradient of diffusive flux and convective flux as well. Thus, equation (5.7) is supposed to be rewritten as

$$-\frac{\partial J_{diff}}{\partial x}=R_0 J_{con}+L_0\frac{\partial J_{con}}{\partial t}. \tag{5.11}$$

In summary, the transmission line equations of oxygen transport in a vessel are developed as follow:

$$\begin{cases} -\dfrac{\partial J_{diff}}{\partial x}=R_0 J_{con}+L_0\dfrac{\partial J_{con}}{\partial t} \\ -\dfrac{\partial J_{con}}{\partial x}=-J_{diff}\Big|_{\text{From blood to wall}}=-2\pi R\left(\Gamma\dfrac{\partial C}{\partial r}\right)_{r=R} \end{cases}, \tag{5.12}$$

where R_0 and L_0 represent the properties of oxygen convection and will be elucidated in the following.

5.1.3 Derivation of the expressions for R_0 and L_0

Oxygen transport equation (Equation (5.6)) is rewritten as

$$\frac{1}{v_x}\frac{\partial J_{con}}{\partial t}-\frac{1}{{v_x}^2}\frac{\partial v_x}{\partial t}\cdot J_{con}+\frac{\partial J_{con}}{\partial x}=\frac{\partial J_{diff}}{\partial x}+J_{diff}\Big|_{\text{From blood to wall}}. \tag{5.13}$$

Subsequently, using equation (5.11) to subtract equation (5.9) in the corresponding side, we yield:

$$-\frac{\partial J_{diff}}{\partial x}+\frac{\partial J_{con}}{\partial x}=R_0 J_{con}+L_0\frac{\partial J_{con}}{\partial t}+J_{diff}\Big|_{\text{From blood to wall}}. \tag{5.14}$$

According to the comparison of equation (5.13) and equation (5.14), R_0 and L_0

are given by the follow expressions:

$$\begin{cases} R_0 = \dfrac{1}{{v_x}^2}\dfrac{\partial v_x}{\partial t} = \dfrac{\partial}{\partial t}\left(-\dfrac{1}{v_x}\right) \\ L_0 = -\dfrac{1}{v_x} \end{cases}. \tag{5.15}$$

Since interval transit time of mass transport is defined as the reciprocal of velocity (Meier and Zierler, 1954, Boulding, 1996, Roberts et al., 1973, Roberts et al., 2000), L_0 represents the transit time of oxygen per unit distance. Moreover, the first derivative of transit time versus time is equal to $1-H(t)$, where $H(t)$ is the cumulative frequency function of transit time and represents the fraction of oxygen transmission (Meier and Zierler, 1954, Zierler, 1965). Thus, R_0 is supposed to represent the fraction of remaining oxygen convection per unit distance. Consequently, both L_0 and R_0 belong to the characteristics of oxygen convection in oxygen transport of a vessel.

In conclusion, transmission line equations of oxygen transport are given by the following expressions: $\begin{cases} -\dfrac{\partial J_{diff}}{\partial x} = R_0 J_{con} + L_0 \dfrac{\partial J_{con}}{\partial t} \\ -\dfrac{\partial J_{con}}{\partial x} = -J_{diff}\Big|_{\text{From blood to wall}} = -2\pi R\left(\Gamma \dfrac{\partial C}{\partial r}\right)_{r=R} \end{cases}$, where $\begin{cases} R_0 = \dfrac{1}{{v_x}^2}\dfrac{\partial v_x}{\partial t} = \dfrac{\partial}{\partial t}\left(-\dfrac{1}{v_x}\right) \\ L_0 = -\dfrac{1}{v_x} \end{cases}$. L_0 and R_0 are the transit time of oxygen per unit distance and the fraction of remaining oxygen convection per unit distance, respectively.

5.2 Verification

A three-dimensional (3D) fluid-structure interaction (FSI) model coupled with oxygen transport equation and a lumped parameter model of oxygen transport were employed for numerically verifying the development of the transmission line equations of oxygen transport.

In the FSI analysis, a straight tube with 9-mm radius and 200-mm length was regarded as the geometric model. The governing equations of blood flow were 3D Navier-Stokes equation and continuity equation. In terms of transient structural simulation, momentum balance equations were solved with fluid-solid interface boundary and constraint conditions. Mass transport equation was used for describing oxygen transport in blood. The density and dynamic viscosity of blood were set as 1050 kg/m^3 and 3.5×10^{-3} kg/m·s (Wentzel et al., 2001), respectively. The thickness of the tube wall was 2 mm. In addition, the density, Poisson's ratio and elastic modulus of the wall were set as 1060 kg/m^3, 0.49 and 5.11 MPa, respectively. The diffusion coefficient of oxygen in blood was 1.2×10^{-9} m^2/s (Stein et al., 1971). In terms of blood flow, the pulsatile profile of flow rate according to in vivo measurements was applied at inlet (van de Vosse and Stergiopulos, 2011), as shown in Fig. 5-1. A pressure boundary condition coupled with constant resistance model was applied at outlet, and the value of the resistance was 0.0865 mmHg·s/cm^3. In terms of oxygen transport, the oxygen tension at inlet was set as 85 mmHg, and oxygen tension at the inner surface of the vascular wall was

specified as 60 mmHg (Buerk and Goldstick, 1982, Qiu and Tarbell, 2000, Moore and Ethier, 1997). The commercial finite element package ANSYS (version 14.0, ANSYS, Inc., USA) was used to simulate blood flow and oxygen transport. Specifically, the user-defined scalar (UDS) in ANSYS Fluent was added for simulating oxygen transport in blood, and the user-defined C-like function (UDF) was compiled in the setting of inlet and outlet boundary conditions.

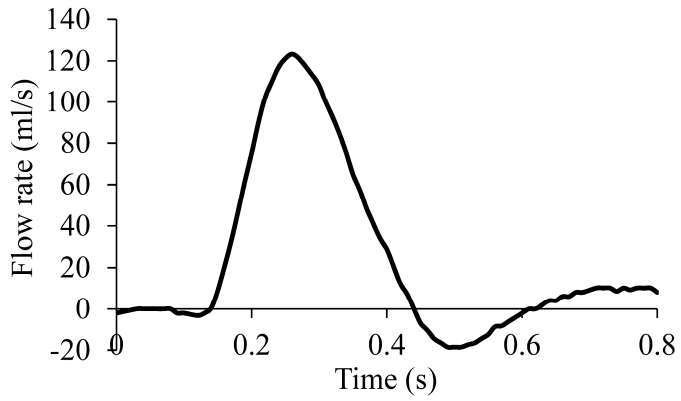

Figure 5-1 Flow rate at inlet of the vessel.

On the other hand, lumped parameter models of blood flow and oxygen transport in the same tube were developed for numerically predicting oxygen concentration distribution. The numerical analysis of lumped parameter model of blood flow was conducted at first in order to provide the blood velocity for the further calculation of parameters (L_0 and R_0) in the lumped parameter model of oxygen transport. In these computational models, the tube was divided into ten segments, and the length of each segment was 20 mm which was short enough for precisely calculating the blood velocity in the lumped parameter model of blood flow (Noordergraaf et al.,

1963, Noordergraaf, 1978). The electric circuits related to transmission line equations of blood flow and oxygen transport were used to represent the lumped parameter models of blood flow and oxygen transport in each segment, as shown in Fig. 5-2. In the electrical analogue of blood flow, the current and voltage were related to the flow rate and pressure, respectively. In the electrical analogue of oxygen transport, the current and voltage represented the convective flux and diffusive flux of oxygen, respectively. The material properties and boundary conditions in lumped parameter models were the same as those of the 3D FSI model. The fourth-order Runge-Kutta method was employed in numerical investigations of these lumped parameter models.

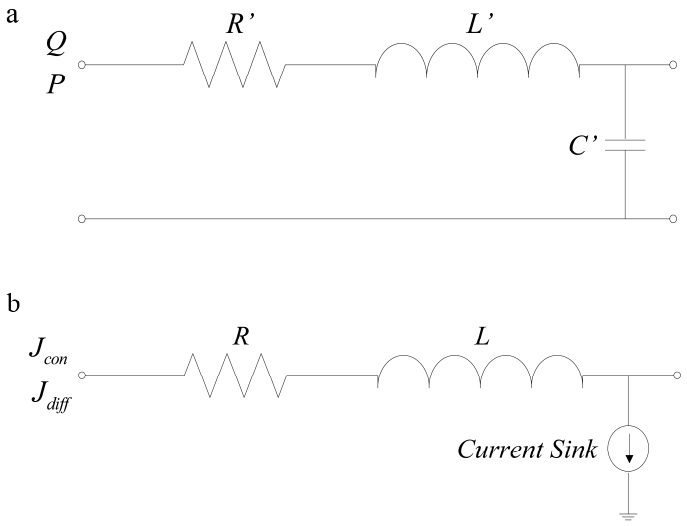

Figure 5-2 Lumped parameter representations of a basic segment. **a** Electrical analogue of blood flow with resistance (*R'*), inductance (*L'*) and capacitance (*C'*). *R'*, *L'* and *C'* represent the resistivity, inertance and compliance, respectively. **b** Electrical analogue of oxygen transport with resistance (*R*), inductance (*L*) and current sink. *R* and *L* represent the properties of oxygen convection. Current sink is

related to the diffusive flux of oxygen from blood to vascular wall.

In summary, the distribution of oxygen concentration in the tube was acquired through numerical analyses of the 3D FSI model coupled with oxygen transport and the lumped parameter model of oxygen transport. As shown in Fig. 5-3, the difference of the oxygen convective flux at the end between the 3D model and lumped parameter model was quite modest. Consequently, the lumped parameter model of oxygen transport based on transmission line equations of oxygen transport could provide the numerical prediction of oxygen concentration distribution which was in accordance with the results of the 3D computational simulation. According to this comparison between the lumped parameter model and 3D computational model, the transmission line equations of oxygen transport are supposed to be reliable.

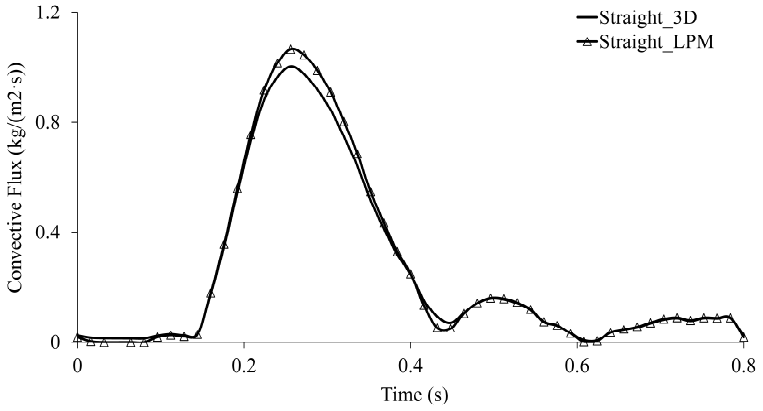

Figure 5-3 The convective flux of oxygen at the end of the tube.

The geometry of the 3D computational model which is compared with the lumped

parameter model is a straight tube. It reveals that the transmission line equations of oxygen transport are reliable in terms of the straight vessel. The geometries of numerous vessels in the entire vascular system are complex and curved. It can be assumed that the curved vessel is divided into a large number of straight tube segments. Since the transmission line equations are applicable to the straight vascular model, the equations are supposed to be reliable in terms of curved vessels, which is also the same for other vessels with branching and complex structure.

5.3 Discussions

This study introduces the process for deducing the development of transmission line equations of oxygen transport in a vessel. More specifically, fluid transmission line equations are regarded as the theoretical reference for the establishment of oxygen transmission line equations. On top of that, the theory of oxygen transport in a vessel, which indicates that the transmitted flux of oxygen convection is equal to the diffusive flux out of the blood, is the theoretical basis for proposing transmission line equations of oxygen transport. The mathematical expressions of the parameters (L_0 and R_0) in oxygen transmission line equations are derived on basis of mass transport equation, and these parameters represent the properties of oxygen convection in oxygen transport. Transmission line equations of oxygen transport could be employed as the theoretical basis for establishing the lumped parameter model of oxygen transport which is coupled with the lumped parameter model of blood flow. The lumped parameter model of oxygen transport is able to provide

numerical predictions for systemic distribution of oxygen concentration in the circulatory system. Having a good knowledge of the systemic distribution of oxygen concentration is supposed to be helpful for assessing the status of human body and further offering valuable guidance for the prevention and intervention of diseases.

In previous studies, oxygen concentration in blood was estimated based on an empirical formula which was mainly related to the hemoglobin in terms of the whole circulatory system (Broomé et al., 2013, Yao et al., 2008). And the value of the hemoglobin concentration which was included in the empirical formula was set as a constant in each part of the circulatory system. Indeed, the hemoglobin concentration is one of the determinant factors for the oxygen concentration in blood. The effects of hemodynamics on the oxygen concentration were not considered in the establishment of the empirical formula. Whereas, hemodynamics plays a significant role in the hemoglobin concentration and oxygen concentration in a vessel. The hemoglobin concentration and oxygen concentration are mainly affected by the convective flow in terms of the hemodynamic effects. Thus, in this study, oxygen convection which is determined by the convective flow is involved in the development of the transmission line equations of oxygen transport. Hemodynamics is treated as a significant factor for calculating oxygen concentration in these transmission line equations of oxygen transport. Although the effect of hemoglobin is not taken into consideration in the development of the

oxygen transmission line equations, oxygen concentration which is numerically predicted with the consideration of oxyhemoglobin transport could be derived from the results of oxygen lumped parameter model developed on the basis of these equations. That is due to the fact that oxygen concentration calculated with oxyhemoglobin transport was linearly related to the numerical results without the consideration of hemoglobin in the computational fluid dynamic (CFD) simulation (Moore and Ethier, 1997). In summary, transmission line equations of oxygen transport could provide a more precise estimation of systemic oxygen distribution in comparison with the previous methods in the numerical simulation. In addition, the systemic distribution of oxygen concentration could be also acquired from the 3D CFD model of the whole arterial system except the aforementioned numerical methods. It needs a large number of computational cost and time to conduct the 3D simulation which consists of the CFD analysis and mass transport computation in the entire arterial system (Xiao et al., 2013, Randles et al., 2015). And the numerical analysis of oxygen lumped parameter model based on the transmission line equations of oxygen transport is supposed to require much less computational resources and time in comparison with the 3D simulation, which demonstrates the significance and value of these equations.

In addition to oxygen, the prediction of other substances concentration in blood is beneficial for the assessment and intervention of disease as well, such as contrast agents for vascular imaging, low-density lipoprotein (LDL) and targeted drugs.

More specifically, determining the systemic distribution of contrast agent concentration is helpful for the optimization of vascular imaging quality (Landis et al., 2000, Bernardino et al., 1994, Calamante et al., 2007); the accumulation of LDL is a risk factor for development of atherosclerosis in an artery (Tarbell, 2003, Ross, 1993), and thus it is beneficial for assessment of atherosclerotic development to figure out the systemic distribution of LDL concentration in the arterial system; numerical kinds of targeted drugs have a detrimental effect on normal tissues due to their toxicities, and it is beneficial for improving targeted drug therapies to understand drug delivery in blood vessels (Langer, 1998, Liu and Kurzrock, 2014, Vasir and Labhasetwar, 2005). Transmission line equations of oxygen transport established in this study could be used as a theoretical reference for developing lumped parameter models of the delivery of the aforementioned substances in blood, and these equations should be modified according to critical characteristics of corresponding substance delivery. Specifically, in order to consider biological and chemical interactions between these substances and blood, the source term in mass transport equation should be added and adjusted on the basis of their biological and chemical properties in blood; since diffusion coefficients of different substances in blood are different, the diffusive term of each substance in transmission line equations of mass transport is supposed to be transformed with substitution of diffusion coefficient; moreover, the parameters (L_0 and R_0) in transmission line equations represent properties of convection term, and thus their values mainly depend on blood flow. The systemic distribution of substance concentration is

obtained from numerical investigations of these lumped parameter models with less computational cost and time. Acquiring the concentration distribution of these substances in the entire vascular system provides guidance for the prevention and treatment of vascular disease. As a consequence, the transmission line equations can be widely applied to determine the concentration distribution of substances in the whole arterial system.

Oxygen delivery in arteries plays a significant role in the physiological status of human body, and prediction of oxygen concentration distribution in the entire vascular system is beneficial for the assessment and intervention of numerous diseases. In order to obtain the distribution of oxygen concentration in the entire arterial system, transmission line equations of oxygen transport are developed in this study with reference to the development of fluid transmission line equations. And the systemic distribution of oxygen concentration could be predicted from a lumped parameter model of oxygen transport which is mainly composed of oxygen transmission line equations. The transmission line equations are widely used as the theoretical basis for the establishment of lumped parameter models of other substances except oxygen in blood.

Although transmission line equations of oxygen transport are innovative and important, there exist a few limitations in the development of the equations. Firstly, the effect of hemoglobin on oxygen concentration distribution is neglected in the

derivation of the transmission line equations. More physiological properties of oxygen in blood will be involved in the further development of these equations for the sake of more precise estimation of oxygen concentration distribution in the arterial system. Secondly, the diffusive flux of oxygen from blood to arterial wall dominates the distribution of the convective flux in blood, and it is difficult to obtain the value of the diffusive flux into arterial wall. In general, oxygen consumption in the arterial wall could be regarded as an estimation of the diffusive flux into wall, which would affect the numerical prediction of oxygen concentration in the lumped parameter model of oxygen transport based on these transmission line equations. A noninvasive method to measure the gradient of oxygen concentration near the arterial wall is beneficial to acquire the accurate value of the oxygen flux into wall, and it would enhance the accuracy of oxygen concentration prediction in the lumped parameter model of oxygen transport.

CHAPTER 6 TRANSMISSION LINE EQUATIONS OF MASS TRANSPORT IN ARTERIOLES AND CAPILLARIES

Understanding the concentration distribution of the substances in the entire circulatory system could offer guidance for the assessment and treatment of diseases (e.g., oxygen, contrast agents for vascular imaging, low-density lipoprotein (LDL), and targeted drugs). Specifically, an abnormality in the oxygen tension (PO_2) distribution causes hypoxia in the arterial wall (Moore and Ethier, 1997), which further contributes to the development of atherosclerosis plaque (Crawford and Blankenhorn, 1991, Lattimore et al., 2005, Zemplenyi et al., 1989, Matsushita et al., 2000). Acquiring the systemic distribution of contrast agent concentration is beneficial in the optimization of vascular imaging quality (Landis et al., 2000, Bernardino et al., 1994, Calamante et al., 2007). LDL accumulation is a risk factor for the atherosclerosis development in an artery (Tarbell, 2003, Ross, 1993), and thus determining the LDL concentration distribution in arteries is helpful in evaluating the development of atherosclerosis. A number of targeted drugs and chemotherapeutic drugs detrimentally affect normal tissues due to their toxicities. Consequently, understanding drug transport in the whole vascular system is beneficial for the improvement of targeted drug therapies (Langer, 1998, Liu and Kurzrock, 2014, Vasir and Labhasetwar, 2005).

There are few *in vivo* noninvasive methods of systematically measuring the

concentration distribution of the substances in the circulatory system. And a 3D CFD simulation of an entire vascular tree coupled with mass transport is complicated and requires considerable computational resources and time due to the complex vasculature of the arteries and microvessels. It is currently almost impossible for most of the research groups and clinical measurements to perform a 3D simulation of the systemic arterial tree or microvascular tree. An efficient scheme is required for understanding the oxygen distribution in terms of the systemic circulation perspective.

The numerical analysis of the lumped parameter model of blood flow, which is performed according to the fluid transmission line model, is a useful way to obtain the systemic distribution of blood flow and pressure in the arterial tree. Mass transport was not involved in most of numerical simulations of lumped parameter models. In the previous chapter, the transmission line equations of oxygen transport in arteries were developed with reference to fluid transmission line equations (Yan et al., 2018), and these proposed equations could provide an efficient scheme for investigating the systemic distribution of oxygen in the arterial tree. Moreover, these equations could also be treated as the theoretical basis for obtaining the systemic distribution of other substances in the arterial tree. However, the derivation of these equations in arterioles and capillaries is lacked.

The cellular metabolism in tissues necessitates the nutrient derived from the

substance transfer in microcirculation, where the substance transfer from the blood to the tissue mainly depends on transport from the arteriole and capillary to the tissue (Barrett and Suresh, 2013). The concentration distribution of the substance in microvessels plays a significant role in the function of the tissue (Herbst et al., 1979, Tateishi et al., 1997, Tsukada et al., 2004) and has an influence on the treatment and recovery of the diseases (Sonveaux et al., 2004, Brunstein et al., 2006, Wang et al., 2007, Ratliff et al., 1984). An empirical expression comprised of time, longitudinal distance, and diffusion coefficient was proposed for predicting the concentration distribution of the substance in capillary based on Taylor-Aris dispersion theory (d'Orlye et al., 2008, Lewandrowska et al., 2013, Bello et al., 1994, Beard and Wu, 2009), while effects of convection on diffusion in mass transport were not considered in these numerical predictions. Mass transport in microvessels consists of convection and diffusion as well (Leonard and Jorgensen, 1974), and a portion of diffusion arises from convective flow in capillaries (Adler, 1985, Leonard and Jorgensen, 1974, Overman and Miller, 1968). We proposed transmission line equations of mass transport in the arteriole and capillary to systematically understand the concentration distribution of the substance, and these equations were derived based on the transmission line equations of oxygen transport in arteries and mass transport theory in microvessels. The verification was carried out through the comparison of the numerical prediction based on the developed equations with the previous *in vitro* experimental studies.

6.1 Theoretical considerations

6.1.1 Transmission line equations of mass transport in the arteriole

The blood flow in the arteriole is assumed to be Poiseuille flow. In terms of cylindrical polar coordinates (r, θ, z), the velocity is given by the expression:

$$V = 2\bar{V}\left(1-\frac{r^2}{a^2}\right), \tag{6.1}$$

where $\bar{V}$ is the average velocity over the cross-section of the vessel, and a is the radius. Mass transport equation is described by

$$\frac{\partial c}{\partial t}+V\frac{\partial c}{\partial z}=D\left(\frac{\partial^2 c}{\partial z^2}+\frac{1}{r}\frac{\partial}{\partial r}\left(r\frac{\partial c}{\partial r}\right)\right), \tag{6.2}$$

where c is the concentration of the substance, and D is the diffusion coefficient.

The concentration (c) is divided into two parts (cross-sectional average and r-dependent), writing $c(r,z,t)=\bar{c}(z,t)+c'(r,z,t)$, where $\bar{c}(z,t)$ is the cross-sectional average concentration and independent on the radius. $c'(r,z,t)$ is the part of the concentration related to the radius, and its cross-sectional average is zero, that is, $\bar{c}'(r,z,t)=0$.

The mass transport equation is transformed into

$$\frac{\partial \bar{c}}{\partial t}+\frac{\partial c'}{\partial t}+V\frac{\partial \bar{c}}{\partial z}+V\frac{\partial c'}{\partial z}=D\left(\frac{\partial^2 \bar{c}}{\partial z^2}+\frac{\partial^2 c'}{\partial z^2}+\frac{1}{r}\frac{\partial}{\partial r}\left(r\frac{\partial c'}{\partial r}\right)\right). \tag{6.3}$$

Taking the cross-sectional average of each term in equation (6.3), we obtain

$$\frac{\partial \bar{c}}{\partial t}+\bar{V}\frac{\partial \bar{c}}{\partial z}+\overline{V\frac{\partial c'}{\partial z}}=D\left(\frac{\partial^2 \bar{c}}{\partial z^2}\right)+\frac{\int_0^a 2\pi rD\frac{1}{r}\frac{\partial}{\partial r}\left(r\frac{\partial c'}{\partial r}\right)dr}{\pi a^2} \quad (6.4)$$

The second term at the right-hand side is rewritten as

$$\frac{\int_0^a 2\pi rD\frac{1}{r}\frac{\partial}{\partial r}\left(r\frac{\partial c'}{\partial r}\right)dr}{\pi a^2}=\frac{2\pi D\left(r\frac{\partial c'}{\partial r}\right)\Big|_{r=0}^{r=a}}{\pi a^2}=\frac{2\pi aD\left(\frac{\partial c'}{\partial r}\right)\Big|_{r=a}}{\pi a^2}=\frac{2\pi aD\left(\frac{\partial c}{\partial r}\right)\Big|_{r=a}}{\pi a^2}$$

. Thus, equation (6.4) can be written as follows:

$$\frac{\partial \bar{c}}{\partial t}+\bar{V}\frac{\partial \bar{c}}{\partial z}+\overline{V\frac{\partial c'}{\partial z}}=D\left(\frac{\partial^2 \bar{c}}{\partial z^2}\right)+\frac{2\pi aD\left(\frac{\partial c}{\partial r}\right)\Big|_{r=a}}{\pi a^2} \quad (6.5)$$

Subsequently, subtracting equation (6.5) from equation (6.3) yields:

$$\frac{\partial c'}{\partial t}+\left(V-\bar{V}\right)\frac{\partial \bar{c}}{\partial z}+V\frac{\partial c'}{\partial z}-\overline{V\frac{\partial c'}{\partial z}}=D\left(\frac{\partial^2 c'}{\partial z^2}+\frac{1}{r}\frac{\partial}{\partial r}\left(r\frac{\partial c'}{\partial r}\right)\right)-\frac{2\pi aD\left(\frac{\partial c}{\partial r}\right)\Big|_{r=a}}{\pi a^2} \quad (6.6)$$

The concentration variation in the r-direction is assumed to be almost smoothed out after a short time (Taylor, 1953), which means $\bar{c}\gg c'$ and $\frac{\partial c'}{\partial t}=0$. Moreover, we apply the hypothesis that the gradient of c' in the r-direction is much greater than that in the z-direction. In summary, we simplify equation (6.6) to

$$\left(V-\bar{V}\right)\frac{\partial \bar{c}}{\partial z}=\frac{D}{r}\frac{\partial}{\partial r}\left(r\frac{\partial c'}{\partial r}\right)-\frac{2\pi aD\left(\frac{\partial c}{\partial r}\right)\Big|_{r=a}}{\pi a^2} \quad (6.7)$$

Substituting (6.1) into (6.7) yields:

$$\frac{\partial}{\partial r}\left(r\frac{\partial c'}{\partial r}\right)=\frac{\bar{V}}{D}\left(r-\frac{2r^3}{a^2}\right)\frac{\partial \bar{c}}{\partial z}+\frac{2\pi aD\left(\frac{\partial c}{\partial r}\right)\Big|_{r=a}}{\pi a^2 D}r \quad (6.8)$$

Integrating equation (6.8) twice finds

$$c'=\frac{\bar{V}}{D}\left(\frac{1}{4}r^2-\frac{r^4}{8a^2}+A+B\ln r\right)\frac{\partial \bar{c}}{\partial z}+\frac{2\pi aD\left(\frac{\partial c}{\partial r}\right)\Big|_{r=a}}{\pi a^2 D}\frac{r^2}{4}+l\ln r+h \quad (6.9)$$

Since the value of the radius (r) could be zero, we find $B=l=0$. In addition, the

cross-sectional average of $c'(r,z,t)$ is zero, namely, $\frac{\int_0^a 2\pi r c'(r,z,t)\,dr}{\pi a^2}=0$. The solution of equation (6.8) is

$$c'=\frac{\bar{V}}{D}\left(\frac{1}{4}r^2-\frac{r^4}{8a^2}\right)\frac{\partial \bar{c}}{\partial z}+\frac{2\pi aD\left(\frac{\partial c}{\partial r}\right)|_{r=a}}{4\pi a^2 D}r^2-\left(\frac{\bar{V}a^2}{12D}\frac{\partial \bar{c}}{\partial z}+\frac{2\pi aD\left(\frac{\partial c}{\partial r}\right)|_{r=a}}{8\pi D}\right). \tag{6.10}$$

Furthermore, we use equation (6.1) and equation (6.10) to determine $\overline{V\frac{\partial c'}{\partial z}}$:

$$\overline{V\frac{\partial c'}{\partial z}}=\frac{\int_0^a 2\pi rV\frac{\partial c'}{\partial z}dr}{\pi a^2}=-\frac{a^2\bar{V}^2}{48D}\frac{\partial^2 \bar{c}}{\partial z^2}. \tag{6.11}$$

Consequently, the mass transport equation in terms of the cross-sectional average concentration ($\bar{c}(z,t)$) is derived through the substitution of equation (6.11) into (6.5):

$$\frac{\partial \bar{c}}{\partial t}+\bar{V}\frac{\partial \bar{c}}{\partial z}=\left(D+\frac{a^2\bar{V}^2}{48D}\right)\frac{\partial^2 \bar{c}}{\partial z^2}+\frac{2\pi aD\left(\frac{\partial c}{\partial r}\right)|_{r=a}}{\pi a^2}=D_{eff}\frac{\partial^2 \bar{c}}{\partial z^2}+\frac{2\pi aD\left(\frac{\partial c}{\partial r}\right)|_{r=a}}{\pi a^2}, \tag{6.12}$$

where D_{eff} is defined as the effective diffusion coefficient.

The convective flux in terms of the average concentration is expressed as $J_{con}=\rho\bar{V}\bar{c}$, and the diffusive flux is expressed as $J_{diff}=-\rho D_{eff}\frac{\partial \bar{c}}{\partial z}$, where ρ is blood density. Subsequently, equation (6.12) is changed into: J_{con} J_{diff}

$$\frac{\partial}{\partial t}\left(\frac{J_{con}}{\bar{V}}\right)+\frac{\partial J_{con}}{\partial z}=-\frac{\partial J_{diff}}{\partial z}+\frac{2\pi a\rho D\left(\frac{\partial c}{\partial r}\right)|_{r=a}}{\pi a^2}. \tag{6.13}$$

Based on the previous transmission line equations of oxygen transport in arteries (Yan et al., 2018) and mass transport in microcirculation (Tsai et al., 2003),

transmission line equations of mass transport in arterioles are developed as follows:

$$-\frac{\partial J_{diff}}{\partial z}=R_0 J_{con}+L_0\frac{\partial J_{con}}{\partial t}, \tag{6.14}$$

$$-\frac{\partial J_{con}}{\partial z}=-\frac{2\pi a\rho D\left(\frac{\partial c}{\partial r}\right)\Big|_{r=a}}{\pi a^2}, \tag{6.15}$$

where $-\frac{2\pi a\rho D\left(\frac{\partial c}{\partial r}\right)\Big|_{r=a}}{\pi a^2}$ represents the cross-sectional average of the diffusive flux of the substance from the blood in arterioles to the tissue, and z-direction is the direction of blood flow. According to equations of (6.13), (6.14) and (6.15), R_0 and L_0 are determined by the following expressions: $\begin{cases} R_0=\frac{\partial}{\partial t}\left(\frac{1}{\overline{V}}\right) \\ L_0=\frac{1}{\overline{V}} \end{cases}$. Our previous study demonstrates that L_0 is defined as the transit time of substance per unit distance and R_0 is the portion of the remaining substance convection per unit distance. R_0 and L_0 represent the resistivity and inertance of the convection to mass transport of substances in arterioles. In summary, the transmission line equations of the substance transfer in an arteriole are derived as follows:

$$\begin{cases} -\frac{\partial J_{diff}}{\partial z}=R_0 J_{con}+L_0\frac{\partial J_{con}}{\partial t} \\ -\frac{\partial J_{con}}{\partial z}=-\frac{2\pi a\rho D\left(\frac{\partial c}{\partial r}\right)\Big|_{r=a}}{\pi a^2} \end{cases}, \tag{6.16}$$

where $\begin{cases} R_0=\frac{\partial}{\partial t}\left(\frac{1}{\overline{V}}\right) \\ L_0=\frac{1}{\overline{V}} \end{cases}$.

6.1.2 Transmission line equations of mass transport in the capillary

Krogh cylinder, which includes a capillary and a part of the surrounding tissue, is applied in the modeling of the capillary (Krogh, 1919). The surrounding tissue is a cylindrical annulus in the model. Thus, the blood velocity in the Krogh cylinder is assumed as follows:

$$V(r)=\begin{cases}V, & 0<r<a_i\\ 0, & a_i<r<a_o\end{cases}, \tag{6.17}$$

where a_i and a_o are the radii of the capillary and the entire cylinder. The value of a_o is usually determined by $a_o=\frac{1}{\sqrt{\pi\rho'}}$, where ρ' is the capillary density. Blood velocity (V) in the capillary is regarded as a random variable with the normal distribution. And the probability function ($P(V)$) is conventionally specified by

$$P(V)=\frac{e^{-(V-V_m)^2/2\sigma_V{}^2}}{\sqrt{2\pi}\sigma_V}, \tag{6.18}$$

where V_m and σ_V are the mean velocity and the standard deviation of velocity, respectively. The mean velocity (V_m) in the capillary is denoted as the following expression:

$$V_m=\frac{Fla_o{}^2}{a_i{}^2}, \tag{6.19}$$

where F is the volume flow rate of blood per unit tissue volume and l is the length of the cylinder.

Mass transport in the capillary model can be described by the convection-diffusion equation as well:

$$\frac{\partial c}{\partial t}+V(r)\frac{\partial c}{\partial z}=D\left(\frac{\partial^2 c}{\partial z^2}+\frac{1}{r}\frac{\partial}{\partial r}\left(r\frac{\partial c}{\partial r}\right)\right). \tag{6.20}$$

Same as the derivation of the transmission line equations of mass transport in the arteriole, we separate the substance concentration in the capillary model into the cross-sectional average part and r -dependent part, writing $c(r,z,t)=\bar{c}(z,t)+c'(r,z,t)$. The average concentration of the substance ($\bar{c}(z,t)$) over the cross-section is determined by the following expression:

$$\bar{c}(z,t)=\frac{1}{\pi {a_o}^2}\int_0^{a_o}\int_{-\infty}^{+\infty}P(V)c(r,z,t)\,dV\,2\pi r dr\,, \tag{6.21}$$

where $\int_{-\infty}^{+\infty}P(V)c(r,z,t)\,dV$ is the mean concentration.

Subsequently, the derivation process, which is same as that in the development of the transmission line equations of mass transport in the arteriole, is employed in the transformation of the convection-diffusion equation in the capillary model. Thus, mass transport equation in the capillary model is changed into the form which is consistent with that in the arteriole:

$$\frac{\partial \bar{c}}{\partial t}+\bar{V}\frac{\partial \bar{c}}{\partial z}+\overline{V\frac{\partial c'}{\partial z}}=D\left(\frac{\partial^2 \bar{c}}{\partial z^2}\right)+\frac{2\pi a_o D\left(\frac{\partial c}{\partial r}\right)\Big|_{r=a_o}}{\pi {a_o}^2}\,, \tag{6.22}$$

where $-\frac{2\pi a_o D\left(\frac{\partial c}{\partial r}\right)\Big|_{r=a_o}}{\pi {a_o}^2}$ is the diffusive flux at the boundary from the Krogh-cylinder model to outer tissue and is assumed to be zero (Frankel and Brenner, 2006); $\bar{V}$ is the cross-sectional average velocity of the Krogh-cylinder model and

is calculated by $\bar{V} = \frac{1}{\pi {a_o}^2}\int_0^{a_o}\int_{-\infty}^{+\infty}|V|P(V)dV\,2\pi r dr = Fl$; the expression of $\overline{V\frac{\partial c'}{\partial z}}$ is obtained on the basis of equation (6.21):

$$\begin{aligned}\overline{V\frac{\partial c'}{\partial z}} &= \frac{1}{\pi {a_o}^2}\int_0^{a_o}\int_{-\infty}^{+\infty}P(V)V\frac{\partial c'}{\partial z}dV\,2\pi r dr \\ &= -\frac{1}{8D}\left[\left({a_i}^2-\frac{1}{\pi\rho'}\right)\left({\sigma_V}^2{a_i}^4\pi^2\rho'^2+2F^2l^2\right)-\left(4\pi\rho'{\sigma_V}^2{a_i}^4+\frac{4F^2l^2}{\pi\rho'}\right)\ln\left(a_i\sqrt{\pi\rho'}\right)\right]\frac{\partial^2\bar{c}}{\partial z^2}\end{aligned} \quad (6.23)$$

As a result, the mass transport equation in the capillary model is given as follows:

$$\frac{\partial\bar{c}}{\partial t}+Fl\frac{\partial\bar{c}}{\partial z}=D_{eff}\frac{\partial^2\bar{c}}{\partial z^2}, \quad (6.24)$$

where $D_{eff}=D+\frac{1}{8D}\left[\left({a_i}^2-\frac{1}{\pi\rho'}\right)\left({\sigma_V}^2{a_i}^4\pi^2\rho'^2+2F^2l^2\right)-\left(4\pi\rho'{\sigma_V}^2{a_i}^4+\frac{4F^2l^2}{\pi\rho'}\right)\ln\left(a_i\sqrt{\pi\rho'}\right)\right]$.

Moreover, according to the previous definitions of the convective flux and the diffusive flux, this equation is transformed into:

$$\frac{1}{Fl}\frac{\partial J_{con}}{\partial t}+\frac{\partial J_{con}}{\partial z}=-\frac{\partial J_{diff}}{\partial z}. \quad (6.25)$$

According to the definition of Péclet number (Pe), the gradient of the convective flux along the flow direction is converted into the expression with the diffusive flux:

$$-\frac{\partial J_{con}}{\partial z}=-Pe\frac{\partial J_{diff}}{\partial z}=-\frac{N_{con}}{N_{diff}}\frac{\partial J_{diff}}{\partial z}=-\frac{1}{\frac{N_{total}}{N_{con}}-1}\frac{\partial J_{diff}}{\partial z}, \quad (6.26)$$

where N_{con}, N_{diff} and N_{total} are the rate of convection, the rate of diffusion and the total rate of mass transport (Beard and Wu, 2009, Cussler, 1984), respectively. Substituting equation (6.26) into equation (6.25) yields

$$\frac{1}{Fl}\frac{\partial J_{con}}{\partial t}=-\left(1+\frac{1}{\frac{N_{total}}{N_{con}}-1}\right)\frac{\partial J_{diff}}{\partial z}. \quad (6.27)$$

Regarding the previous transmission line equations in the artery and arteriole as reference, the transmission line equations of mass transport in the capillary model are expressed by

$$\begin{cases} -\dfrac{\partial J_{diff}}{\partial z} = R_0 J_{con} + L_0 \dfrac{\partial J_{con}}{\partial t} \\ -\dfrac{\partial J_{con}}{\partial z} = G_0 J_{diff} + C_0 \dfrac{\partial J_{diff}}{\partial t} \end{cases}, \tag{6.28}$$

where R_0 and L_0 represent the resistivity and inertance of the convection to mass transport; G_0 and C_0 represent the permeability and compliance. Since the capillary behaves as the rigid vessel (Fung et al., 1966, Leonard and Jorgensen, 1974), the compliance of the capillary wall could be ignored. Based on the aforementioned understanding of the resistance, the resistance to diffusion is correlated with the time-derivative of the velocity. Moreover, the experimental studies showed that the time-varying nature of capillary flow hardly altered the oxygen gradient (the diffusion) in comparison with the constant velocity model (Aroesty and Gross, 1970, Graeser et al., 1969). Thus, the resistance of the convection to the diffusion is neglected as well. In summary, the transmission line equations of mass transport in the capillary model are developed as follows:

$$-\frac{\partial J_{diff}}{\partial z} = L_0 \frac{\partial J_{con}}{\partial t}, \tag{6.29}$$

$$-\frac{\partial J_{con}}{\partial z} = G_0 J_{diff}. \tag{6.30}$$

L_0 and G_0 are determined by the comparison of a new equation, which is derived through the substitution of equation (6.30) into equation (6.29), with equation (6.27):

$$\begin{cases} L_0 = \dfrac{1}{Fl} \\ G_0 = \dfrac{N_{con} / N_{total}}{l} \end{cases}. \tag{6.31}$$

According to the proposed transmission line equations in the artery and equation (6.31), L_0 is the transit time per unit distance, and G_0 is the ratio of the rate of convection to the total rate per unit distance. Moreover, L_0 represents the inertance of the convection to mass transport of substances in the capillary, and G_0 represents the proportion of the convection which is converted into the diffusion. In summary, the transmission line equations of substance transfer in the capillary are expressed by the following equations:

$$\begin{cases} -\dfrac{\partial J_{diff}}{\partial z} = L_0 \dfrac{\partial J_{con}}{\partial t} \\ -\dfrac{\partial J_{con}}{\partial z} = G_0 J_{diff} \end{cases}, \tag{6.32}$$

where $\begin{cases} L_0 = \dfrac{1}{Fl} \\ G_0 = \dfrac{N_{con} / N_{total}}{l} \end{cases}$.

6.2 Verifications

The transmission line equations of mass transport and mass dispersion phenomenon in the arteriole are consistent with the developed equations of oxygen transport in the artery. The transmission line equations of oxygen transport are determined to be reliable in our study through the comparison of the lumped parameter model of oxygen transport with the 3D computational model. Thus, the transmission line equations of mass transport in the arteriole is supposed to be reliable. In addition,

eight studies (shown in Tab. 6-1) which concentrated on the concentration distribution of the substance in the capillary were employed in the verification of the transmission line equations of mass transport in the capillary. The corresponding lumped parameter models of mass transport based on the transmission line equations of mass transport were established to investigate the concentration distributions of different substances in different capillaries. We used an electric circuit (shown in Fig. 6-1), which was proposed according to the transmission line equations of mass transport, to show the basic element of the lumped parameter model of mass transport in the capillary. Moreover, the parameters and boundary conditions applied in the lumped parameter models were derived from the previous studies correspondingly.

Table 6-1 The previous studies used in the verification of the transmission line equations of mass transport.

Category	Sub-category	Previous study
Capillary geometry	Straight	Beard et al. Bello et al.
	Coiled	Lewandrowska et al.
	Rectangular cross-section	Yan et al.
Substance category	Drug	Ye et al.
	Nanoparticle	d'Orlyé et al.
Animal experiment	Rat brain	Tao et al. Thorne et al.

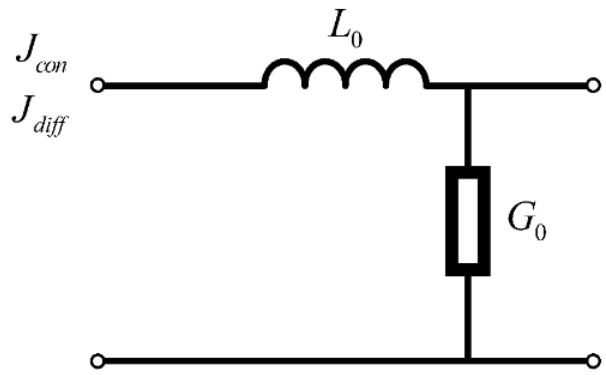

Figure 6-1 Electrical analogue of mass transport with inductance (L_0) and conductance (G_0), which represents the basic element of the lumped parameter model. The convective flux and diffusive flux of the substance in the capillary is regarded as the current and voltage in the circuit, respectively.

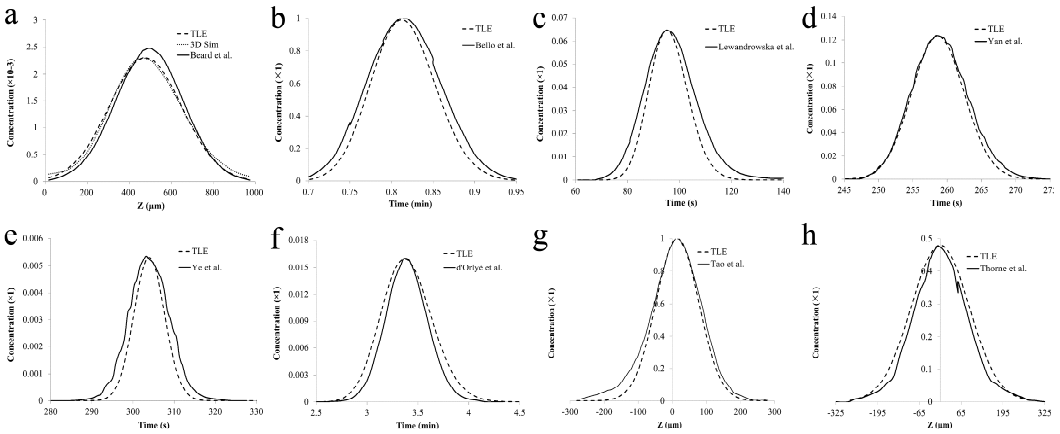

Figure 6-2 Comparisons of concentration distributions of substances in straight capillaries (**a** and **b**) (Bello et al., 1994, Beard and Wu, 2009), in **c** coiled capillary (Lewandrowska et al., 2013), in **d** capillary with rectangular cross-section (Yan et al., 2015), in terms of **e** drug (Ye et al., 2012) and **f** nanoparticle (d'Orlye et al., 2008), in rat brains (**g** and **h**) (Tao and Nicholson, 1996, Thorne and Nicholson, 2006). The method with transmission line equations of mass transport is abbreviated to TLE.

The substance concentration distributions in capillaries were determined through the literatures and the lumped parameter models of the substance transport based on the transmission line equations of mass transport. The differences of the substance concentration distributions between the experimental studies and the lumped parameter models were quite modest as shown in Fig. 6-2. As a consequence, the concentration distribution of the substance in the capillary could be provided by the lumped parameter model of mass transport based on the transmission line equations of mass transport, and the results of the lumped parameter model were consistent with those of the measurements in previous studies. In summary, the transmission line equations of mass transport in the arteriole and capillary are reliable for investigating the concentration distribution of the substance in blood.

Few *in vivo* non-invasive methods can be used in the measurement of the systemic distribution of the substance in capillaries. Most of studies focused on the numerical predictions of the substance distribution in the Krogh-cylinder model, *in vitro* experiments of investigating the concentration distribution of the substance in capillaries with different geometries, experiments of measuring the distributions of different substances in the capillary tube, and measurements of the substance distribution in animal experiments. Thus, the numerical prediction proposed by Beard et al. and the 3D simulation were selected as the references for verifying the

theoretical prediction with the transmission line equations of mass transport. Thereafter, three capillary geometries (straight, coiled, and rectangular cross-section), two types of substances (drug and nanoparticle), and two animal experiments of measuring the substance concentration in rat brains were included in the selection of these studies which were compared with the lumped parameter model of mass transport for the verification of the transmission line equations of mass transport in capillaries.

6.3 Discussions

The processes of proposing the transmission line equations of mass transport in arterioles and capillaries are introduced in this study. Specifically, the developed transmission line equations of oxygen transport in arteries are applied as the theoretical reference for the development of the transmission line equations of mass transport in arterioles and capillaries. Moreover, mass transport theory in an arteriole demonstrates that the changes in the convective flux of the substance transfer is converted into the diffusive flux from the blood to the tissue, which is treated as the basis of developing the transmission line equations of mass transport in arterioles. This theory is applicable for the development of the transmission line equations of mass transport in capillaries as well. Meanwhile, the Krogh cylinder model is introduced in this development, and the model is usually used for the numerical investigation of the concentration distribution of the substance in the capillary with the surrounding tissue. Consequently, the transmission line equations

of mass transport in capillaries are proposed on the basis of mass transport theory in capillaries and the Krogh cylinder model. Additionally, the convection-diffusion equations in arterioles and capillaries are transformed into the forms including the cross-sectional average concentration based on the Taylor-Aris dispersion theory. The mathematical expressions of the parameters (R_0 and L_0) in the transmission line equations of mass transport in arterioles and the parameters (L_0 and G_0) in the equations of capillaries are found through the transformation of the convection-diffusion equations with the replacement of the concentration by the cross-sectional average variable. R_0 and L_0 in the equations of arterioles represent the properties of the convection in mass transfer, while L_0 and G_0 in the equations of capillaries represent the properties of the convection and diffusion, respectively. The transmission line equations of mass transport in arterioles and capillaries can be applied in constructing the lumped parameter model of mass transport for predicting the systemic distribution of the substance concentration in the microvascular tree. Investigating the concentration distribution of the substance in the microvascular system of the corresponding tissue is supposed to be beneficial in the evaluation of the organ function, the assessment and intervention of illnesses, and the disease recovery.

The parameters in the transmission line equations of mass transport in arterioles and capillaries depend on the transformation of the convection-diffusion equation which includes the replacement of the concentration with the cross-sectional average

concentration based on Taylor-Aris dispersion theory. Taylor-Aris dispersion theory offers an efficient scheme for understanding the convection-diffusion mass transport process (Frankel and Brenner, 2006), and is conventionally applied to determine the diffusion coefficient in the *in vitro* measurement of the substance distribution (Bello et al., 1994, Cottet et al., 2010). This theory is applicable for the thin tube which satisfies the condition $\frac{4l}{a} \geq 690$ (Taylor, 1954), where l and a is the length and the radius of the tube, respectively. The average length and average diameter of arterioles are 950 μm and 7 μm (Wiedeman, 1963). The average capillary length is 412 μm, and the capillary diameter is from 5 μm to 10 μm (Tsai et al., 2003). Therefore, Taylor-Aris dispersion theory is applicable in the arteriole and capillary. Some scholars used Taylor-Aris dispersion theory to develop an empirical expression for numerically predicting the substance concentration distribution in the capillary (Bello et al., 1994, d'Orlye et al., 2008, Lewandrowska et al., 2013, Beard and Wu, 2009). The expression is analogous to the probability function of the normal distribution and is composed of time, longitudinal distance, and effective diffusion coefficient. Whereas, the effect of substance convection on diffusion in mass transport is not involved in the expression for estimating the substance concentration. The concentration distribution of the substance in the capillary is mainly dependent on convection and diffusion. The change in the convective flux along the flow direction significantly affects the amount of the diffusive flux. Thus, the mutual relationships between convection and diffusion are considered in the development of the transmission line equations of mass transport

in the capillary to acquire a more precise prediction of the substance concentration distribution. Specifically, the convection in mass transport equation is converted into the diffusion based on the definition of Péclet number, and the equation which expresses the correlation between the gradient of the convective flux and the diffusive flux is proposed according to the phenomenon that the transmitted flux of the convection is converted into the diffusion in the capillary with the surrounding tissue. The interaction between convection and diffusion in mass transport theory is regarded as the theoretical basis for developing the transmission line equations of mass transport in arterioles and capillaries.

The 3D CFD simulation of the entire vascular system can be carried out to obtain the systemic distribution of the substance concentration in arteries, arterioles, and capillaries. The entire vascular system is comprised of complex arterial vasculature and a large number of microvessels. This simulation would cost considerable computational resources and consume an amount of time (Xiao et al., 2013, Randles et al., 2015). Whereas, the aforementioned numerical analysis with the empirical expression and the method with the transmission line equations of mass transport simplify the spatial structure of the whole vascular system and just require fewer computational resources and time to investigate the substance concentration distribution in arteries, arterioles, and capillaries. Thereafter, since the influence of convection on diffusion is considered in the development of the transmission line equations, the lumped parameter model of mass transport based on the transmission

line equations provides a more precise prediction of the concentration distribution of the substance in the whole vascular system in comparison with the previous numerical studies. Joint consideration of the correlation between convection and diffusion in the transmission line equations of mass transport is helpful for enhancing the accuracy of the prediction of the substance concentration in the vascular system, which further indicates the advantage and significance of these equations.

The prediction of the substance distribution in the microvascular system could be acquired through the numerical analysis of the lumped parameter model of mass transport based on the transmission line equations and offers quantitative guidance for the evaluation of the organ function, the assessment and treatment of illnesses, and the disease recovery. Mass transfer from arterioles and capillaries to the tissue is the principal source of the substance in tissue, and the content of the substance in arterioles and capillaries plays a significant role in the function of the corresponding tissue. Tissue needs nutrients to perform normal function, and the nutrients generally come from blood in arterioles and capillaries. Nutrients primarily transmit through blood flow in the vascular system including arteries, arterioles, and capillaries. Thus, having a good knowledge of the concentration distribution of nutrient is fundamental for evaluating the tissue status. For instance, low oxygen concentration causes a reduction of protein in muscle tissue (Caron et al., 2009). The status of the tumor is assessed through the prediction of the change in

microvascular vasculature (Kimura et al., 1996, Deb et al., 2012). Vascular imaging with contrast agent provides an evaluation of the spatial structure of microvessels (Turetschek et al., 2001). Vascular imaging quality mainly depends on the concentration distribution of the contrast agent. Having a more precise prediction of the distribution of the contrast agent is in favor of improving the vascular imaging quality and further enhances the monitoring of tumor growth.

Since the substance in microcirculation is derived from blood in arteries, the development of the lumped parameter model of mass transport in the microvascular system requires the data of the mass flux from arteries to microvessels. The mass flux is generally equal to that at the terminal site of the lumped parameter model of mass transport in arteries. Understanding the systemic distribution of the substance concentration in the whole circulatory system needs the coupling method of the lumped parameter models of mass transport in arteries, arterioles, and capillaries. Figuring out the interactions among these three lumped parameter models is of great significance in establishing the coupling model of mass transport in the entire vascular system. The development of the boundary condition of mass transport in each model is a way to realize the interactions among these models (Esmaily Moghadam et al., 2013, Grote and Kirsch, 2004). Based on the law of mass conservation and the continuity of mass flux, the convective flux at the outlet of an artery is distributed into the inlet fluxes of convection in the downstream arterioles, while the sum of diffusive fluxes in the arterioles is applied in the outlet boundary

condition of the artery (Fig. 6-3). This development of the boundary conditions in arteries and arterioles is applicable at the interfaces between arterioles and capillaries as well. Thereafter, mass transfer in human body mainly depends on blood flow in the entire vascular system including arteries, arterioles, and capillaries. In summary, in order to investigate the distribution of the substance concentration in the whole vascular system, the combination of the transmission line equations of mass transport in arteries, arterioles, and capillaries is utilized as the theoretical basis of the derivation of the lumped parameter model in the entire vascular tree, and the interactions among these three types of vessels are realized through employing the aforementioned boundary conditions. The transmission line equations are used to establish a lumped parameter model of oxygen transport in the vascular system including arteries, arterioles, and capillaries, and the distribution of oxygen concentration along the vascular system is numerically predicted through using the model. On the other hand, the model is also applied for acquiring oxygen consumption along the vascular system when oxygen distribution in tissues of human organs is obtained. Thereafter, oxygen tension in main organs is listed in Tab. 6-2. Consequently, based on the transmission line equations of mass transport, having a good knowledge of oxygen distribution in tissues is beneficial for understanding the oxygen consumption along the vascular system (Fig. 6-3). Moreover, the lumped parameter model of mass transport in the whole vascular system is used to predict the concentration distribution of targeted drug and chemotherapeutic drug in vessels and tissues, which is further helpful for improving

the efficiency of drug therapy. Enhancing the drug concentration in the targeted site and diseased region needs the clear understanding of the systemic distribution of drug in vessels and tissues. In addition, numerous targeted drugs and chemotherapeutic drugs affect normal tissues detrimentally due to their toxicities. Predicting the concentration distribution of drug in the entire vascular system is beneficial in alleviating the adverse effect on normal tissues. Determining the drug concentration distribution in vessels and tissues provides guidance for putting forward several ways of improving the efficiency of targeted drug therapy and chemotherapy. Clinicians can use the lumped parameter model of mass transport in the whole vascular system to find out the systemic distribution of drug concentration in vessels and tissues and further optimize the injection site and system. The purposes of the optimization are to increase the drug content in the targeted site and diseased region, and to decrease the drug content in normal tissues eventually. In conclusion, transmission line equations of mass transport in arterioles and capillaries developed in this study are treated as a complement to the theoretical basis for constructing the whole lumped parameter model of mass transport in the circulatory system, which is valuable for improving the assessment and treatment of diseases.

Table 6-2 Oxygen tension in main human organs.

Organ	Oxygen tension (mmHg)	Source
Brain	37	(Samaja, 1988)
Heart	27	(Woodson and Auerbach, 1982)
Kidneys	65	(Samaja, 1988)
Legs	34	(Jorfeldt and Wahren, 1971)

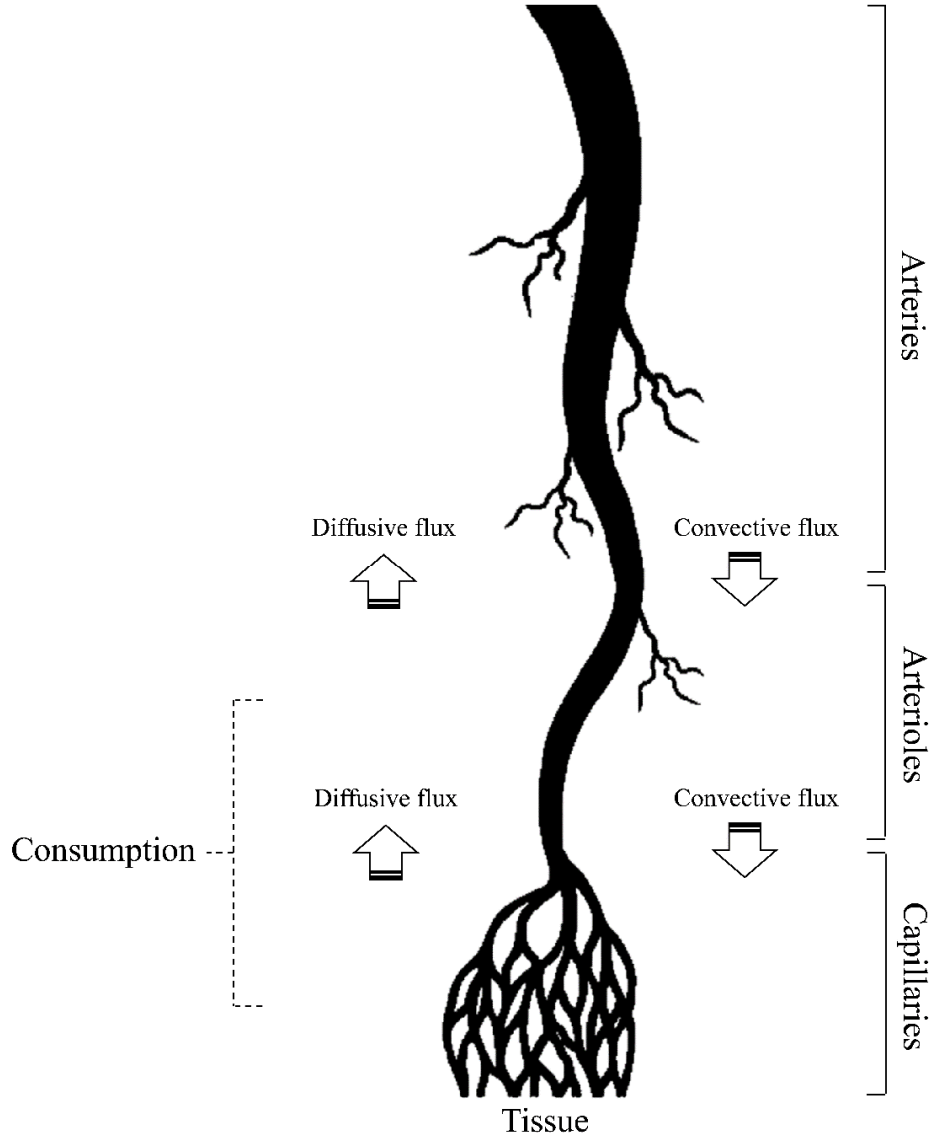

Figure 6-3 Mass transfer in the vascular system.

This study derives the transmission line equations of oxygen transport in arteries, arterioles, and capillaries. These equations are included in the lumped parameter model of oxygen transport in order to numerically predict the oxygen concentration distribution in the systemic arterial tree. I believe that my study makes a significant contribution to the literature because the developed method allows us to reduce the computational requirements for estimating the oxygen concentration distribution. A 3D simulation of oxygen transport in the entire vascular system needs a large number of computational resources and time to obtain the systemic distribution of oxygen concentration in the vessels. The advantages of the proposed lumped parameter model are presented in two aspects according to the transmission line equations: in mathematics, partial differential equations are converted into ordinary differential equations, which simplifies the numerical analysis; in physics, the complex vascular network is divided into a few lumped parameter elements, while it requires a large number of grid elements to acquire accurate results in the 3D simulation. Moreover, my method is also more accurate than the previously proposed empirical expression because the hemodynamics is considered as a significant factor for calculating the oxygen concentration in the transmission line equations. The advantages and disadvantages of the 3D computational model, the empirical expression, and the transmission line equations of oxygen transport in terms of the systemic circulation perspective are summarized in Tab. 6-3.

Table 6-3 Advantages and disadvantages of the 3D computational model, the empirical expression, and the transmission line equations of oxygen transport

Method	Advantage	Disadvantage
3D model	Considering hemodynamics and complex vascular geometries	Numerous computational resources and time
Empirical expression	Reducing computational requirements	Ignoring hemodynamics and complex vascular geometries
Transmission line equations	Simplifying numerical analysis and complex vascular network	Difficult to calculating parameters in equations

There exist some limitations of these novel transmission line equations of mass transport in arterioles and capillaries. First, for the sake of having a better understanding of the substance distribution, these equations are supposed to be adjusted with the consideration of more physiological properties of substance transmitting in the microvascular system. Second, the transmitted flux of substance from microcirculation to tissue affects the accuracy of the numerical prediction of the substance distribution in the microvascular system and is composed of the diffusive fluxes from arteriole and capillary to tissue. In terms of arteriole, the diffusive flux is hardly measured by noninvasive methods and is generally substituted with the substance consumption in the surrounding tissue at rest. Since the Krogh cylinder model utilized as the capillary model in the development of the transmission line equations of mass transport includes the surrounding tissue, the mass flux in the lumped parameter model of mass transport contains the diffusive flux from capillary to tissue. Third, the substance consumption in the surrounding

tissue of a capillary is ignored in the development of the transmission line equations of mass transport, which has an impact on the time-varying nature of the substance concentration in the capillary model with the surrounding tissue. A noninvasive way of measuring the consumption in the local tissue around a capillary is required for more precisely determining the concentration distribution of the substance, and this consumption will be considered in our future study.

CHAPTER 7 USE OF TRANSMISSION LINE EQUATIONS OF OXYGEN TRANSPORT FOR UNDERSTANDING OXYGEN DISTRIBUTION IN TRANS-FEMORAL RESIDUUM ARTERIES

Health problems in residual limb after trans-femoral amputation have an adverse effect on amputees' rehabilitation process and might further be harmful for their physical health. The underlying biomechanical mechanisms of these issues have not been clearly figured out. The spatial structure of residuum vessels changes significantly after amputation, and the change in vasculature affects blood flow and oxygen transport in residuum arteries. Moreover, change in oxygen distribution of the residuum plays a significant role in the fundamental mechanisms of these problems. Consequently, as oxygen in tissues of the residual limb is derived from blood flow in arteries, investigations of blood flow and oxygen concentration distribution in the transformed arterial vasculature are required for more fully elucidating the mechanisms of these problems in residuum.

Previous studies about arterial responses in the residuum after trans-femoral amputation mainly concentrated on changes in the residuum vasculature (Dong et al., 2016), the relationship between hemodynamic state and health problems after amputation (Dong et al., 2015), and oxygen transport in an artery of the residual limb (Yan et al., 2017). Nevertheless, studies focusing on oxygen transport in the arterial tree of the residuum after trans-femoral amputation were few.

A number of numerical investigations of oxygen transport in 3D arteries were performed and coupling models of blood flow and oxygen transport were employed in these 3D simulations to predict the oxygen concentration distribution in the arteries (Moore and Ethier, 1997, Buerk and Goldstick, 1982, Qiu and Tarbell, 2000, Tada, 2010). The convection-diffusion equation was conventionally applied as the governing equation of oxygen transport in these computational models. These studies mainly focused on the local distribution of oxygen concentration in arterial wall and hardly paid attention to the overall nature of oxygen distribution in the arteries. Moreover, oxygen concentration at the outlet boundary conditions of numerical investigations was generally simplified as a constant value. Thus, effects of the downstream arteries and microvessels on oxygen transport in arteries of interest were ignored in these computational simulations.

Ignorance of arteries and microvessels causes a decrease in the accuracy of the numerical prediction of oxygen distribution and blood flow in the vessels of interest. In terms of blood flow, the values of pressure or flowrate fraction at the outlet of the vascular model are assumed to be constant without the consideration of effects of the downstream vasculature. Compliance and resistance of the downstream arterial bed and microvascular bed are neglected in these settings of outlet boundary conditions. Several schemes have been developed for coupling the effects of the downstream vessels in the 3D computational fluid dynamic (CFD) simulations of

the arteries. Lumped parameter models and one-dimensional vascular tree model in these numerical methods are conventionally applied at outlets of these computational models (Schaaf and Abbrecht, 1972, Stettler et al., 1981, Stergiopulos et al., 1992, Stergiopulos et al., 1999, Stergiopulos et al., 1995, Olufsen et al., 2000). Studies have proved that blood flow closely correlates with oxygen transport in arteries and microvessels (Qiu and Tarbell, 2000, Liu et al., 2011, Coppola and Caro, 2008, Duling, 1972, Prewitt and Johnson, 1976, Sullivan and Johnson, 1981). Oxygen consumption in tissue is primarily supplied by oxygen transfer from blood to tissue. The way of transferring oxygen from blood to tissue is dependent on blood flow in arteries, arterioles, and capillaries. Eventually, oxygen in tissue is derived from mass transport from microvessels to tissues in microcirculation. Moreover, oxygen content in arteries of interest relates to oxygen transport in the downstream arteries and the corresponding microcirculation (Ivanov et al., 1999, Pittman and Duling, 1975, Swain and Pittman, 1989). In summary, to acquire a more precise prediction of oxygen concentration distribution in the artery of interest, the consideration of effects of oxygen transport in the downstream vessels is required in the 3D simulation of blood flow and oxygen transport. Although the 3D model of the whole vascular tree including the artery of interest, the downstream arteries, and microvessels is supposed to be used for performing the coupling of the artery of interest and the downstream vessels, it needs considerable computational resources and consumes a large amount of time. Most of research groups barely have enough resources to perform the simulation of

the entire vascular tree.

We have proposed transmission line equations of oxygen transport for simulating oxygen mass transfer in the entire vascular tree (Yan et al., 2018). In this study, the transmission line equations of oxygen transport were applied as the theoretical basis for developing the lumped parameter models of oxygen transport in the downstream vascular beds of the residuum arteries. These lumped parameter models were used in the settings of the outlet boundary conditions of the thigh arteries in the residual limb after trans-femoral amputation. The 3D computational model of the residuum vasculature coupling with the lumped parameter model of oxygen transport was established to provide a more accurate estimation of oxygen distribution in arteries of the residual limb after trans-femoral amputation. Moreover, the *in vitro* experiment with a 3D printing vascular model of the residuum arteries was carried out to validate the aforementioned computational simulation.

Details in the numerical simulation and the *in vitro* experimental study are introduced in section 3.3. In order to acquire a more precise prediction of oxygen distribution in the 3D vascular model, the boundary condition with the lumped parameter model of oxygen transport was employed at outlets of the residuum arteries, which added the consideration of effects of downstream vessels on the residuum vasculature. The study in this chapter is divided into three parts; first, the proposed boundary condition of oxygen transport is verified through the

comparisons between elongated models and non-elongated models with this boundary condition; second, blood flow and oxygen distribution in residuum arteries are numerically predicted in the CFD simulation coupled with oxygen transport, and the effect of downstream vascular beds on oxygen transport in residuum vasculature is considered in the numerical prediction; third, the comparison between the *in vitro* experiment and the computational simulation is conducted to validate the computational model of oxygen transport in residuum arteries.

7.1 Results in numerical verifications, computational simulation, and *in vitro* experiment

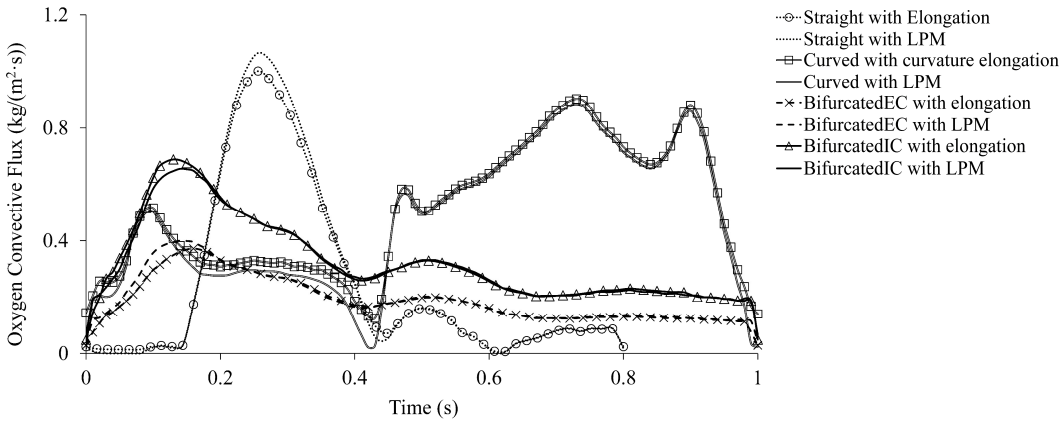

Figure 7-1 Oxygen convective fluxes at the ends of the non-elongated vessels and at the corresponding locations of the vessel with elongation. In the bifurcated model, the external carotid branch was abbreviated to bifurcatedEC, while the internal carotid branch was abbreviated to bifurcatedIC.

The comparisons between the elongated vessels and the non-elongated vessels were

carried out in terms of three regular geometries of vascular models in order to numerically verify the boundary condition of oxygen transport with the lumped parameter model of oxygen transport. The results of these computational investigations showed that the difference of oxygen content between the computational models with elongations and those with lumped parameter models was quite modest (Fig. 7-1). The developed boundary condition of oxygen transport with the lumped parameter model was supposed to be consistent with the extension of the vascular model, which could further describe the effect of downstream vascular tree on oxygen distribution in the artery of interest. In summary, the proposed boundary condition of a lumped parameter model of oxygen transport showed consistency with the elongation of the vascular model and provided a reliable and efficient method to demonstrate the response of downstream vascular bed to the oxygen transport in the vascular region of interest.

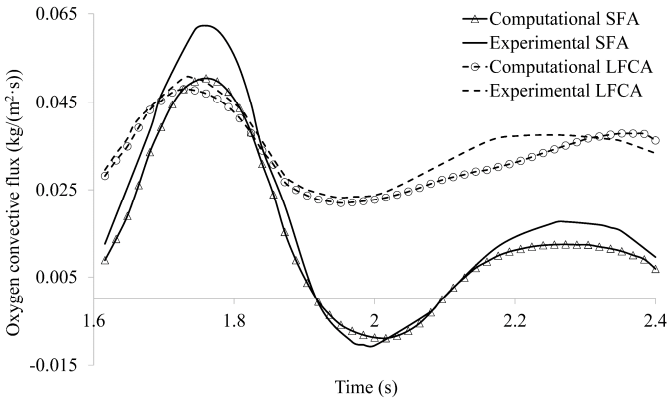

Figure 7-2 Comparisons of the oxygen convective fluxes between the computational simulation and the experimental measurement.

In addition, an experimental platform with a 3D printing replica of trans-femoral residuum vasculature was built to validate the computational simulation of oxygen transport and blood flow in the residuum arterial tree with the lumped parameter model of oxygen transport and blood flow of the downstream vessels. The measured oxygen convective flux in the experimental study was in accordance with that of the numerical prediction in the computational model as shown in Fig. 7-2. The maximum difference of the convective flux in SFA between the experimental measurement and the numerical investigation was 19.02%, which the maximum difference of this flux in LFCA was 15.30%. Moreover, the maximum differences in SFA and LFCA were observed at peak values of the systole and diastole, respectively. As a consequence, the computational simulation of the residuum arteries with the lumped parameter model of oxygen transport was generally determined to be reliable through the comparison between the simulation and the experiment.

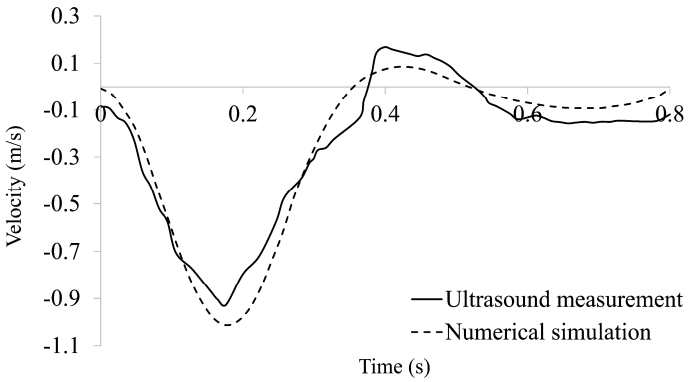

Figure 7-3 Comparison of blood velocity in residuum DFA between the ultrasound measurement and the numerical simulation of the residuum vasculature.

For the sake of precisely understanding blood velocity distribution and oxygen concentration distribution in the vessels of interest, the Windkessel model and the lumped parameter model of oxygen transport were coupled in the computational simulation of blood flow and oxygen transport in the arterial vasculature of the residuum limb. These numerical methods were applied to add the effects of downstream vascular beds on blood flow and oxygen transport in this simulation. And parameters in the Windkessels model were derived from the ultrasound data and literatures. Blood velocity in residuum DFA obtained by the ultrasound measurement was compared with the velocity predicted through the numerical investigation of the residuum arteries with the Windkessel model and the lumped parameter model of oxygen transport. It was indicated that the numerical prediction of blood velocity in residuum DFA was consistent with the ultrasound measurement (Fig. 7-3). The maximum difference of blood velocity between the ultrasound measurement and the numerical investigation was 15.94%. The difference of blood velocity between the measurement and the simulation was quite modest, thus, the computational model of residuum vasculature in this study was validated in terms of blood flow.

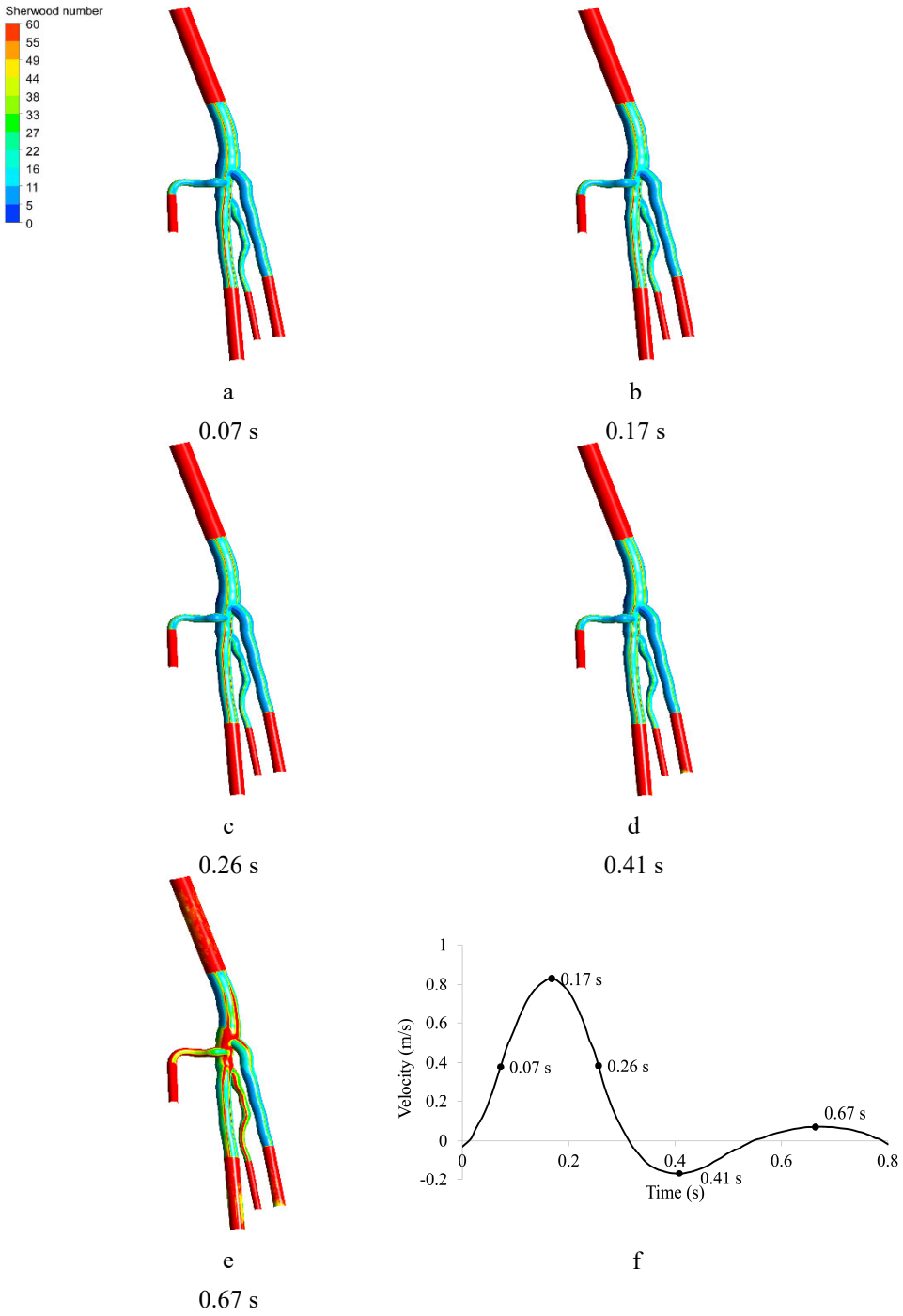

Figure 7-4 The distributions of Sherwood number at five moments of a cycle.

A dimension number (Sherwood number) was applied to describe the oxygen distribution in the arterial wall of the residuum vasculature. Sherwood number is defined as the ratio of convection rate to diffusion rate in mass transport and is

generally abbreviated to Sh. Sh is a dominant factor in evaluating the development of hypoxia in the arterial wall and plays a significant role in determining the appearance region of atherosclerosis (Qiu and Tarbell, 2000, Tarbell, 2003, Okamoto et al., 1983), as hypoxia causes the development of atherosclerotic plaque (Ogawa et al., 1990, Matsushita et al., 2000, Hulten and Levin, 2009). In this study, Sh was regarded as an index for evaluating the status of the arteries in the residual limb. Oxygen concentration distribution in residuum vasculature was obtained through conducting the numerical analysis of the computational model, while we acquired the Sh distribution at the arterial wall of the residuum vessels. Forward blood flow hardly caused the changes in the Sh distribution of the residuum arteries, whereas backflow contributed to the increment of the Sh values at the arterial wall (Fig. 7-4). Low Sh values were observed at regions with the most complex geometries in the spatial vasculature. Specifically, these regions located at the curved branches of the entire arterial tree. The geometry of the residuum vasculature was indicated to be the main factor for determining the Sh distribution at the vascular wall during forward blood flow in a cycle. The increase in Sh at the arterial wall referred to the augmentation in the flux of oxygen transfer into the wall during flow recirculation, thus, backflow supplied more oxygen for the vascular wall at the diastolic phase of a cycle.

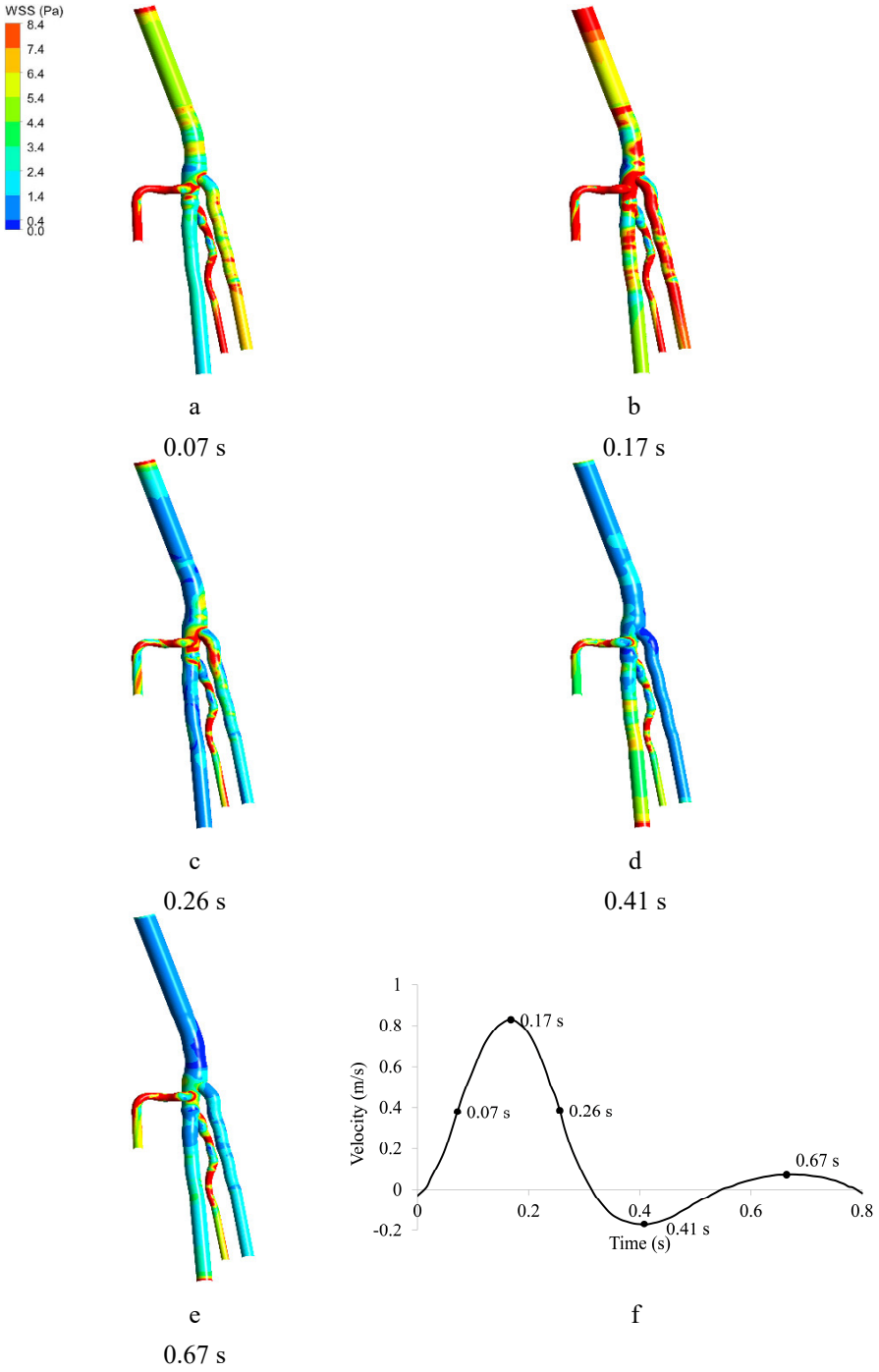

Figure 7-5 The distributions of wall shear stress at five moments of a cycle.

Wall shear stress (WSS) significantly affects the development of atherosclerosis and plays a key role in the function of the vascular wall as well (Palumbo et al., 2002, Chatzizisis et al., 2011). Low WSS (< 0.4 Pa) has a detrimental effect on the arterial

wall and leads to the formation of the atherosclerotic plaque. The values of WSS in the residuum arteries were calculated by this numerical simulation. The distribution of WSS depended on the blood velocity and the spatial vasculature. The increase in velocity caused the increment of WSS, and the reduction of velocity contributed to the decrease in WSS. Thereafter, backflow led to the appearance of low WSS region, and low WSS regions were found near the recirculation zone. Higher WSS was observed in MFCA and LFCA, as their diameters were smaller. Low WSS zones located at the curved portions of the vessels, and there barely existed low WSS zones in the straight tube. Specifically, most of low WSS zones were observed in CFA, SFA, and DFA, as backflow appeared in these three arteries. In summary, the WSS distribution in residuum vasculature closely correlated to blood velocity in a cycle and the geometries of these arteries. The geometries of arteries and blood flow in residual limb significantly altered due to the trans-femoral amputation and muscle atrophy, and the changes in the geometries and blood velocity further had an influence in the distributions of WSS and Sh.

7.2 Summary and discussion

A coupling computational model of blood flow and oxygen transport in residuum arteries was employed to understand the status of the residual limb in terms of hemodynamic responses and oxygen distribution. The Windkessel model and the lumped parameter model of oxygen transport were treated as the outlet boundary conditions of blood flow and oxygen transport in this computational model for the

sake of considering the effects of downstream vascular beds on hemodynamic responses and oxygen concentration distribution, and parameters in these numerical models were derived from literatures and the clinical measurement. The novel boundary condition of the lumped parameter model of oxygen transport was developed on the basis of transmission line equations of oxygen transport proposed in our previous study, while the Windkessel model was generally applied as the boundary condition at outlet of the vascular model and was established based on the fluid transmission line equations. The developed boundary condition of oxygen transport was numerically verified through the comparisons between the elongated models and the non-elongated models with the lumped parameter models of oxygen transport, and three regular vascular models (straight, curved, and bifurcated vessels) were employed in this verification. Moreover, oxygen transport in the computational model of residuum vasculature was validated through carrying out the *in vitro* experiment with a 3D printing replica of arteries in the residuum limb, while blood velocity measured by the ultrasound was compared with the numerical result of this computational model to validate this simulation of blood flow in residuum arteries. Consequently, the proposed boundary condition of the lumped parameter model of oxygen transport was supposed to provide a reliable estimation of oxygen concentration distribution in residuum vasculature and offer an efficient scheme for simulating the effect of downstream vessels on oxygen transport in the artery of interest.

In this study, the effect of hemoglobin was not considered in the computational simulation of oxygen transport in residuum vessels. Indeed, oxyhemoglobin transfer is the key factor to oxygen transport in the circulatory system. The computational simulation of oxygen transport without the consideration of hemoglobin could offer a reliable prediction of oxygen distribution in an artery as well. This is because oxygen concentration predicted by the simulation with oxyhemoglobin transport linearly correlated to that in the computational model without considering hemoglobin (Moore and Ethier, 1997). And a number of computational investigations of oxygen transport in arteries, which did not involve the effects of hemoglobin, have been conducted to understand the relationship between oxygen distribution and the status of vessels (Qiu and Tarbell, 2000, Liu et al., 2010, Tada, 2010, Caputo et al., 2013). Thus, the numerical simulation of oxygen transport in residuum arteries is available for determining the correlation between oxygen distribution and residuum status under the assumption that the effect of hemoglobin on oxygen transport is ignored. In addition, the arterial wall in this computational model of residuum vessels was assumed to be rigid. The previous study has found that the elasticity of the arterial wall slightly affected the hemodynamic response in the CFD model of thigh arteries (Kim et al., 2008). Moreover, numerous scholars applied the assumption of rigid vascular wall in the numerical investigations of blood flow and oxygen transport and acquired the qualitative distribution of oxygen concentration in vascular models (Qiu and Tarbell, 2000, Liu et al., 2010, Kolandavel et al., 2006). Consequently, the prediction of

oxygen concentration distribution in the computational model of residuum vasculature was determined to be reliable under these aforementioned assumptions.

Three regular geometries of vessels were employed to numerically verifying the developing boundary conditions of the lumped parameter model of oxygen transport. The comparison between the non-elongated model with this oxygen boundary condition and the elongated model was conducted, and the influence of the boundary condition of oxygen transport on oxygen concentration distribution in these regular models was suggested to be similar with that of the elongation of the vascular model. Thereafter, the effect of the oxygen boundary condition at outlet of the vascular model on oxygen transport was proved to be almost eliminated in the elongated model. The prediction of oxygen distribution in the vascular model with the developed boundary condition of oxygen transport was herein supposed to be reliable in understanding oxygen transport in arteries. Vascular geometries in the circulatory system are mainly composed of straight, curved and bifurcated vessel. These basic vessels are the main components of the branching and complex vasculatures in the entire vascular system. Parameters used in the proposed boundary condition of oxygen transport would be adjusted to be applicable in these complex vasculatures. Thus, straight, curved and bifurcated vessels were selected in the verification of this developed boundary condition of oxygen transport.

Blood velocity and oxygen distribution in arteries of the residual limb were

calculated by the computational simulation of the residuum vasculature with the employment of the lumped parameter model of oxygen transport. The numerical analysis of this computational simulation was validated by the comparison with the experiment of fluid flow and oxygen content in 3D vascular replica. We found that the oxygen content in the experimental measurement was slightly more than that of the computational model. This was because oxygen consumption in the arterial wall of the 3D residuum vasculature cannot be involved in the vascular replica of the *in vitro* experiment. Whereas, the oxygen consumption was considered in the computational simulation of the residuum arteries through setting the oxygen concentration at the wall as a lower value than that at inlet of the vascular model. Thus, oxygen content at the end of the computational vascular model reduced by the amount of the oxygen consumption in arterial wall in comparison with the experimental data. Additionally, the blood velocity numerically predicted in the computational model was compared with that of the ultrasound measurement, and the difference was quite modest. Overall, the computational model of the residuum arteries developed in this study could offer the reasonable estimation of oxygen distribution and hemodynamic parameters in the vasculature of the residual limb.

Sh is an important index to determine the amount of oxygen transmitted into the arterial wall, and oxygen content in the wall is a significant factor in the development of the vascular diseases. The Sh distribution in the residuum vasculature was acquired in the computational simulation with the boundary

condition of the lumped parameter model of oxygen transport. As the lumped parameter model of oxygen transport provided a numerical scheme for coupling the effect of downstream vessels with the 3D computational model of residuum arteries, the prediction of Sh distribution in vasculature of the residual limb was supposed to be more precise. We found that the change in blood velocity of the residuum vasculature hardly affected the Sh distribution during forward blood flow, which was consistent with our previous study. Our previous study has indicated that the difference of Sh distribution among different blood velocities in the residuum artery was quite modest (Yan et al., 2017), and the boundary condition of zero flux was utilized in the computational simulation of oxygen transport. The velocity of the forward blood flow herein had a slight effect on Sh distribution in the arteries of the residual limb. Moreover, the mean Sh under the maximum forward velocity was 15.92 in this study with the lumped parameter model of oxygen transport, while the mean Sh under the minimum velocity was 42.4 in the previous computational investigation with zero-flux boundary condition. As the effect of the downstream vascular beds on oxygen transport in the residuum artery was not considered in our previous computational simulation, the Sh value in the computational model with the zero-flux condition was higher than that with the lumped parameter model of oxygen transport. The numerical investigation of residuum vasculature with the developed boundary condition of oxygen transport provided the prediction of oxygen distribution with lower Sh value during forward blood flow. Smaller Sh in the residuum arteries enhances the rate of the development of atherosclerotic plaque

(Tarbell, 2003, Okamoto et al., 1983, Matsushita et al., 2000), and severe atherosclerosis in the arterial system of the residual limb causes reamputation (Martin et al., 1967, Dillingham et al., 2005). The possibility of the atherosclerosis development predicted by the computational simulation with the lumped parameter model of oxygen transport is supposed to be higher than that with the zero-flux boundary condition of oxygen transport. Thus, a high rate of the formation of atherosclerotic plaque in arteries of the trans-femoral residual limb was figured out by the coupling computational model of blood flow and oxygen transport in residual vasculature during forward blood flow, as applying the developed boundary condition with the lumped parameter model of oxygen transport contributed to smaller Sh in the vascular model. In summary, a smaller amount of oxygen content in the residuum vasculature was predicted by the computational model with the lumped parameter model of oxygen transport during forward blood flow, and the effect of the downstream vessels on oxygen transport in residuum arteries, which was implemented by the lumped parameter model of oxygen transport, was the key factor to the reduction of the oxygen content in the computational investigation.

Additionally, the result of the computational investigation showed that backflow caused the increase in the Sh values in the residuum arteries. The flux of oxygen transmitted into the arterial wall of the residuum vasculature raised with the reference to the increment of Sh at the wall during flow recirculation, thus, backflow supplied more oxygen for the vascular wall at the diastolic phase of a

cycle. The backflow brought the specified amount of oxygen from the downstream vascular beds back to the residuum vasculature, which played a dominant role in the augmentation of oxygen content during the diastolic phase of a cycle. The increased amount of oxygen in residuum arteries during flow recirculation mainly depended on the backflow velocity and oxygen content in backflow. Oxygen transport and blood flow in the downstream vessels of the residuum vasculature intrinsically affect the backflow velocity and oxygen content in backflow. In terms of blood flow, the effect of the downstream vessels was simulating through applying the Windkessel model as the outlet boundary condition of the computational model of the residuum vasculature, while the lumped parameter model of oxygen transport was treated as the boundary condition of oxygen transport at outlet of the vascular model to consider the effect of oxygen transport in downstream vessels. Consequently, backflow in the residuum vasculature enhanced the amount of oxygen in the arteries, and blood velocity and oxygen content of the backflow were determined by the Windkessel model and the lumped parameter model of oxygen transport, respectively. The increment of the backflow was supposed to lead to a more marked augmentation of oxygen content in the residuum arteries during a whole pulsatile cycle in comparison with the increase in blood velocity of the forward flow. However, backflow caused the reduction of the WSS at the arterial wall of the residuum vasculature. As low WSS detrimentally affects the arteries, backflow had an adverse influence on the arteries of the residual limb in terms of WSS. In summary, backflow contributed to the augmentation of oxygen content in

residuum vasculature which was beneficial to reduce the rate of the atherosclerosis development in residuum arteries, whereas, the decrease in WSS caused by backflow enhanced the possibility of the formation of the atherosclerotic plaque and had a detrimental effect on the arteries of the residual limb. Thus, the joint consideration of WSS and oxygen distribution was required to enhance the advantageous effect and alleviate the adverse effect of backflow on the arteries of the residual limb. Specifically, appropriately enhancing backflow in the branches of the residuum vasculature during the systolic phase of a pulsation cycle at inlet would lead to the increment of oxygen content and be beneficial to reduce the rate of the formation of the atherosclerotic plaque, as the WSS value was much higher than the threshold value of low WSS and the Sh value was quite lower at the systolic phase. Moreover, a modest decrease in backflow of the branch vessels during the diastolic phase could contribute to the increase in WSS and further have a favorable effect on the residuum arteries, as the WSS value became lower and the Sh value became higher at the diastolic phase of a pulsation cycle. In terms of arteries in the trans-femoral residuum, the adjustment of the backflow in branches vessels during a pulsation cycle would be favorable to alleviate the risk of vascular disease under the joint consideration of hemodynamic response and oxygen distribution.

Backflow is modestly adjusted to reduce the rate of the development of vascular disease. Oxygen is brought back to the residuum arteries by backflow, and the oxygen supply from arteries to muscular tissues is impeded. Oxygen content in

tissues of the residual limb decreases due to the hindrance of the backflow in residuum vasculature. Low oxygen concentration induces muscle dysfunction and contributes to muscle atrophy in the residuum (Ottenheijm et al., 2006, Caron et al., 2009). As a consequence, backflow causes the reduction of oxygen content in muscular tissues of the residual limb and further has a detrimental effect on the residuum muscles. Thus, oxygen content in tissues is another key factor in determining the adjustment of inflow and backflow in order to alleviate the risk of the development of vascular disease and muscle atrophy in the residual limb. In summary, backflow in branch vessels of the residuum vasculature positively correlates with Sh at the arterial wall and associates inversely with the WSS and oxygen content in tissues, while inflow positively correlates with Sh, WSS, and oxygen content in tissues. With the joint consideration of Sh, WSS, and oxygen content in tissues, enhancing inflow and backflow during the systolic phase is beneficial for arteries and muscles in the residual limb, while augmentation of inflow and reduction of backflow during the diastolic phase contribute to the decrease in the risk of the residuum disorder.

Although the novel computational model of the residuum vasculature with the lumped parameter model of oxygen transport can provide a reliable prediction of the oxygen distribution in residuum arteries and offer the basis for proposing a way to alleviate the risk of the residuum disorder, the numerical model has several limitations. As oxygen consumption in downstream vessels is hardly acquired by

the noninvasive measurement, the value of the oxygen consumption used in the development of the lumped parameter model of oxygen transport is derived from literatures. Oxygen consumption in downstream vascular beds affects the amount of oxygen brought back by backflow. A method for noninvasive measurement of oxygen consumption in vascular beds and tissues is beneficial for proposing a precise adjustment of inflow and backflow at a pulsation cycle, and this adjustment further leads to the reduction of the risk of vascular disease. Thereafter, the distributions of other substances in arteries except oxygen affect development and intervention of vascular disease as well, such as low-density lipoprotein (LDL). The lumped parameter model of other substances transfer can be established with reference to the lumped parameter model of oxygen transport and be regarded as the boundary condition in the computational simulation of the residuum vasculature, which provides a more precise prediction of the distributions of other substances. Investigations of other substances transfer will be carried out in the future study.

CHAPTER 8 CONCLUSIONS AND FUTURE WORK

8.1 Conclusions

For sake of determining the blood flow and oxygen transport systematically in the arterial system of the residual limb after amputation, theoretical developments, computational simulations, and experimental investigations about oxygen distribution and hemodynamic responses were implemented in this study.

1) Computational fluid dynamics models of the descending branches of the lateral femoral circumflex artery (DLFCA) coupled with oxygen transport in both the residuum and the sound limb were established, and three inflow velocities were applied at inlet to figure out the effect of exercise on oxygen transport in residuum DLFCA. Consequently, the investigation of oxygen transport in the residuum vasculature was suggested to be valuable in understanding the health status of the residuum after amputation, and the joint consideration of WSS and oxygen distribution was required in determining the rate of the atherosclerosis development in residuum arteries. Additionally, exercise was indicated to be favourable for enhancing oxygen content in DLFCA of the residual limb and reducing the possibility of the formation of the atherosclerotic plaque in residuum arteries.

2) The oxygen concentration in the arteries could not be noninvasively monitored in clinical research and a three-dimensional (3D) numerical simulation of the

systemic arterial tree is complicated and requires considerable computational resources and time. Thus, transmission line equations of oxygen transport in the arteries were firstly proposed according to the theory of oxygen transport and fluid transmission line equations. And these equations were numerically verified through the comparison between a 3D computational simulation of oxygen transport in the vascular model and a lumped parameter model of oxygen transport. These transmission line equations are treated as the theoretical basis for the establishment of the lumped parameter model of oxygen transport, and this model can be applied for numerically predicting the oxygen distribution in the systemic arterial tree with fewer computational resources and less time. Moreover, these transmission line equations of oxygen transport can also be regarded as the theoretical basis for developing transmission line equations of other substances in blood.

3) Transmission line equations of mass transport in arteries have been proposed, and these equations offer a more efficient scheme for investigating the systemic distribution of the substance in the arterial tree. Whereas, the derivation of these equations in arterioles and capillaries is lacked. Transmission line equations of mass transport in arterioles and capillaries were developed, and these equations were derived based on the transmission line equations of mass transport in arteries and mass transport theory in microvessels. These equations were verified through the comparison of the numerical prediction based on the

developed equations with the previous *in vitro* experimental studies. Parameters in the equations of arterioles represent the properties of the convection in mass transfer, while those in the equations of capillaries represent the properties of the convection and diffusion, respectively. The transmission line equations of mass transport in arterioles and capillaries are not only applied in constructing the lumped parameter model of mass transport for predicting the systemic distribution of the substance concentration in the microvascular tree, but also regarded as the supplement to the theoretical basis for establishing the lumped parameter model of the entire vascular system including arteries, arterioles, and capillaries.

4) Oxygen distribution in the residual limb changes due to the vasculature transformation after trans-femoral amputation, and changes in oxygen content play a significant role in the developments of health problems of the trans-femoral residuum. Oxygen content in the residual limb mainly depends on oxygen transport in the residuum vasculature. Few studies focused on oxygen transport in the arteries of the residual limb. We developed a coupling computational model of blood flow and oxygen transport in the residuum arteries to predict oxygen distribution, and the Windkessel model and the lumped parameter model of oxygen transport were applied as the boundary conditions at outlets of the vascular model. The boundary condition with the lumped parameter model of oxygen transport was verified through the

comparisons between the non-elongated vascular models with the lumped parameter models and the elongated models. Moreover, an in vitro experiment with a three-dimensional (3D) printing replica of the residuum vasculature was carried out to validate the computational simulation. The proposed boundary condition with the lumped parameter model was determined to be reliable for simulating the effect of downstream vessels on oxygen transport in the vascular model. According to the numerical results of the 3D computational model with the developed boundary condition of oxygen transport, the effect of inflow velocity on oxygen distribution was indicated to be much smaller than that of backflow during a pulsation cycle. Moreover, with the joint consideration of Sh, WSS, and oxygen content in tissues, the adjustment of inflow and backflow during a cycle was proposed to alleviate the risk of the residuum disorder.

8.2 Directions of future studies

Although this study is innovative and valuable for providing a reliable prediction of the oxygen distribution in residuum arteries and offering the basis for developing a way to alleviate the risk of the residuum disorder, there exist a few limitations in the development of the transmission line equations of oxygen transport and the establishment of the computational simulation of oxygen transport in residuum arteries.

First, the effect of hemoglobin on oxygen concentration distribution is neglected in the derivation of the transmission line equations. More physiological properties of oxygen in blood will be involved in the further development of these equations for the sake of more precise estimation of oxygen concentration distribution in the arterial system.

Second, the transmitted fluxes of oxygen from blood to arterial wall and from microcirculation to tissue affect the accuracy of the numerical prediction of the oxygen distribution in the residuum arteries and the microvascular system. A noninvasive method to measure the gradient of oxygen concentration near the arterial wall and between microvessels and tissues is favourable to acquire the accurate values of the oxygen fluxes into wall and tissues, and the method would enhance the accuracy of oxygen concentration prediction in the lumped parameter model of oxygen transport and the vascular model.

Third, as oxygen consumption in downstream vessels is hardly acquired by the noninvasive measurement, the value of the oxygen consumption used in the development of the lumped parameter model of oxygen transport is derived from literatures. Oxygen consumption in downstream vascular beds affects the amount of oxygen brought back by backflow. A method for noninvasive measurement of oxygen consumption in vascular beds and tissues is beneficial for proposing a

precise adjustment of inflow and backflow at a pulsation cycle, and this adjustment further leads to the reduction of the risk of vascular disease.

Forth, the distributions of other substances in arteries except oxygen affect development and intervention of vascular disease as well, such as low-density lipoprotein (LDL). The lumped parameter model of other substances transfer can be established with reference to the lumped parameter model of oxygen transport and be regarded as the boundary condition in the computational simulation of the residuum vasculature, which provides a more precise prediction of the distributions of other substances. Investigations of other substances transfer will be carried out in the future study.

In addition, the animal experiment and more clinical trials will be beneficial for the validation and development of the proposed theory and the computational simulation. Specifically, the transmission line equations of oxygen transport can be used for understanding the systemic distribution of oxygen concentration in the entire arterial system of the animal, and the measurement of oxygen concentration in the animal would be employed to validate this numerical prediction. My study finds that backflow is a key factor for comprehending the development of muscle atrophy, and the change in the spatial structure of residuum arteries increases vascular resistance and further leads to the augmentation of backflow. Conducting more clinical trials is beneficial for making these findings more convincing.

REFERENCES

ADLER, P. M. 1985. Transport processes in fractals III. Taylor despersion in two examples of fractal capillary networks. *International Journal of Multiphase Flow,* 11**,** 241-254.

AROESTY, J. & GROSS, J. F. 1970. Convection and diffusion in the microcirculation. *Microvascular Research,* 2**,** 247-267.

AUSTIN, L. R. & SEADER, J. D. 1973. Fully developed viscous flow in coiled circular pipes. *AICHE Journal,* 19**,** 85-94.

BACK, L. H., RADBILL, J. R. & CRAWFORD, D. W. 1977. Analysis of oxygen transport from pulsatile, viscous blood flow to diseased coronary arteries of man. *Journal of Biomechanics,* 10**,** 763-774.

BARRETT, M. J. & SURESH, V. 2013. Extra permeability is required to model dynamic oxygen measurements: evidence for functional recruitment? *Journal of Cerebral Blood Flow & Metabolism,* 33**,** 1402–1411.

BATEMAN, R. M., SHARPE, M. D. & ELLIS, C. G. 2003. Bench-to-bedside review: microvascular dysfunction in sepsis–hemodynamics, oxygen transport, and nitric oxide. *Critical Care,* 7**,** 359.

BATRA, R. & JENA, B. 1991. Flow of a Casson fluid in a slightly curved tube. *International Journal of Engineering Science,* 29**,** 1245-1258.

BAUMGARTNER, R. & LANGLOTZ, M. 1980. Amputee stump radiology. *Prosthetics and Orthotics International,* 4**,** 97-100.

BEARD, D. A. & WU, F. 2009. Apparent diffusivity and Taylor dispersion of water and solutes in capillary beds. *Bulletin of Mathematical Biology,* 71**,** 1366-1377.

BELLO, M. S., REZZONICO, R. & RIGHETTI, P. G. 1994. Use of taylor-aris dispersion for measurement of a solute diffusion coefficient in thin capillaries. *Science,* 266**,** 773-776.

BERNARDINO, M. E., WEINREB, J. C., MITCHELL, D. G., SMALL, W. C. & MORRIS, M. 1994. Safety and optimum concentration of a manganese chloride-based oral MR contrast agent. *Journal of Magnetic Resonance Imaging,* 4**,** 872-876.

BODINE, S. C., STITT, T. N., GONZALEZ, M., KLINE, W. O., STOVER, G. L., BAUERLEIN, R., ZLOTCHENKO, E., SCRIMGEOUR, A., LAWRENCE, J. C. & GLASS, D. J. 2001. Akt/mTOR pathway is a crucial regulator of skeletal muscle hypertrophy and can prevent muscle atrophy in vivo. *Nature Cell Biology,* 3**,** 1014-1019.

BOILEAU, E., NITHIARASU, P., BLANCO, P. J., MULLER, L. O., FOSSAN, F. E., HELLEVIK, L. R., DONDERS, W. P., HUBERTS, W., WILLEMET, M. & ALASTRUEY, J. 2015. A benchmark study of numerical schemes for one-dimensional arterial blood flow modelling. *International Journal for Numerical Methods in Biomedical Engineering,* 31**,** e02732.

BOONYAROM, O., KOZUKA, N., MATSUYAMA, K. & MURAKAMI, S. 2009. Effect of electrical stimulation to prevent muscle atrophy on morphologic

and histologic properties of hindlimb suspended rat hindlimb muscles. *American Journal of Physical Medicine & Rehabilitation,* 88**,** 719-726.

BOULDING, J. R. 1996. *Subsurface characterization and monitoring techniques: a desk reference guide*, DIANE Publishing.

BRIGGS, S. M. 2006. Earthquakes. *Surgical Clinics of North America,* 86**,** 537-544.

BROOM , M., MAKSUTI, E., BJ LLMARK, A., FRENCKNER, B. & JANEROT-SJ BERG, B. 2013. Closed-loop real-time simulation model of hemodynamics and oxygen transport in the cardiovascular system. *Biomedical Engineering Online,* 12**,** 1-20.

BRUNSTEIN, F., RENS, J., VAN TIEL, S. T., EGGERMONT, A. M. & TEN HAGEN, T. L. 2006. Histamine, a vasoactive agent with vascular disrupting potential, improves tumour response by enhancing local drug delivery. *British Journal of Cancer,* 95**,** 1663-1669.

BUERK, D. G. & GOLDSTICK, T. K. 1982. Arterial wall oxygen consumption rate varies spatially. *American Journal of Physiology-Heart and Circulatory Physiology,* 243**,** H948-H958.

CALAMANTE, F., VONKEN, E. J. & VAN OSCH, M. J. 2007. Contrast agent concentration measurements affecting quantification of bolus-tracking perfusion MRI. *Magnetic Resonance in Medicine,* 58**,** 544–553.

CAPUTO, M., CHIASTRA, C., CIANCIOLO, C., CUTR , E., DUBINI, G., GUNN, J., KELLER, B., MIGLIAVACCA, F. & ZUNINO, P. 2013. Simulation of

oxygen transfer in stented arteries and correlation with in-stent restenosis. *International Journal for Numerical Methods in Biomedical Engineering,* 29**,** 1373-1387.

CARO, C. G., PEDLEY, T., SCHROTER, R., SEED, W. & PARKER, K. 1978. *The mechanics of the circulation*, Oxford University Press.

CARON, M. A., TH RIAULT, M. E., PAR , M. È., MALTAIS, F. & DEBIGAR , R. 2009. Hypoxia alters contractile protein homeostasis in L6 myotubes. *FEBS Letters,* 583**,** 1528-1534.

CHATZIZISIS, Y. S., BAKER, A. B., SUKHOVA, G. K., KOSKINAS, K. C., PAPAFAKLIS, M. I., BEIGEL, R., JONAS, M., COSKUN, A. U., STONE, B. V., MAYNARD, C., SHI, G. P., LIBBY, P., FELDMAN, C. L., EDELMAN, E. R. & STONE, P. H. 2011. Augmented expression and activity of extracellular matrix-degrading enzymes in regions of low endothelial shear stress colocalize with coronary atheromata with thin fibrous caps in pigs. *Circulation,* 123**,** 621-630.

CHEN, J., GUTMARK, E., MYLAVARAPU, G., BACKELJAUW, P. F. & GUTMARK-LITTLE, I. 2014. Numerical investigation of mass transport through patient-specific deformed aortae. *Journal of Biomechanics,* 47**,** 544-552.

CHEN, J. & LU, X.-Y. 2006. Numerical investigation of the non-Newtonian pulsatile blood flow in a bifurcation model with a non-planar branch. *Journal of Biomechanics,* 39**,** 818-832.

COPPOLA, G. & CARO, C. 2008. Oxygen mass transfer in a model three-dimensional artery. *Journal of The Royal Society Interface,* 5**,** 1067-1075.

COTTET, H., BIRON, J. P., CIPELLETTI, L., MATMOUR, R. & MARTIN, M. 2010. Determination of individual diffusion coefficients in evolving binary mixtures by taylor dispersion analysis: application to the monitoring of polymer reaction. *Analytical Chemistry,* 82**,** 1793-1802.

CRAWFORD, D. W. & BLANKENHORN, D. H. 1991. Arterial wall oxygenation, oxyradicals, and atherosclerosis. *Atherosclerosis,* 89**,** 97-108.

CUSSLER, E. L. 1984. *Diffusion: mass transfer in fluid systems*, Cambridge University Press.

CUSSLER, E. L. 2009. *Diffusion: mass transfer in fluid systems*, Cambridge University Press.

D'ORLYE, F., VARENNE, A. & GAREIL, P. 2008. Determination of nanoparticle diffusion coefficients by Taylor dispersion analysis using a capillary electrophoresis instrument. *Journal of Chromatography A,* 1204**,** 226-232.

DEB, P., BORUAH, D. & DUTTA, V. 2012. Morphometric study of microvessels in primary CNS tumors and its correlation with tumor types and grade. *Microvascular Research,* 84**,** 34-43.

DEEN, W. M. 1998. *Analysis of transport phenomena (topics in chemical engineering)*, Oxford University Press.

DILLINGHAM, T. R., PEZZIN, L. E. & SHORE, A. D. 2005. Reamputation, mortality, and health care costs among persons with dysvascular lower-limb

amputations. *Archives of Physical Medicine and Rehabilitation,* 86**,** 480-486.

DONG, R., JIANG, W., ZHANG, M., LEUNG, A. & WONG, M. S. 2015. Review: hemodynamic studies for lower limb amputation and rehabilitation. *Journal of Mechanics in Medicine and Biology,* 15**,** 1530005.

DONG, R., LI, X., YAN, F., FAN, Y., JIANG, W. & WONG, M. S. 2016. The spatial structure changes of thigh arterial trees after transfemoral amputation: case studies. *Journal of Medical Imaging and Health Informatics,* 6**,** 688-692.

DOUGLAS, J. & RUSSELL, T. F. 1982. Numerical methods for convection-dominated diffusion problems based on combining the method of characteristics with finite element or finite difference procedures. *SIAM Journal on Numerical Analysis,* 19**,** 871-885.

DULING, B. R. 1972. Microvascular responses to alterations in oxygen tension. *Circulation Research,* 31**,** 481-489.

ERIKSON, U. & HULTH, A. 1962. Circulation of amputation stumps. Arteriographic and skin temperature studies. *Acta Orthopaedica Scandinavica,* 32**,** 159-170.

ESMAILY MOGHADAM, M., VIGNON-CLEMENTEL, I. E., FIGLIOLA, R. & MARSDEN, A. L. 2013. A modular numerical method for implicit 0D/3D coupling in cardiovascular finite element simulations. *Journal of Computational Physics,* 244**,** 63-79.

FAN, Y., JIANG, W., ZOU, Y., LI, J., CHEN, J. & DENG, X. 2009. Numerical simulation of pulsatile non-Newtonian flow in the carotid artery bifurcation. *Acta Mechanica Sinica,* 25**,** 249-255.

FANNJIANG, A. & PAPANICOLAOU, G. 1994. Convection enhanced diffusion for periodic flows. *SIAM Journal on Applied Mathematics,* 54**,** 333-408.

FANNJIANG, A. & PAPANICOLAOU, G. 1997. Convection-enhanced diffusion for random flows. *Journal of Statistical Physics,* 88**,** 1033-1076.

FEDERSPIEL, W. J. & POPEL, A. S. 1986. A theoretical analysis of the effect of the particulate nature of blood on oxygen release in capillaries. *Microvascular Research,* 32**,** 164-189.

FERRARI, M. & QUARESIMA, V. 2012. A brief review on the history of human functional near-infrared spectroscopy (fNIRS) development and fields of application. *Neuroimage,* 63**,** 921-935.

FERREIRA, R., NEUPARTH, M. J., VITORINO, R., APPELL, H. J., AMADO, F. & DUARTE, J. A. 2008. Evidences of apoptosis during the early phases of soleus muscle atrophy in hindlimb suspended mice. *Physiological Research,* 57**,** 601-611.

FITTS, R. H., METZGER, J. M., RILEY, D. A. & UNSWORTH, B. R. 1986. Models of disuse: a comparison of hindlimb suspension and immobilization. *Journal of Applied Physiology,* 60**,** 1946-1953.

FITTS, R. H., RILEY, D. R. & WIDRICK, J. J. 2000. Physiology of a microgravity environment invited review: microgravity and skeletal muscle. *Journal of Applied Physiology,* 89**,** 823-839.

FOURNIER, R. L. 2011. *Basic transport phenomena in biomedical engineering*, CRC Press.

FRAISSE, N., MARTINET, N., KPADONOU, T. J., PAYSANT, J., BLUM, A. & ANDRE, J. M. 2008. [Muscles of the below-knee amputees]. *Annales de Réadaptation et de Médecine Physique,* 51**,** 218-227.

FRANKEL, I. & BRENNER, H. 2006. On the foundations of generalized Taylor dispersion theory. *Journal of Fluid Mechanics,* 204**,** 97-119.

FRIEDMAN, M., BARGERON, C., HUTCHINS, G., MARK, F. & DUNCAN, D. 1992. Effects of arterial compliance and non-Newtonian rheology on correlations between intimal thickness and wall shear. *Journal of Biomechanical Engineering,* 114**,** 317-320.

FUNG, Y. C., ZWEIFACH, B. W. & INTAGLIETTA, M. 1966. Elastic environment of the capillary bed. *Circulation Research,* 19**,** 441-461.

GLASS, D. J. 2005. Skeletal muscle hypertrophy and atrophy signaling pathways. *The International Journal of Biochemistry & Cell Biology,* 37**,** 1974-1984.

GOLBRANSON, F. L., WIRTA, R., KUNCIR, E., LIEBER, R. & OISHI, C. 1988. Volume changes occurring in postoperative below-knee residual limbs. *Journal of Rehabilitation Research and Development,* 25**,** 11-18.

GONZALEZ, D. 2005. Crush syndrome. *Critical Care Medicine,* 33**,** S34-S41.

GRAESER, H. J., KIM, Y. G. & CRANDALL, E. D. 1969. The effects of time-varying blood flow on diffusional resistance to oxygen transfer in the pulmonary capillaries. *Biophysical Journal,* 9**,** 1100-1114.

GROTE, M. J. & KIRSCH, C. 2004. Dirichlet-to-Neumann boundary conditions for multiple scattering problems. *Journal of Computational Physics,* 201**,** 630-650.

GUDMUNDSSON, G., MATTHIASSON, S. E., ARASON, H., JOHANNSSON, H., RUNARSSON, F., BJARNASON, H., HELGADOTTIR, K., THORISDOTTIR, S., INGADOTTIR, G., LINDPAINTNER, K., SAINZ, J., GUDNASON, V., FRIGGE, M. L., KONG, A., GULCHER, J. R. & STEFANSSON, K. 2002. Localization of a gene for peripheral arterial occlusive disease to chromosome 1p31. *American Journal of Human Genetics,* 70**,** 586-592.

HELLUMS, J. D. 1977. The resistance to oxygen transport in the capillaries relative to that in the surrounding tissue. *Microvascular Research,* 13**,** 131-136.

HERBST, T. J., RAICHLE, M. E. & FERRENDELLI, J. A. 1979. beta-Adrenergic regulation of adenosine 3',5'-monophosphate concentration in brain microvessels. *Science,* 204**,** 330-332.

HORSTEN, J. J., STEENHOVEN, V. A. A. & DONGEN, V. M. R. 1989. Linear propagation of pulsatile waves in viscoelastic tubes. *Journal of Biomechanics,* 22**,** 477-484.

HULTEN, L. M. & LEVIN, M. 2009. The role of hypoxia in atherosclerosis. *Current Opinion in Lipidology,* 20**,** 409-414.

ISAKOV, E., BURGER, H., GREGORIC, M. & MARINCEK, C. 1996. Stump length as related to atrophy and strength of the thigh muscles in trans-tibial amputees. *Prosthetics and Orthotics International,* 20**,** 96-100.

IVANOV, K. P., SOKOLOVA, I. B. & VOVENKO, E. P. 1999. Oxygen transport in the rat brain cortex at normobaric hyperoxia. *European Journal of Applied Physiology and Occupational Physiology,* 80**,** 582-587.

JAEGERS, S. M. H. J. 1993. The morphology and functions of the muscles around the hip joint after a unilateral transfemoral amputation. *Ph. D Thesis, University of Groningen, Netherland*.

JIM DOUGLAS, J. & RUSSELL, T. F. 1982. Numerical methods for convection-dominated diffusion problems based on combining the method of characteristics with finite element or finite difference procedures. *Siam Journal on Numerical Analysis,* 19**,** 871-885.

JOHNSTON, B. M., JOHNSTON, P. R., CORNEY, S. & KILPATRICK, D. 2006. Non-Newtonian blood flow in human right coronary arteries: transient simulations. *Journal of Biomechanics,* 39**,** 1116-1128.

JORFELDT, L. & WAHREN, J. 1971. Leg blood flow during exercise in man. *Clinical Science,* 41**,** 459-473.

KATZ, I. R., WITTENBERG, J. B. & WITTENBERG, B. A. 1984. Monoamine oxidase, an intracellular probe of oxygen pressure in isolated cardiac myocytes. *Journal of Biological Chemistry,* 259**,** 7504-7509.

KIM, Y. H., KIM, J. E., ITO, Y., SHIH, A. M., BROTT, B. & ANAYIOTOS, A. 2008. Hemodynamic analysis of a compliant femoral artery bifurcation model using a fluid structure interaction framework. *Annals of Biomedical Engineering,* 36**,** 1753-1763.

KIMURA, H., BRAUN, R. D., ONG, E. T., HSU, R., SECOMB, T. W., PAPAHADJOPOULOS, D., HONG, K. & DEWHIRST, M. W. 1996. Fluctuations in red cell flux in tumor microvessels can lead to transient hypoxia and reoxygenation in tumor parenchyma. *Cancer Research,* 56**,** 5522-5528.

KOLANDAVEL, M. K., FRUEND, E.-T., RINGGAARD, S. & WALKER, P. G. 2006. The effects of time varying curvature on species transport in coronary arteries. *Annals of Biomedical Engineering,* 34**,** 1820-1832.

KREUZER, F., HOOFD, L. & KREUZER, F. 2011. *Facilitated diffusion of oxygen and carbon dioxide*, John Wiley & Sons, Inc.

KROGH, A. 1919. The number and distribution of capillaries in muscles with calculations of the oxygen pressure head necessary for supplying the tissue. *The Journal of Physiology,* 52**,** 409-415.

KU, D. N. 1997. Blood flow in arteries. *Annual Review of Fluid Mechanics,* 29**,** 399-434.

KUSHMERICK, M. J., MEYER, R. A. & BROWN, T. R. 1992. Regulation of oxygen consumption in fast-and slow-twitch muscle. *American Journal of Physiology,* 263**,** C598-C606.

LACOURSE, J. R., MOHANAKRISHNAN, G. & SIVAPRASAD, K. 1986. Simulations of arterial pressure pulses using a transmission line model. *Journal of Biomechanics,* 19**,** 771-780.

LANDIS, C. S., LI, X., TELANG, F. W., CODERRE, J. A., MICCA, P. L., ROONEY, W. D., LATOUR, L. L., V TEK, G., P LYKA, I. & SPRINGER, C. S. 2000. Determination of the MRI contrast agent concentration time course in vivo following bolus injection: Effect of equilibrium transcytolemmal water exchange. *Magnetic Resonance in Medicine,* 44**,** 563–574.

LANGER, R. 1998. Drug delivery and targeting. *Nature,* 392**,** 5-10.

LATTIMORE, J., WILCOX, I. & NAKHLA, S. 2005. Repetitive hypoxia increases lipid loading in human macrophages-a potentially atherogenic effect. *Atherosclerosis,* 179**,** 255-259.

LEE, P. H. U. & VANDENBURGH, H. H. 2013. Skeletal muscle atrophy in bioengineered skeletal muscle: a new model system. *Tissue Engineering Part A,* 19**,** 2147-2155.

LEE, W. C., ZHANG, M., JIA, X. & CHEUNG, J. 2004. Finite element modeling of the contact interface between trans-tibial residual limb and prosthetic socket. *Medical Engineering & Physics,* 26**,** 655-662.

LEONARD, E. F. & JORGENSEN, S. B. 1974. The analysis of convection and diffusion in capillary beds. *Annual Review of Biophysics and Bioengineering,* 3**,** 293-339.

LEWANDROWSKA, A., MAJCHER, A., OCHAB-MARCINEK, A., TABAKA, M. & HOLYST, R. 2013. Taylor dispersion analysis in coiled capillaries at high flow rates. *Analytical Chemistry,* 85**,** 4051-4056.

LIANG, F., SENZAKI, H., KURISHIMA, C., SUGHIMOTO, K., INUZUKA, R. & LIU, H. 2014a. Hemodynamic performance of the Fontan circulation compared with a normal biventricular circulation: a computational model study. *American Journal of Physiology-Heart and Circulatory Physiology,* 307**,** H1056-H1072.

LIANG, F., SUGHIMOTO, K., MATSUO, K., LIU, H. & TAKAGI, S. 2014b. Patient-specific assessment of cardiovascular function by combination of clinical data and computational model with applications to patients undergoing Fontan operation. *International Journal for Numerical Methods in Biomedical Engineering,* 30**,** 1000-1018.

LILJA, M., HOFFMANN, P. & ÖBERG, T. 1998. Morphological changes during early trans-tibial prosthetic fitting. *Prosthetics and Orthotics International,* 22**,** 115-122.

LILJA, M. & ÖBERG, T. 1997. Proper time for definitive transtibial prosthetic fitting. *Journal of Prosthetics and Orthotics,* 9**,** 90-95.

LIU, S. & KURZROCK, R. 2014. Toxicity of targeted therapy: Implications for response and impact of genetic polymorphisms. *Cancer Treatment Reviews,* 40**,** 883-891.

LIU, X., FAN, Y. & DENG, X. 2010. Effect of spiral flow on the transport of oxygen in the aorta: a numerical study. *Annals of Biomedical Engineering,* 38**,** 917-926.

LIU, X., FAN, Y., DENG, X. & ZHAN, F. 2011. Effect of non-Newtonian and pulsatile blood flow on mass transport in the human aorta. *Journal of Biomechanics,* 44**,** 1123-1131.

LIU, X., PU, F., FAN, Y., DENG, X., LI, D. & LI, S. 2009. A numerical study on the flow of blood and the transport of LDL in the human aorta: the physiological significance of the helical flow in the aortic arch. *American Journal of Physiology-Heart and Circulatory Physiology,* 297**,** H163-H170.

LUO, Y. & SUN, W. 2009. The development of Chinese prostheses since the founding. *Orthopaedic Journal of China,* 17**,** 1325-1328.

LYON, C. C., KULKARNI, J., ZIMERSONC, E., VAN ROSS, E. & BECK, M. H. 2000. Skin disorders in amputees. *Journal of the American Academy of Dermatology,* 42**,** 501-507.

MA, P., LI, X. & KU, D. 1994. Heat and mass transfer in separated flow region for high Prandtl and Schmidt numbers under pulsatile conditions. *International Journal of Heat and Mass Transfer,* 37**,** 2723-2736.

MA, P., LI, X. & KU, D. 1997. Convective mass transfer at the carotid bifurcation. *Journal of Biomechanics,* 30**,** 565-571.

MACCHI, C., CASSIGOLI, S., LOVA, R. M., ROCCUZZO, A., MINIATI, B., CEPPATELLI, S., CONTI, A. A. & GENSINI, G. F. 2004. Prosthesis

intolerance in patients with transfemoral amputation: a videocapillaroscopic study. *American Journal of Physical Medicine & Rehabilitation,* 83**,** 486-491.

MAK, A. F. T., ZHANG, M. & BOONE, D. A. 2001. State-of-the-art research in lower-limb prosthetic biomechanics-socket interface: a review. *Journal of Rehabilitation Research & Development,* 38**,** 161-173.

MARTIN, P., RENWICK, S. & THOMAS, E. M. 1967. Gritti-Stokes amputation in atherosclerosis: a review of 237 cases. *British Medical Journal,* 3**,** 837-838.

MASAMOTO, K., VAZQUEZ, A., WANG, P. & KIM, S. G. 2008. Trial-by-trial relationship between neural activity, oxygen consumption, and blood flow responses. *Neuroimage,* 40**,** 442-450.

MATSUSHITA, H., MORISHITA, R., NATA, T., AOKI, M., NAKAGAMI, H., TANIYAMA, Y., YAMAMOTO, K., HIGAKI, J., YASUFUMI, K. & OGIHARA, T. 2000. Hypoxia-induced endothelial apoptosis through nuclear factor-kappaB (NF-kappaB)-mediated bcl-2 suppression: in vivo evidence of the importance of NF-kappaB in endothelial cell regulation. *Circulation Research,* 86**,** 974-981.

MCCULLY, K. K. & HAMAOKA, T. 2000. Near-infrared spectroscopy: what can it tell us about oxygen saturation in skeletal muscle? *Exercise and Sport Sciences Reviews,* 28**,** 123-127.

MEIER, P. & ZIERLER, K. L. 1954. On the theory of the indicator-dilution method for measurement of blood flow and volume. *Journal of Applied Physiology,* 6**,** 731-744.

MILLIKAN, G. 1939. Muscle hemoglobin. *Physiological Reviews,* 19**,** 503-523.

MOORE, J. & ETHIER, C. 1997. Oxygen mass transfer calculations in large arteries. *Journal of Biomechanical Engineering,* 119**,** 469-475.

MOORE, J., MAIER, S. E., KU, D. N. & BOESIGER, P. 1994. Hemodynamics in the abdominal aorta: a comparison of in vitro and in vivo measurements. *Journal of Applied Physiology,* 76**,** 1520-1527.

MULVEY, J., AWAN, S., QADRI, A. & MAQSOOD, M. 2008. Profile of injuries arising from the 2005 Kashmir Earthquake: The first 72h. *Injury,* 39**,** 554-560.

MURKIN, J. M. & ARANGO, M. 2009. Near-infrared spectroscopy as an index of brain and tissue oxygenation. *British Journal of Anaesthesia,* 103**,** i3-i13.

MURPHY, E. A., DUNNE, A. S., MARTIN, D. M. & BOYLE, F. J. 2015. Oxygen mass transport in stented coronary arteries. *Annals of Biomedical Engineering,* 44**,** 1-15.

NAGANO, K., SUZAKI, E., NAGANO, Y., KATAOKA, K. & OZAWA, K. 2008. The activation of apoptosis factor in hindlimb unloading-induced muscle atrophy under normal and low-temperature environmental conditions. *Acta Histochemica,* 110**,** 505-518.

NOORDERGRAAF, A. 1978. *Circulatory system dynamics*, Academic Press.

NOORDERGRAAF, A., VERDOUW, P. D. & BOOM, H. B. K. 1963. The use of an analog computer in a circulation model. *Progress in Cardiovascular Diseases,* 5**,** 419-439.

OGAWA, S., GERLACH, H., ESPOSITO, C., PASAGIAN-MACAULAY, A., BRETT, J. & STERN, D. 1990. Hypoxia modulates the barrier and coagulant function of cultured bovine endothelium. Increased monolayer permeability and induction of procoagulant properties. *The Journal of Clinical Investigation,* 85**,** 1090-1098.

OKAMOTO, R., HATANI, M., TSUKITANI, M., SUEHIRO, A., FUJINO, M., IMAI, N., TAKANO, S., WATANABE, Y. & FUKUZAKI, H. 1983. The effect of oxygen on the development of atherosclerosis in WHHL rabbits. *Atherosclerosis,* 47**,** 47-53.

OLUFSEN, M. S. 1999. Structured tree outflow condition for blood flow in larger systemic arteries. *American Journal of Physiology,* 276**,** H257-H268.

OLUFSEN, M. S., PESKIN, C. S., KIM, W. Y., PEDERSEN, E. M., NADIM, A. & LARSEN, J. 2000. Numerical simulation and experimental validation of blood flow in arteries with structured-tree outflow conditions. *Annals of Biomedical Engineering,* 28**,** 1281-1299.

OTTENHEIJM, C. A., HEUNKS, L. M., GERAEDTS, M. C. & DEKHUIJZEN, P. N. 2006. Hypoxia-induced skeletal muscle fiber dysfunction: role for reactive nitrogen species. *American Journal of Physiology-Lung Cellular and Molecular Physiology,* 290**,** L127-L135.

OVERMAN, A. R. & MILLER, R. J. 1968. Convective diffusion in capillaries. *The Journal of Physical Chemistry,* 72**,** 155-158.

PALUMBO, R., GAETANO, C., ANTONINI, A., POMPILIO, G., BRACCO, E., RONNSTRAND, L., HELDIN, C. H. & CAPOGROSSI, M. C. 2002. Different effects of high and low shear stress on platelet-derived growth factor isoform release by endothelial cells: consequences for smooth muscle cell migration. *Arteriosclerosis Thrombosis and Vascular Biology,* 22**,** 405-411.

PATANKAR, S. 1980a. *Numerical heat transfer and fluid flow*, CRC Press.

PATANKAR, S. V. 1980b. *Numerical heat transfer and fluid flow*, Hemisphere Publishing Corporation.

PATTENGALE, P. K. & HOLLOSZY, J. O. 1967. Augmentation of skeletal muscle myoglobin by a program of treadmill running. *American Journal of Physiology,* 213**,** 783-785.

PITTMAN, R. N. 2000. Oxygen supply to contracting skeletal muscle at the microcirculatory level: diffusion vs convection. *Acta Physiologica Scandinavica,* 168**,** 593-602.

PITTMAN, R. N. & DULING, B. R. 1975. Measurement of percent oxyhemoglobin in the microvasculature. *Journal of Applied Physiology,* 38**,** 321-327.

POPEL, A. S. 1989. Theory of oxygen transport to tissue. *Critical Reviews in Biomedical Engineering,* 17**,** 257-321.

PORTNOY, S., SIEV-NER, I., SHABSHIN, N., KRISTAL, A., YIZHAR, Z. & GEFEN, A. 2009. Patient-specific analyses of deep tissue loads post transtibial amputation in residual limbs of multiple prosthetic users. *Journal of Biomechanics,* 42**,** 2686-2693.

POWERS, S. K., KAVAZIS, A. N. & DERUISSEAU, K. C. 2005. Mechanisms of disuse muscle atrophy: role of oxidative stress. *American Journal of Physiology-Regulatory Integrative and Comparative Physiology,* 288**,** R337-R344.

PREWITT, R. L. & JOHNSON, P. C. 1976. The effect of oxygen on arteriolar red cell velocity and capillary density in the rat cremaster muscle. *Microvascular Research,* 12**,** 59-70.

QIU, Y. & TARBELL, J. M. 2000. Numerical simulation of oxygen mass transfer in a compliant curved tube model of a coronary artery. *Annals of Biomedical Engineering,* 28**,** 26-38.

RAINES, J., JAFFRIN, M. & SHAPIRO, A. 1974. A computer simulation of arterial dynamics in the human leg. *Journal of Biomechanics,* 7**,** 77-91.

RAMACHANDRAN, P. A. 2014. *Advanced transport phenomena: analysis, modeling, and computations*, Cambridge University Press.

RANDLES, A., DRAEGER, E. W. & BAILEY, P. E. 2015. Massively parallel simulations of hemodynamics in the primary large arteries of the human vasculature. *Journal of Computational Science,* 9**,** 70-75.

RATLIFF, D. A., CLYNE, C. A., CHANT, A. D. & WEBSTER, J. H. 1984. Prediction of amputation wound healing: the role of transcutaneous pO2 assessment. *British Journal of Surgery,* 71**,** 219-222.

RENSTR M, P., GRIMBY, G., MORELLI, B. & PALMERTZ, B. 1982. Thigh muscle atrophy in below-knee amputees. *Scandinavian Journal of Rehabilitation Medicine,* 9**,** 150-162.

REYMOND, P., BOHRAUS, Y., PERREN, F., LAZEYRAS, F. & STERGIOPULOS, N. 2011. Validation of a patient-specific one-dimensional model of the systemic arterial tree. *American Journal of Physiology-Heart and Circulatory Physiology,* 301**,** H1173-H1182.

REYMOND, P., MERENDA, F., PERREN, F., RUFENACHT, D. & STERGIOPULOS, N. 2009. Validation of a one-dimensional model of the systemic arterial tree. *American Journal of Physiology-Heart and Circulatory Physiology,* 297**,** H208-H222.

RICHARDSON, R. B. 2008. Age-dependent changes in oxygen tension, radiation dose and sensitivity within normal and diseased coronary arteries-Part B: modeling oxygen diffusion into vessel walls. *International Journal of Radiation Biology,* 84**,** 849-857.

ROBERTS, G. W., LARSON, K. B. & SPAETH, E. E. 1973. The interpretation of mean transit time measurements for multiphase tissue systems. *Journal of Theoretical Biology,* 39**,** 447-475.

ROBERTS, M. S., ANISSIMOV, Y. G. & WEISS, M. 2000. Commentary: using the convection–dispersion model and transit time density functions in the

analysis of organ distribution kinetics. *Journal of Pharmaceutical Sciences,* 89**,** 1579-1586.

ROSS, R. 1993. Rous-Whipple Award Lecture. Atherosclerosis: a defense mechanism gone awry. *American Journal of Pathology,* 143**,** 987-1002.

SAMAJA, M. 1988. Prediction of the oxygenation of human organs at varying blood oxygen carrying properties. *Respiration Physiology,* 72**,** 211-217.

SANDERS, J. E., GARBINI, J. L., LESCHEN, J. M., ALLEN, M. S. & JORGENSEN, J. E. 1997. A bidirectional load applicator for the investigation of skin response to mechanical stress. *IEEE Transactions on Biomedical Engineering,* 44**,** 290-296.

SANDERS, J. E., GREVE, J. M., CLINTON, C. & HAFNER, B. J. 2000. Changes in interface pressure and stump shape over time: preliminary results from a trans-tibial amputee subject. *Prosthetics and Orthotics International,* 24**,** 163-168.

SANDERS, J. E., HARRISON, D. S., ALLYN, K. J. & MYERS, T. R. 2009. Clinical utility of in-socket residual limb volume change measurement: case study results. *Prosthetics and Orthotics International,* 33**,** 378-390.

SANTILLI, S. M., STEVENS, R. B., ANDERSON, J. G., PAYNE, W. D. & CALDWELL, M. D. 1995. Transarterial wall oxygen gradients at the dog carotid bifurcation. *American Journal of Physiology,* 268**,** H155-H161.

SCHAAF, B. W. & ABBRECHT, P. H. 1972. Digital computer simulation of human systemic arterial pulse wave transmission: a nonlinear model. *Journal of Biomechanics,* 5**,** 345-364.

SCHMALZ, T., BLUMENTRITT, S. & REIMERS, C. 2001. Selective thigh muscle atrophy in trans-tibial amputees: an ultrasonographic study. *Archives of Orthopaedic and Trauma Surgery,* 121**,** 307-312.

SCHNEIDERMAN, G. & GOLDSTICK, T. K. 1978. Significance of luminal plasma layer resistance in arterial wall oxygen supply. *Atherosclerosis,* 31**,** 11-20.

SEELEY, R. R. 2011. *Seeley's anatomy & physiology*, McGraw-Hill.

SHERK, V. D., BEMBEN, M. G. & BEMBEN, D. A. 2010. Interlimb muscle and fat comparisons in persons with lower-limb amputation. *Archives of Physical Medicine and Rehabilitation,* 91**,** 1077-1081.

SHOEMAKER, J. K., PHILLIPS, S. M., GREEN, H. J. & HUGHSON, R. L. 1996. Faster femoral artery blood velocity kinetics at the onset of exercise following short-term training. *Cardiovascular Research,* 31**,** 278-286.

SNYDER, M. F., RIDEOUT, V. C. & HILLESTAD, R. J. 1968. Computer modeling of the human systemic arterial tree. *Journal of Biomechanics,* 1**,** 341-353.

SONVEAUX, P., DESSY, C., MARTINIVE, P., HAVAUX, X., JORDAN, B. F., GALLEZ, B., GREGOIRE, V., BALLIGAND, J. L. & FERON, O. 2004.

Endothelin-1 is a critical mediator of myogenic tone in tumor arterioles: implications for cancer treatment. *Cancer Research,* 64**,** 3209-3214.

STAINSBY, W. N. & OTIS, A. B. 1964. Blood flow, blood oxygen tension, oxygen uptake, and oxygen transport in skeletal muscle. *American Journal of Physiology-Legacy Content,* 206**,** 858-866.

STANDRING, S., ELLIS, H., HEALY, J., JHONSON, D., WILLIAMS, A. & COLLINS, P. 2005. Gray's anatomy: the anatomical basis of clinical practice. *American Journal of Neuroradiology,* 26**,** 1825-1831.

STEIN, T., LESKIW, M., SCHLUTER, M., DONALDSON, M. & LARINA, I. 1999. Protein kinetics during and after long-duration spaceflight on MIR. *American Journal of Physiology-Endocrinology and Metabolism,* 276**,** E1014-E1021.

STEIN, T. R., MARTIN, J. C. & KELLER, K. H. 1971. Steady-state oxygen transport through red blood cell suspensions. *Journal of Applied Physiology,* 31**,** 397-402.

STERGIOPULOS, N., MEISTER, J. J. & WESTERHOF, N. 1995. Evaluation of methods for estimation of total arterial compliance. *American Journal of Physiology,* 268**,** H1540-H1548.

STERGIOPULOS, N., SEGERS, P. & WESTERHOF, N. 1999. Use of pulse pressure method for estimating total arterial compliance in vivo. *American Journal of Physiology,* 276**,** H424-H428.

STERGIOPULOS, N., YOUNG, D. F. & ROGGE, T. R. 1992. Computer simulation of arterial flow with applications to arterial and aortic stenoses. *Journal of Biomechanics,* 25**,** 1477-1488.

STETTLER, J. C., NIEDERER, P. & ANLIKER, M. 1981. Theoretical analysis of arterial hemodynamics including the influence of bifurcations. Part I: mathematical models and prediction of normal pulse patterns. *Annals of Biomedical Engineering,* 9**,** 145-164.

SULLIVAN, S. M. & JOHNSON, P. C. 1981. Effect of oxygen on arteriolar dimensions and blood flow in cat sartorius muscle. *American Journal of Physiology,* 241**,** H547-H556.

SWAIN, D. P. & PITTMAN, R. N. 1989. Oxygen exchange in the microcirculation of hamster retractor muscle. *American Journal of Physiology,* 256**,** H247-H255.

TADA, S. 2010. Numerical study of oxygen transport in a carotid bifurcation. *Physics in Medicine and Biology,* 55**,** 3993-4010.

TADA, S. & TARBELL, J. M. 2006. Oxygen mass transport in a compliant carotid bifurcation model. *Annals of Biomedical Engineering,* 34**,** 1389-1399.

TAO, L. & NICHOLSON, C. 1996. Diffusion of albumins in rat cortical slices and relevance to volume transmission. *Neuroscience,* 75**,** 839-847.

TARBELL, J. M. 2003. Mass transport in arteries and the localization of atherosclerosis. *Annual Review of Biomedical Engineering,* 5**,** 79-118.

TATEISHI, N., SUZUKI, Y., TANAKA, J. & MAEDA, N. 1997. Imaging of oxygen saturation and distribution of erythrocytes in microvessels. *Microcirculation,* 4**,** 403-412.

TAYLOR, C. R., WEIBEL, E. R., KARAS, R. H. & HOPPELER, H. 1987. Adaptive variation in the mammalian respiratory system in relation to energetic demand: VIII. Structural and functional design principles determining the limits to oxidative metabolism. *Respiration Physiology,* 69**,** 117-127.

TAYLOR, G. 1953. Dispersion of soluble matter in solvent flowing slowly through a tube. *Proceedings of the Royal Society of London. Series A, Mathematical and Physical Sciences,* 219**,** 186-203.

TAYLOR, G. 1954. Conditions under which dispersion of a solute in a stream of solvent can be used to measure molecular diffusion. *Proceedings of the Royal Society of London. Series A, Mathematical and Physical Sciences,* 225**,** 473-477.

THORNE, R. G. & NICHOLSON, C. 2006. In vivo diffusion analysis with quantum dots and dextrans predicts the width of brain extracellular space. *Proceedings of the National Academy of Sciences of the United States of America,* 103**,** 5567-5572.

TRENDELENBURG, A. U., MEYER, A., ROHNER, D., BOYLE, J., HATAKEYAMA, S. & GLASS, D. J. 2009. Myostatin reduces Akt/TORC1/p70S6K signaling, inhibiting myoblast differentiation and

myotube size. *American Journal of Physiology-Cell Physiology,* 296**,** C1258-C1270.

TROEDSSON, B. S. 2013. Stump arterial circulation and its relationship to the prescription of a prosthesis for the geriatric patient. *Journal of Rehabilitation Research & Development,* 50**,** 39-53.

TSAI, A. G., JOHNSON, P. C. & INTAGLIETTA, M. 2003. Oxygen gradients in the microcirculation. *Physiological Reviews,* 83**,** 311-322.

TSUKADA, K., SEKIZUKA, E., OSHIO, C., TSUJIOKA, K. & MINAMITANI, H. 2004. Red blood cell velocity and oxygen tension measurement in cerebral microvessels by double-wavelength photoexcitation. *Journal of Applied Physiology,* 96**,** 1561-1568.

TUGCU, I., SAFAZ, I., YILMAZ, B., GOKTEPE, A. S., TASKAYNATAN, M. A. & YAZICIOGLU, K. 2009. Muscle strength and bone mineral density in mine victims with transtibial amputation. *Prosthetics and Orthotics International,* 33**,** 299-306.

TURETSCHEK, K., HUBER, S., FLOYD, E., HELBICH, T., ROBERTS, T. P., SHAMES, D. M., TARLO, K. S., WENDLAND, M. F. & BRASCH, R. C. 2001. MR imaging characterization of microvessels in experimental breast tumors by using a particulate contrast agent with histopathologic correlation. *Radiology,* 218**,** 562-569.

VAN DE VOSSE, F. N. & STERGIOPULOS, N. 2011. Pulse wave propagation in the arterial tree. *Annual Review of Fluid Mechanics,* 43**,** 467-499.

VANDENBURGH, H., CHROMIAK, J., SHANSKY, J., DEL TATTO, M. & LEMAIRE, J. 1999. Space travel directly induces skeletal muscle atrophy. *The FASEB Journal,* 13**,** 1031-1038.

VASIR, J. K. & LABHASETWAR, V. 2005. Targeted drug delivery in cancer therapy. *Technology in Cancer Research & Treatment,* 4**,** 363-374.

VAZQUEZ, A. L., FUKUDA, M., TASKER, M. L., MASAMOTO, K. & KIM, S. G. 2010. Changes in cerebral arterial, tissue and venous oxygenation with evoked neural stimulation: implications for hemoglobin-based functional neuroimaging. *Journal of Cerebral Blood Flow & Metabolism,* 30**,** 428-439.

WAGENMAKERS, A. J. M. 1998. Protein and amino acid metabolism in human muscle. *In:* RICHTER, E. A., KIENS, B., GALBO, H. & SALTIN, B. (eds.) *Skeletal Muscle Metabolism in Exercise and Diabetes.* Boston, MA: Springer US.

WANG, B., SCOTT, R. C., PATTILLO, C. B., PRABHAKARPANDIAN, B., SUNDARAM, S. & KIANI, M. F. 2007. Microvascular transport model predicts oxygenation changes in the infarcted heart after treatment. *American Journal of Physiology-Heart and Circulatory Physiology,* 293**,** H3732-H3739.

WENTZEL, J. J., KRAMS, R., SCHUURBIERS, J. C., OOMEN, J. A., KLOET, J., VAN DER GIESSEN, W. J., SERRUYS, P. W. & SLAGER, C. J. 2001. Relationship between neointimal thickness and shear stress after Wallstent implantation in human coronary arteries. *Circulation,* 103**,** 1740-1745.

WESTERHOF, N., BOSMAN, F., DE VRIES, C. J. & NOORDERGRAAF, A. 1969. Analog studies of the human systemic arterial tree. *Journal of Biomechanics,* 2**,** 121-143.

WIEDEMAN, M. P. 1963. Dimensions of blood vessels from distributing artery to collecting vein. *Circulation Research,* 12**,** 375-378.

WILKINSON, D. S. 2000. *Mass transport in solids and fluids*, Cambridge University Press.

WITTENBERG, B. A. & WITTENBERG, J. B. 1985. Oxygen pressure gradients in isolated cardiac myocytes. *Journal of Biological Chemistry,* 260**,** 6548-6554.

WITTENBERG, B. A. & WITTENBERG, J. B. 1989. Transport of oxygen in muscle. *Annual Review of Physiology,* 51**,** 857-878.

WITTENBERG, J. B. 1970. Myoglobin-facilitated oxygen diffusion: role of myoglobin in oxygen entry into muscle. *Physiological Reviews,* 50**,** 559-636.

WITTENBERG, J. B. & WITTENBERG, B. A. 1981. Facilitated oxygen diffusion by oxygen carriers. *Oxygen and Living Processes.* Springer.

WOLF, M., FERRARI, M. & QUARESIMA, V. 2007. Progress of near-infrared spectroscopy and topography for brain and muscle clinical applications. *Journal of Biomedical Optics,* 12**,** 062104.

WOODSON, R. D. & AUERBACH, S. 1982. Effect of increased oxygen affinity and anemia on cardiac output and its distribution. *Journal of Applied*

Physiology: Respiratory, Environmental and Exercise Physiology, 53**,** 1299-1306.

XIAO, N., HUMPHREY, J. D. & FIGUEROA, C. A. 2013. Multi-scale computational model of three-dimensional hemodynamics within a deformable full-body arterial network. *Journal of Computational Physics,* 244**,** 22-40.

YAN, F., JIANG, W., DONG, R., WANG, Q., FAN, Y. & ZHANG, M. 2017. Blood flow and oxygen transport in the descending branch of lateral femoral circumflex arteries after transfemoral amputation: a numerical study. *Journal of Medical and Biological Engineering,* 37**,** 63-73.

YAN, F., JIANG, W., XU, Z., WANG, Q., FAN, Y. & ZHANG, M. 2018. Developing transmission line equations of oxygen transport for predicting oxygen distribution in the arterial system. *Scientific Reports,* 8**,** 5369.

YAN, X., LIU, M., ZHANG, J., ZHU, H., LI, Y. & LIANG, K. 2015. On-chip investigation of the hydrodynamic dispersion in rectangular microchannels. *Microfluidics and Nanofluidics,* 19**,** 435-445.

YAO, W., ZHU, B., DING, G., DANG, R. & CHEN, E. 2008. A dynamic model describing oxygen metabolism in human and it's physiological analysis. *Chinese Journal of Biomedical Engineering,* 27**,** 50-55.

YASEEN, M. A., SRINIVASAN, V. J., SAKADŽIĆ, S., RADHAKRISHNAN, H., GORCZYNSKA, I., WU, W., FUJIMOTO, J. G. & BOAS, D. A. 2011. Microvascular oxygen tension and flow measurements in rodent cerebral

cortex during baseline conditions and functional activation. *Journal of Cerebral Blood Flow & Metabolism,* 31**,** 1051-1063.

YE, F., JENSEN, H., LARSEN, S. W., YAGHMUR, A., LARSEN, C. & OSTERGAARD, J. 2012. Measurement of drug diffusivities in pharmaceutical solvents using Taylor dispersion analysis. *Journal of Pharmaceutical and Biomedical Analysis,* 61**,** 176-183.

ZEMPLENYI, T., CRAWFORD, D. W. & COLE, M. A. 1989. Adaptation to arterial wall hypoxia demonstrated in vivo with oxygen microcathodes. *Atherosclerosis,* 76**,** 173-179.

ZHANG, M., MAK, A., CHUNG, A. I. & CHUNG, K. 1988. MRI investigation of musculoskeletal action of transfemoral residual limb inside a prosthetic socket. *In:* IEEE, ed. Proceedings of the 20th Annual International Conference of the IEEE Engineering in Medicine and Biology Society, Hong Kong. 2741-2743.

ZHANG, M. & ROBERTS, V. 1993. The effect of shear forces externally applied to skin surface on underlying tissues. *Journal of Biomedical Engineering,* 15**,** 451-456.

ZHAO, M., ZHANG, Y., ZHANG, Z., LIU, W. & PENG, J. 2008. Characteristics and staged rescue of severe cases in "5.12" Wenchuan megaseism. *China Journal of Modern Medicine,* 18**,** 2287-2290.

ZIERLER, K. L. 1965. Equations for measuring blood flow by external monitoring of radioisotopes. *Circulation Research,* 16**,** 309-321.